CONDUCTING POLYMERS AS ELECTROCHEMICAL ENERGY STORAGE PLATFORMS

A Dissertation

Presented to the Faculty of the Graduate School

of Cornell University

In Partial Fulfillment of the Requirements for the Degree of

Doctor of Philosophy

by

Gabriel Rodriguez-Calero

August 2014

CONDUCTING POLYMERS AS ELECTROCHEMICAL ENERGY STORAGE PLATFORMS

Gabriel Rodriguez-Calero, Ph. D.

Cornell University 2014

Solving the energy crisis and putting a halt to climate change is the greatest challenge of this century. In order to solve the energy crisis, harvesting energy from renewable sources needs to be economically and technologically feasible. Renewable energy sources are intermittent, but for our society to keep functioning uninterrupted access to electricity is a must. For this uninterrupted access, electrochemical energy storage (EES) is needed to provide energy when the renewable source is not available. Among EES, batteries and electrochemical capacitors (ECs) have shown the most promise, providing higher energy and power densities than other EES. In this publication conducting polymers as electrode materials are demonstrated to have improved performance over commercially available electrodes for EES applications. Conducting polymers are proven to be both electrocatalysts towards the redox reactions of organosulfur compounds and high gravimetric capacity electrode materials. Studies of the origin of the electrocatalytic effect yielded poly-3,4-ethylenedioxythiophene (PEDOT) as the best electrocatalyst. The idea of incorporating small redox active substituents (RAS) is proven effective and the understanding of the electropolymeriation reaction of RAS-CP is achieved. A RAS-CP that had practical capacities of 80 mAh/g was designed; this capacity was higher than

any other CP reported in the literature to date. Finally, the post-polymerization reaction was proven effective for the synthesis of RAS-CPs yielding polymers with enhanced capacity retention.

BIOGRAPHICAL SKETCH

Gabriel G. Rodríguez-Calero received his PhD in Chemistry from the Department of Chemistry and Chemical Biology at Cornell University. His research in Prof. Héctor D. Abruña's research group focuses on the investigation of novel materials for electrochemical energy generation and storage. Specifically his dissertation work involved the investigation of the electrochemical, electronic, and chemical properties of organic materials and their behavior during their electrochemical reactions using spectroscopy and electro-analytical techniques. Prior to joining Cornell University, he pursued his undergraduate studies at the University of Puerto Rico, Río Piedras Campus, graduating Magna Cum Laude with a Bachelor of Science with a major in Chemistry. During his studies at UPR-RP he worked under Prof. Carlos R. Cabrera's guidance researching materials and electro-synthesis techniques for electrochemical biosensors and fuel cell applications.

ACKNOWLEDGMENTS

The completion of this dissertation was only possible thanks to a great support network in my personal and professional life. I would not be here if it were not for specific individuals, who without expecting anything in return, helped me obtain the PhD degree. In the end, I feel blessed for having so many opportunities swing my way over the years and to be able to fulfill one of my goals.

First of all, I want to thank my parents Gabriel Rodríguez Quijano and Ida M. Calero Toledo. Mom and Dad, you have been an inspiration in how to live life in a way that matters. You taught me the important things in life, which are: feeling happy with what you are doing, following your "heart" to make decisions, not worrying about materialistic needs, preserving family values, among so many others lessons that would fill the entire dissertation on its own. Without your advice and support over the years, I am sure, I would not have aspired or being able to obtain a higher education. You are also, in great part, the reason why I have a scientific mind. You taught me how to look for facts and question why things happen in a certain way and not another. I am sure it was not easy at times but thanks for always being there no matter what.

I also want to thank other members of my family who have given me their support and have always believed I "had what it takes" to pursue and finish the PhD degree. My grandmothers Carmen D. Toledo Amador and Milagros Quijano Ocasio, you are why my parents are the way they are and have taught me many values that I still preserve to this day. My aunt and uncle Lymari Calero Toledo and Miguel

Medina Cintrón, you have always been supportive and role models in many ways. You gave me my first job and helped me appreciate the value of hard work. My sister Ilka B. Rodriguez Calero, your motivation and passion towards life and making a difference in the world is second to none. You have made me want to be a better person and brother by being an inspiration in how things should be done. As I tell everyone I meet that asks me about you, my sister is like me in many ways, but more responsible, smart and dedicated.

I would also like to thank my close friends who I consider family: Martin Samara, Davier Alfaro, Juan C. Cruz, and Pito Quiñones you have always believed in me and are a huge part of who I am since we have lived so many life experiences together. I truly appreciate your support and friendship. I have also been fortunate enough to meet new friends in Ithaca. Fefy Rivera, Joaquin Rodriguez Lopez, Manuel Plaza Dominguez and Fernando Uribe Romo thanks for being great friends and for all the advice in life and science. Anjuli Ramos Busot , thank you for your friendship, you were there through the ups and downs of my early PhD days, you always heard me out and understood the situations I was in. You made much of the transition from college to graduate school go by smoothly. Kenneth Hernández Burgos you are great friend, thanks for your friendship and for sharing 4/5 of my PhD life with me, I consider you part of my family. I would like to thank my partner Alyssa J. de Villiers. Alyssa, you have assisted me in the decision making process of making the “right” career choice and have kept me sane while writing my dissertation, also, you have provided me with the resolve, emotional stability, and wise advise necessary to complete this dissertation. You are most supportive and I am thankful to have you as my partner.

My colleagues and friends, Michael Lowe, Stephen Burkhardt, Sean Conte, Jie Gao, Joerg Werner, and all the other who due to an oversight on my part I have not mentioned you by name. Thanks for collaborating with me and providing me with invaluable guidance and more importantly your friendship. I have enjoyed enormously working with great scientists such as you. The intellectual conversations we have had will always remain with me. My contemporary colleagues in the Abruña group, Nicole Ritzert and Yingchao Yu, you have been great laboratory mates and friends that have helped shape the scientist I am today. I would also like to thank the members of the Abruña group who have made me feel appreciated and have provided me with a wonderful working environment.

I would also like to thank specific people who have helped me be here today. Carlos Velazquez, my godfather, you helped me decide to study chemistry and were facilitated my decisions to start doing research as an undergrad. You have provided me advice and wisdom over the years for which I am truly thankful. Prof. Carlos R. Cabrera, my undergraduate research advisor, you are the facilitator for my being in Cornell University. If it not were for that time you asked me, after class, where I was going for a summer internship, soon to discover that I had not been accepted anywhere, I would not have made it to Cornell. You are an inspiration to any scientist. Dr. Yasuyuki Kiya, thanks for introducing me to the fascinating world of conducting polymers and for making my stay at Cornell in the summer of 2008 so good that I decided to apply for graduate school at Cornell.

I would also like to thank my committee members Prof. Francis J. DiSalvo and Prof. Geoffrey W. Coates. Your open door policy, research advice and more

importantly decision-making guidance have made research and life at Cornell significantly easier. You have always been there to help out and I am truly grateful for that. You are role models in the academic field of professors who care about science and the graduate students they mentor.

Finally, I would like to thank my advisor Prof. Héctor D. Abruña. You have created a working environment in which I felt appreciated and understood since the first day I started working in your lab. You gave me the freedom to investigate scientific phenomena that I thought was interesting, while also making sure I did not chase at loose straws. You have come through every time and have provided me with the tools necessary to succeed. It is thanks to you that I was able to achieve the PhD title and for that I can't thank you enough. Thanks for being a great scientist, advisor and friend.

I would also like to thank my funding sources over the course of my PhD: the Rohm and Haas Fellowship, the SAGE fellowship, the Department of Energy, the Energy Materials Center at Cornell, the King Abdullah University of Science and Technology at Cornell University, and the Colin Garfield Fink ECS summer fellowship. Also, I would like to thank the journals that have allowed me to publish my research over the years.

TABLE OF CONTENT

CHAPTER 1

INTRODUCTION

Renewable Energy

Renewable energy is harvested from resources that can be replenished in a short time frame. The ideal future relies on harvesting energy from renewable energy sources. The case of solar, hydroelectric, geothermal, tidal, and wind as energy sources has to be the only option moving forward if we are to tackle the serious issues that are affecting our planet today. If we restrict ourselves by not moving away from fossil-fuel resources as our main energy source, the earth will experience continued climate change and the nation's (and, indeed, global) energy security will be compromised.

So far, the use of fossil fuels has created severe climatological changes on planet earth. Fortunately, in the last 20 years there has been a newfound interest in the development of technologies that are powered by, or that harvest, renewable energy sources. Fuel cells, photovoltaic panels, and wind turbines, to mention a few, have seen an increase in commercialization and adoption. More importantly, several companies have now accepted the promise of these innovative technologies, allowing for their further widespread utilization.

Renewable energy sources are inherently intermittent. However, our society is accustomed to uninterrupted use of electricity. If we are to successfully incorporate these renewable energy technologies into the electric grid with a seamless transition, there must be efficient ways of storing energy for instances when the renewable energy source is not available.

There are currently several options to store energy: fuel generation, pumped-hydro, compressed gas and electrochemical energy storage. In this dissertation, the study of a specific family of materials for electrochemical energy storage will be detailed.

Electrochemical Energy Storage

Electrochemical energy storage (EES) devices are used today in a variety of application spaces. These devices store energy in the form of physical charge or as chemical reactants. They are primarily divided into two devices, batteries and electrochemical capacitors (Figure 1.1).

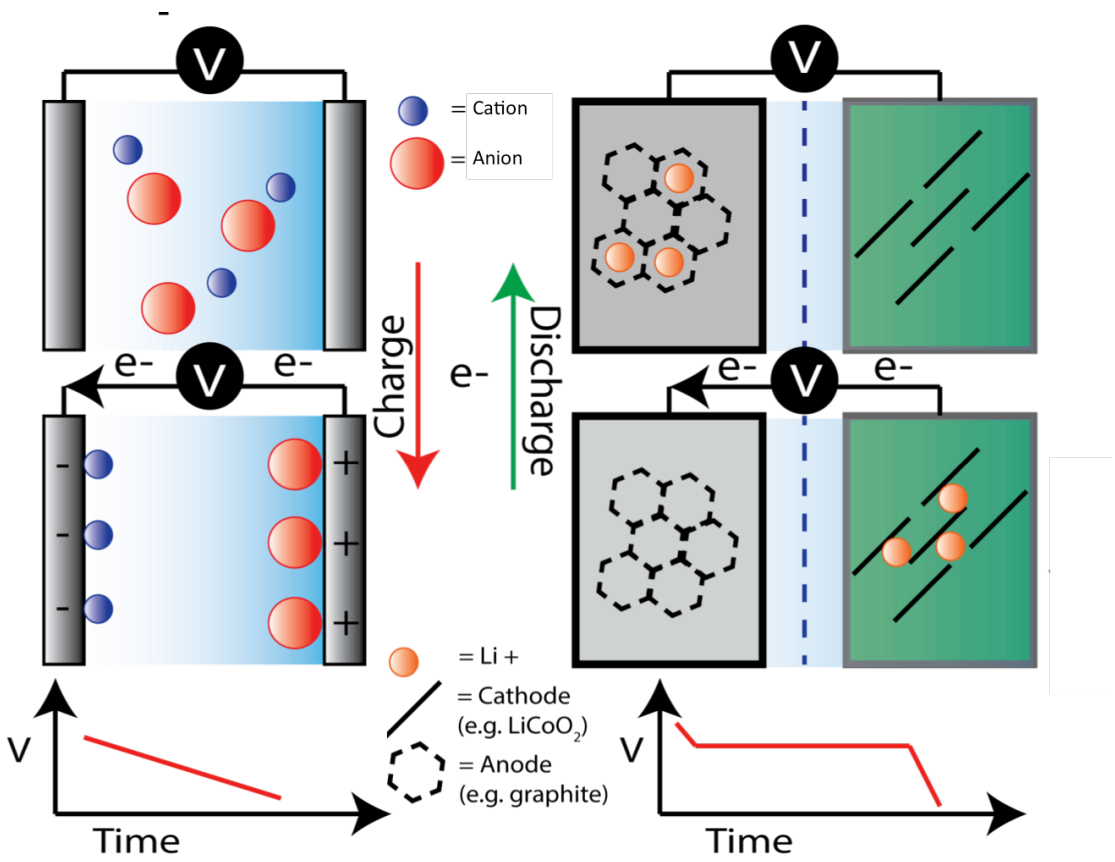

Figure 1.1. Pictorial representation of a capacitor (left) and a lithium ion battery (right).

Capacitors store energy electrostatically as physical charge on the electrode plates. The electrode materials in capacitors suffer virtually no change in structure or chemical composition during the device operation. In large part, these two characteristics of capacitors allow them to inherently possess high power densities and very long device lifetimes. However, since the charges are stored only at the electrode surface, they typically suffer from low energy densities.[1]

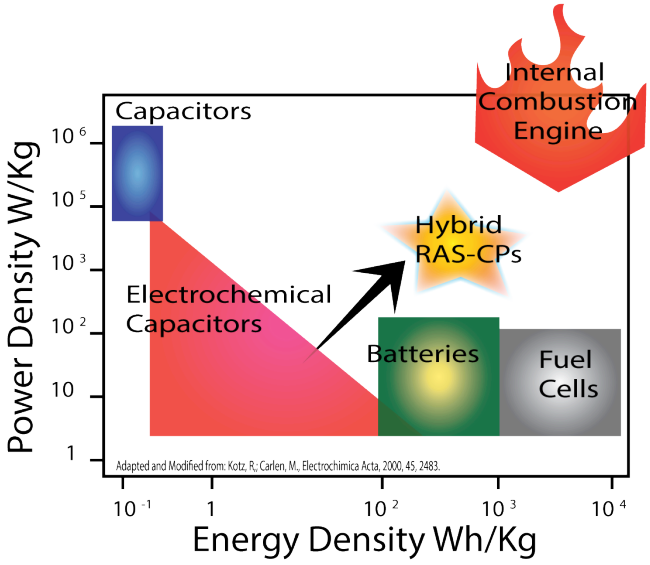

Figure 1.2. Ragone plot with the theoretical gravimetric power and energy densities of redox active substituted conducting polymers (RAS-CP)

Batteries store energy in the form of chemical reactants. Alessandro Volta invented the first battery in the 1880s. The application space for batteries ranges from grid-energy storage and transportation to smaller electronic devices like portable computers and cellphones. The electrodes in batteries undergo structural and chemical changes during device operation and, depending on their nature, these changes can be reversible or not. Because of the structural and chemical changes undergone by battery electrodes, the device lifetime of batteries is significantly shorter than that of

capacitors by 2-3 orders of magnitude. On the other hand, since batteries store energy in the bulk of the electrodes, the energy density of batteries is 3-4 orders of magnitude higher than traditional capacitors. These properties of EES devices are graphically represented in the Ragone plot shown in Figure 1.2.

In the work described herein, I will illustrate how organic materials, specifically conducting polymers, can be used as energy storage platforms for EES applications.

Organic Materials as EES Platforms

Organic materials represent a most attractive alternative to traditional electrode materials for EES applications. They are composed of abundant elements (such as C, H, N, S, and O) making them inherently inexpensive. The use of organic synthesis allows control over the electronic structure and physical properties; making them tunable. Also, since they are lightweight, the theoretical gravimetric capacity and energy density is high, in some cases exceeding 300 mAh/g and 1000 KWh/g.

The electrode that has the lower capacity limits the overall capacity of an EES device. Currently, in state-of-the-art high energy density devices (i.e. lithium ion batteries) the cathode limits performance; therefore, that will be the electrode under study in this dissertation.

Traditionally, cathode electrodes in batteries are composed primarily of metal oxides. These electrodes undergo phase changes upon battery operation and are composed of expensive and often toxic elements such as Cobalt. The most common cathode material in high energy density EES devices is $LiCoO_2$. This electrode has a practical capacity of 140 mAh/g.

Several groups have investigated organic materials for EES applications.[1] Electrochemical studies of these materials have revealed promising properties including high gravimetric capacities and high energy density.[1] Synthetic methodologies have also been developed to extract these organic compounds from renewable feedstocks (in this case plants), making these materials even more attractive.

In the past 10 years, the majority of the work on organic materials has focused on the use of carbonyl functionalities as the redox active component of the molecule.[2] Carbonyl based materials are electrochemically reversible and can bind small metal ions very well (our group recently published an article illustrating these ionic effects on the electrochemical reactions of carbonyl based molecules).[3] However, they typically suffer from low operating voltages.[2,3] Other groups, including ours, have studied organic materials with alternate electroactive functionalities such as thiolates, thioethers, and tertiary amines with varying degrees of success.[4] I will make the case for conducting polymers (CPs) as additives and active materials in EES devices.

Conducting Polymers as EES Cathodes

Since their discovery in the 1970's, CPs have been extensively studied for a variety of applications ranging from flexible electronics to electrochemical energy storage applications. Shirakawa, Heeger and MacDiarmid received the Nobel prize in Chemistry in 2000 for the discovery of CPs and the study of their properties. They found that polyacetylene could be oxidized and doped with anions to increase conductivity by 7 orders of magnitude.

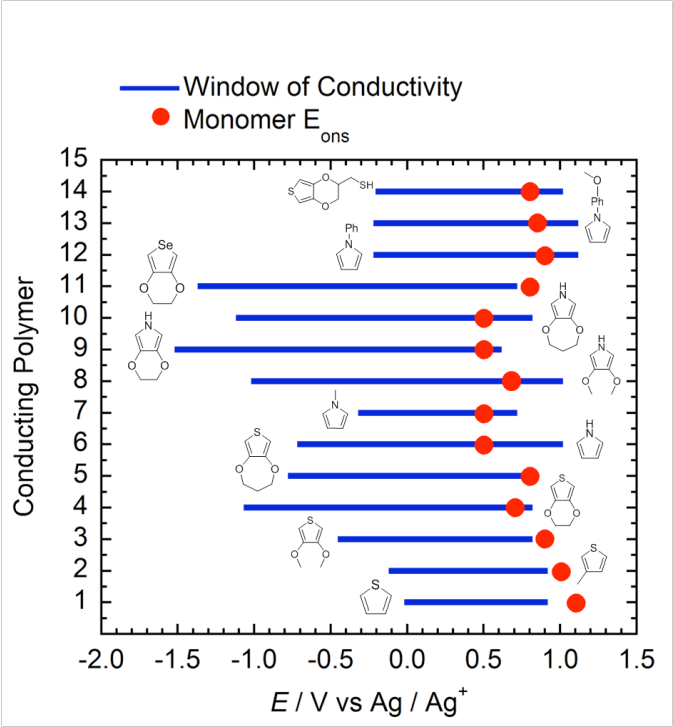

Figure 1.3. Window of conductivity (Blue lines) and monomer oxidation onset potential (Red dots) plot for the indicated monomers.

Similar to organic materials, CPs can be modified using organic synthesis to alter their physical and chemical properties. By changing the substituents or the heteroatoms in the CP structure the position of the window of conductivity and the onset for monomer oxidation can be finely tuned (Figure 1.3)

The representative cyclic voltammogram (CV) of a poly-3,4-ethylenedioxythiophene (PEDOT) can be observed in Figure 1.4. In this CV three distinct regions can be observed: the n-doped region where the polymer is reduced and doped with cations, the insulating region where the polymer is electronically an insulator, and the p-doped region where the polymer is oxidized and doped with anions. The p-doped region is located at potentials where the electrochemical reactions of interest take place. The p-doped conductivity region can also be called the window of conductivity of the CP.

CPs inherently posses high conductivity and chemical stability making them prime candidates for EES electrodes. Most of them are also insoluble in traditional battery electrolytes. The use of CP in EES devices is not new. Several groups have studied the electrochemical performance in prototype devices illustrating their high electrochemical cycling performance.[7] However, the theoretical gravimetric capacity of CPs is from 20-40 mAh/g. This is due, in large part, to the fractions of an electron transferred per monomer unit in the polymer.

In this dissertation the use of conducting polymers as electrocatalysts for organosulfur compounds and as the electroactive material in the cathode of the electrochemical energy storage device is presented. Modifying CPs with redox active substituents, or adding them as electrocatalysts, allows for EES devices with higher energy and power densities (Figure 1.2).

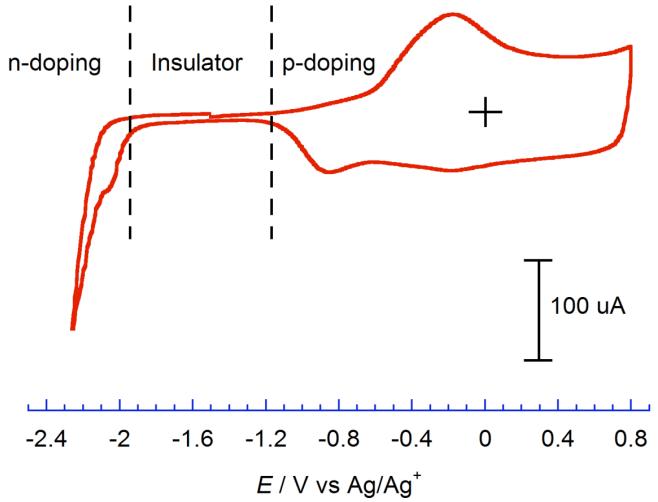

Figure 1.4. Representative cyclic voltammogram of a poly-3,4-ethylenedioxythiophene film modified electrode in 0.1 M lithium perchlorate / acetonitrile solution at a sweep rate of 20 mV/s.

REFERENCES

1. (a) Liang, Y.; Tao, Z.; and Chen.; J. Adv. Energy Mater. 2012, 1, 1.; (b) Burkhardt, S. E.; Lowe M. A.; Conte, S.; Zhou, W.; Qian, H.; Rodríguez-Calero, G. G.; Gao, J.; Hennig, R. G.; and Abruña, H. D.; Energy. Environ. Sci. 2012, 5, 7176. (c) Poizot, P.; and Dolhem, F.; Energy Environ. Sci. 2011, 4, 2003. (d) Chen, H.; Armand, M.; Courty, M.; Jiang, M.; Grey, C. P.; Dolhem, F.; Tarascon, J.-M.; and Poizot, P.; J. Am. Chem. Soc. 2009, 131, 8984. (e) Gao, J., Lowe M. A., Conte S., Burkhardt, S. E., and Abruña H. D.; Chem. Eur. J. 2012, 18, 8521.

2. (a) Tarascon, J. M.; and Armand, M.; Nature 2001, 414, 359.; (b) Chen, H.; Armand, M.; Demailly, G.; Dolhem, F.; Poizot. P.; and Tarascon, J.-M.; ChemSusChem. 2008, 1, 348. (c) Walker, W.; Grugeon, S.; Mentre, O.; Laruelle, S.; Tarascon, J.-M.; and Wudl, F.; J. Am. Chem. Soc. 2010, 132, 6517.

3. Hernández-Burgos, K.; Rodríguez-Calero, G. G.; Zhou, W.; Burkhardt, S. E.; and Abruña, H. D.; J. Am. Chem. Soc. 2013, 135, 14532.

4. (a) Conte, S.; Rodríguez-Calero, G. G.; Burkhardt, S. E.; Lowe, M. A.; and Abruña, H. D.; RSC Adv. 2013, 3, 1957. (b) Burkhardt, S. E.; Lowe, M. A.; Conte, S.; Zhou, W.; Qian, H.; Rodríguez-Calero, G. G.; Gao, J.; Hennig, R. G.; and Abruña, H. D.; Ener. Environ. Sci. 2012, 5, 7176. (c) Burkhardt, S. E.; Conte, S.; Rodríguez-Calero, G. G.; Lowe, M. A.; Qian H.; Zhou, W.; Gao, J.; Hennig, R.; and Abruña, H. D.; J. Mater. Chem. 2011, 21, 9553. (d) Suguro, M.; Iwasa, S.; and Nakahara, K.; Electrochem. Solid-State Lett., 2009, 12, A194.

5. (a) Novak, P.; Müller, K.; Santhanam, K.S.V.; and Haas, O.; Chem. Rev. 1997, 97, 207 (b) Groenendal, L.; Jonas, F.; Freitag, D.; Pielartzik, H.; and Reynolds, J. R.; Adv. Mater. 2000 12, 481

6. Hiang, C. K.; Fincher, C. R., Jr.; Park, Y. W.; Heeger, A. J.; Shirakawa, H.; Louis, E. J.; Gau, S. C.; and MacDiarmid, A. G.; Physical Review Letters 1977, 39, 1098.

7. Park, K.-S.; Schougaard, S. B.; and Goodenough, J. B.; Adv. Mater. 2007, 19, 848.

CHAPTER 2

ELECTROCHEMICAL AND COMPUTATIONAL STUDIES ON THE ELECTROCATALYTIC EFFECT OF CONDUCTING POLYMERS TOWARD THE REDOX REACTIONS OF THIADIAZOLE-BASED THIOLATE COMPOUNDS

Introduction

Organosulfur compounds with multiple thiolate groups have garnered scientific and technological interest as potential cathode materials for lithium-ion rechargeable batteries due, primarily, to their high theoretical gravimetric capacities.[1-15] In general, they are theoretically capable of providing higher gravimetric capacity than conventional cathode materials such as lithium metal oxides and phosphates (e.g., $LiCoO_2$ and $LiFePO_4$, respectively). Organosulfur compounds also offer the advantage of being relatively low cost and derived from abundant resources as opposed to $LiCoO_2$ that has been widely employed in practical applications. Moreover, chemical tunability of organosulfur compounds makes them even more attractive. That is, organosulfur compounds can be modified (designed) to provide additional chemical and/or electrochemical properties of interest. More importantly, disulfide bond formation/cleavage reactions involved in these redox systems are capable of releasing/capturing lithium ions during charge/discharge operations, and thus, they can be easily incorporated into the so-called "rocking-chair" type system.[16]

However, the practical application of organosulfur compounds has been hindered because of their sluggish charge transfer kinetics as well as their lack of electrical conductivity. Therefore, in order for them to be of practical use in lithium-

ion battery technologies, it is necessary to develop efficient electrocatalysts to accelerate the redox (i.e., charge/discharge) processes. In order to accelerate the redox reactions of organosulfur compounds, we have been focusing on the use of conducting polymers as efficient electrocatalysts.[6, 15, 17-20] In particular, we have previously reported on the unprecedented electrocatalytic activity of poly(3,4-ethylenedioxythiophene) (PEDOT) toward the redox reactions of 2,5-dimercapto-1,3,4-thiodiazole (DMcT), one of the most promising organosulfur compounds as a cathode electroactive material.[6,20] As shown in Scheme 2.1, during charge, DMcT is electrochemically oxidized to give the radical, which generates DMcT dimer via the coupling reaction. DMcT dimer is then oxidized to generate its radical species, resulting in the formation of DMcT disulfide oligomers (and polymers). On the other hand, during discharge, DMcT oligomers are electrochemically reduced, resulting in the cleavage of the disulfide bonds and, thus, regeneration of DMcT monomer. These redox reactions are found to be electrocatalyzed at PEDOT film modified electrodes via electron exchange reactions between DMcT and PEDOT. In fact, we have previously demonstrated that the reduction process of the DMcT dimer (i.e., disulfide bond cleavage) is accelerated by a factor of approximately 12000 at a PEDOT film modified glassy carbon electrode (GCE).[20]

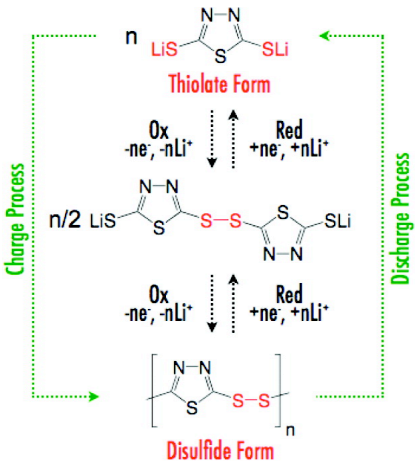

Scheme 2.1. Redox reaction scheme for 2,5-dimercapto-1,3,4-thiadiazole dilithium salt (DMcT-2Li)

In the present chapter, and with the aim of further understanding this dramatic electrocatalytic effect, we have studied the redox reactions of DMcT dilithium salt (DMcT-2Li) at GCEs modified with polythiophene (PTh) and its derivatives, shown in Figure 2.1, via cyclic voltammetry (CV) and rotating-disk electrode voltammetry (RDE). Since the redox behavior of DMcT is strongly influenced by the presence of protons, DMcT-2Li was employed in this study to focus solely on the redox reactions of the dithiolate form.[17,21,22] In particular, we have thoroughly studied the effect of the location of the window of conductivity (i.e., potential range over which a conducting polymer is in its electrically conducting state) on the electrocatalytic activity toward DMcT-2Li. The position of the window of conductivity was tuned by employing different electron-donating groups at the 3- or 3,4-positions of PTh, resulting in different degrees of overlap of the window of conductivity with the formal potential of DMcT-2Li. Due to the fact that the redox reactions of conducting polymers such as PEDOT mediate the redox reactions of organosulfur compounds in the electrocatalytic processes, it was anticipated that higher electrocatalytic activity would be obtained

when the window of conductivity for a conducting polymer had better overlap with the formal potential for an organosulfur compound. The electrocatalytic activity of conducting polymers was compared by estimating the standard charge transfer rate constants, k^0, for the dimerization process of DMcT-2Li at GCEs modified with conducting polymers. To avoid any complications arising from the deposition process of DMcT polymer, we have focused on the dimerization process (i.e., the first one-electron oxidation process). In order to estimate k^0 values at conducting polymer modified GCEs and compare them with that at an unmodified GCE, conducting polymer films were treated as an extension of the GCE.[20] We have also estimated the film resistance of the conducting polymers at the formal potential for the dimerization process of DMcT-2Li via electrochemical impedance spectroscopy (EIS). Furthermore, computational studies were carried out to identify the factors affecting the electrochemical behavior of conducting polymers (and thus the electrocatalytic activity toward DMcT-2Li). The relationships between the molecular structures of conducting polymers and the positions of the window of conductivity, and thus the electrocatalytic activity toward DMcT-2Li, are discussed in detail.

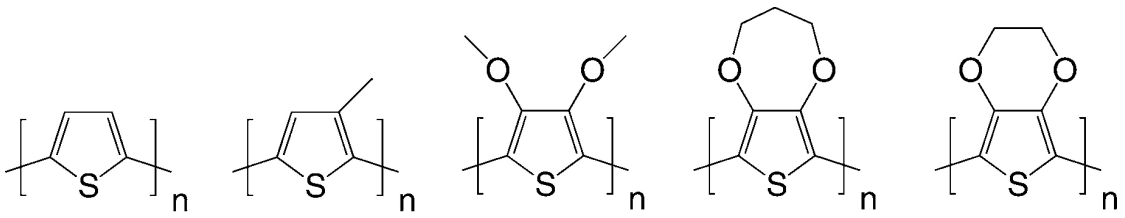

Figure 2.1. Polythiophene derivatives with different substituents at the 3,4-positions employed in this study: polythiophene (PTh), 1; poly(3-methylthiophene) (PMTh), 2; poly(3,4-dimethoxythiophene) (PDMTh), 3; poly(3,4-propylenedioxythiophene) (PProDOT), 4; and poly(3,4-ethylenedioxythiophene) (PEDOT), 5.

Experimental

Materials

2,5-Dimercapto-1,3,4-thiadiazole dilithium salt (DMcT-2Li) was purchased from Toyo Kasei Co. (Japan) and used without further purification. 3,4-Ethylenedioxythiophene (EDOT) was obtained from Bayer Co. (Germany) and used as received. High-purity HPLC-grade acetonitrile (AN) was purchased from Burdick and Jackson, and dried over 3 Å molecular sieves. Lithium perchlorate ($LiClO_4$) (99.99%), thiophene (Th) (99%+), 3-methylthiophene (MTh) (98%), 3,4-dimethoxythiophene (DMTh) (97%), and 3,4-propylenedioxythiophene (ProDOT) (97%) were purchased from Aldrich Chemical Co., Inc., and used as received. Sodium hydroxide (NaOH) was purchased from Mallinckrodt Chemicals and used as received.

Electrochemical Measurements

CV and RDE voltammetry studies were carried out at room temperature using a Hokuto Denko Co., model HSV-100 and HABF1510m, potentiostat. In RDE voltammetry studies, linear sweeps were carried out at 10 mV/s at different rotation rates using a Pine Instrument Co., model AFMSRX, rotator. EIS studies were carried out at room temperature using a frequency response analyzer equipped with a potentiostat/galvanostat (Solartron Analytical, SI 1280B). In EIS studies, the impedance spectra were recorded over the frequency range from 20 kHz to 0.3 Hz by using a sinusoidal signal with an amplitude of 10 mV. Measurements were taken in a three-electrode cell configuration using a GCE (for CV and EIS a 3.0 mm diameter electrode from Bioanalytical Systems, Inc. (BAS) and for RDE a 5.0 mm diameter electrode from Pine Instrument Co.), a large area Pt coil counter electrode, and a

Ag/Ag^+ (0.05 M $AgClO_4$ + 0.1 M $LiClO_4$/AN) reference electrode without regard to the liquid junction potential, and against which all potentials are reported. The working electrodes were polished with 0.3 and 0.05 μm alumina solutions (REFINETEC Ltd.), rinsed with distilled water and acetone, and dried prior to use. The electrodes were then electrochemically cleaned by cycling the potential in a 1 M NaOH solution between 0.0 and +1.3 V versus Ag/AgCl (KCl saturated) (BAS), followed by rinsing with distilled water and acetone. Unless otherwise noted, all experiments were carried out in 0.1 M $LiClO_4$/AN solutions, which were thoroughly purged prior to use with prepurified nitrogen gas.

Films of PTh (**1**), PMTh (**2**), PDMTh (**3**), PProDOT (**4**), and PEDOT (**5**) were prepared on GCEs for CV, RDE, and EIS studies by anodic electrochemical polymerization of the monomers in 0.1 M $LiClO_4$/AN solutions via potential cycling at 20 mV/s. The potential cycling was carried out over the potential regions from −0.60 V to +1.35 V for Th, to +1.30 V for MTh, to +1.05 V for DMTh, to +1.00 V for ProDOT, and to +0.90 V for EDOT. The monomer concentrations employed for the polymerization of Th, MTh, DMTh, ProDOT, and EDOT were 200, 20, 50, 20, and 20 mM, respectively. The film thicknesses of the conducting polymers were approximated by using a coulometer (attached to the HABF 1510 m). After polymerization, the films were thoroughly rinsed with a 0.1 M $LiClO_4$/AN solution and subsequently used for the characterization of the redox reactions of DMcT-2Li. In EIS studies, potentials of the conducting polymer modified GCEs were equilibrated at the potential of interest for 1 min before EIS experiments were initiated.

Quantum Mechanical Calculations

Geometry optimizations for thiophene-based oligomers were performed at the level of density functional theory using Gaussian 03 software. The hybrid functional (B3LYP) and basis set (6-31G*) chosen for optimization have been demonstrated to accurately reproduce experimental band gaps[23] and yield optimized geometries that are consistent with ab initio approaches and other DFT functionals.[24] All oligomers were first optimized in a planar, all-anti-conformation, using the Universal Force Field (UFF) as implemented in the Avogadro 0.8.1 software program. Oligomers were then relaxed without constraint. Geometric trends reported were verified by geometry optimizations on tetramers using an expanded basis set (6-31+G**). Torsion angle calculations were performed using a relaxed potential energy scan about the central dihedral angle of the dimers with the expanded basis set.[24] Bader charge analysis was performed on a high-resolution charge density file (12^3 data points/bohr^3) using a grid-based algorithm for charge decomposition.[25] Calculations were performed on the Intel Cluster at the Cornell Nanoscale Facility (CNF), part of the National Nanotechnology Infrastructure Network (NNIN) funded by the National Science Foundation (NSF).

Results and Discussion

Preparation of Conducting Polymer Film Modified GCEs and Their Redox Behavior

Figure 2.2 presents consecutive cyclic voltammograms (CVs) taken during the electrochemical polymerization of ProDOT (4) in a 0.1 M LiClO4/AN solution containing 20 mM ProDOT. In the first anodic potential scan, the onset of the irreversible anodic current, due to the oxidation of ProDOT, was observed at +0.85 V versus Ag/Ag+. An increase in the double layer capacitance was observed over the

potential region from −0.60 to +0.80 V during continuous potential cycles. The increase in both the anodic and cathodic current responses indicates that PProDOT, formed by coupling reactions of ProDOT radicals generated by the oxidation of ProDOT, is continuously deposited onto the GCE surface. Additionally, the onset potential for the oxidation of ProDOT shifted toward negative potentials as the number of potential cycles increased, indicating that the PProDOT film is capable of self-catalyzing the ProDOT oxidation process as was the case for PEDOT (5).[20] Similar anodic and cathodic current responses were observed for all of the monomer solutions studied.

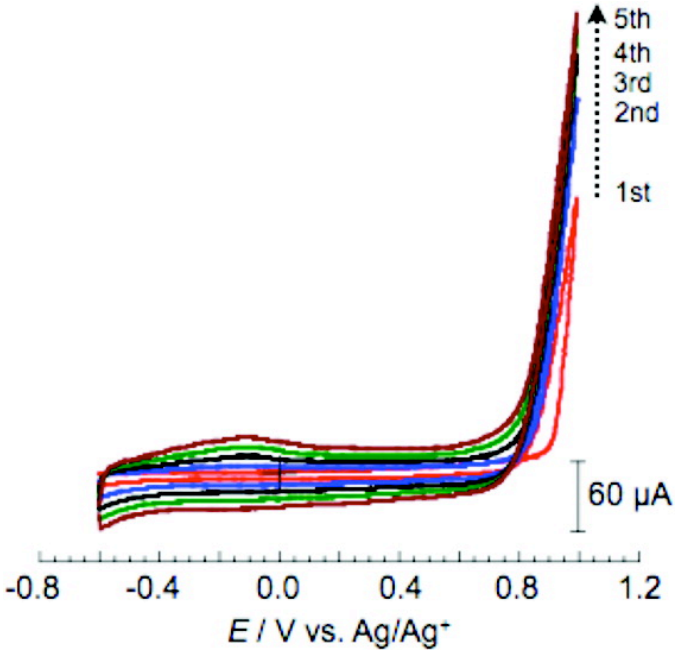

Figure 2.2. Typical CV for 20 mM ProDOT 4 at a bare GCE in 0.1 M LiClO4/AN. Scan rate was 20 mV/s.

Figure 2.3 shows CVs obtained in 0.1 M LiClO4/AN solutions at 20 mV/s for GCEs modified with films of 1, 2, 3, 4, and 5. As is evident, the onset potentials for the oxidation (p-doping) of PMTh, PDMTh, PProDOT, and PEDOT films are shifted

toward negative potentials when compared to the PTh film, thus exhibiting different conducting potential regions (i.e., windows of conductivity). The negative shift in potentials is consistent with the electron-donating nature of the substituents at the 3- or 3,4-positions and enables an analysis of the effects of the position of the window of conductivity on the electrocatalytic activity of each polymer film toward the redox reactions of DMcT-2Li. For instance, the oxidation of PProDOT starts at –0.68 V and anodic current peaks are observed at –0.50 V and +0.02 V, followed by a plateau current response. The corresponding reduction current peaks were observed at –0.65 and –0.08 V. The redox current responses obtained over this potential region exhibited a steady-state voltammetric response, indicating that the stable window of conductivity for PProDOT is approximately 1.5 V. In addition, as can be seen in Figure 2.4, the oxidation peak currents observed at +0.02 V for 4, –0.28 V for 5, and +0.12 V for 3 were directly proportional to scan rates up to 200 mV/s, indicating that the redox reactions of these polymers are surface processes and that charge propagation through the films is facile. Similar results (not shown) were also obtained for 1 and 2.

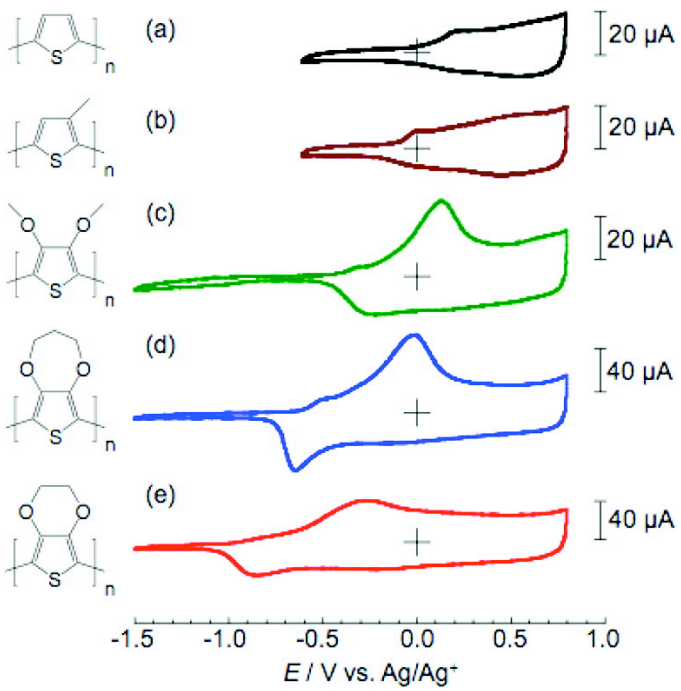

Figure 2.3. CVs for (a) 1, (b) 2, (c) 3, (d) 4, and (e) 5 film-modified GCEs in 0.1 M LiClO4/AN. The scan rate in all cases was 20 mV/s.

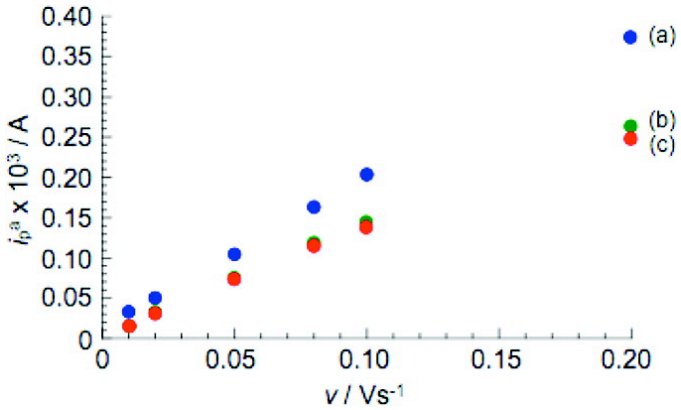

Figure 2.4. Anodic peak current, ipa for (a) 4, (b) 5, and (c) 3, as a function of scan rate *v*.

Effect of Window of Conductivity for Conducting Polymers on the Electrocatalytic Activity toward the Redox Reactions of DMcT-2Li

Next, we studied the effect of the position of the window of conductivity for conducting polymers on the electrocatalytic activity toward the redox reactions of DMcT-2Li. As discussed in the previous section, the window of conductivity for a

conducting polymer can be tuned by employing electron-donating (or withdrawing) substituents at the 3- or 3,4-positions of PTh. The formal potential for the dimerization process of DMcT-2Li was estimated from the redox response obtained at a PEDOT film modified GCE and determined to be –0.54 V versus Ag/Ag+. Note that the redox reactions of DMcT-2Li are electrochemically irreversible at bare GCEs (vide infra), and thus, the electrocatalytic effect by PEDOT toward DMcT-2Li helped estimate the formal potential. It can be seen from Figure 2.3 that the formal potential is located within the windows of conductivity for 4 and 5, while it is located outside of the windows for 1, 2, and 3. From the relationship between the windows of conductivity and the formal potential for DMcT-2Li, it was anticipated that PProDOT as well as PEDOT would electrocatalyze the redox reactions of DMcT-2Li while 1, 2, and 3 would not. In this section we discuss changes in electrocatalytic activity of conducting polymers by exemplifying the redox behavior of DMcT-2Li obtained at PProDOT and PDMTh film modified GCEs.

CVs a and c of Figure 2.5 show representative CVs for 1 mM DMcT-2Li at bare and PProDOT film modified GCEs in 0.1 M LiClO4/AN, respectively. The CV response of a PProDOT film modified GCE in 0.1 M LiClO4/AN (in the absence of DMcT-2Li) is also shown in Figure 2.5b for comparison. In the anodic potential scan at a bare GCE, the oxidation of DMcT-2Li to generate the radical species, resulting in the formation of the dimer and oligomers (or polymer), was observed with anodic current peaks at –0.30 and +0.01 V versus Ag/Ag+. A cathodic peak corresponding to the reductive stripping of DMcT oligomers (or polymer) from the GCE surface was observed at –0.92 V. The large separation between the anodic and cathodic current

peaks indicates that the redox processes of DMcT-2Li are electrochemically irreversible under the experimental conditions employed. The redox behavior observed was consistent with that previously reported.[18] At a PProDOT film modified GCE, on the other hand, the anodic current peaks due to the oxidation of DMcT-2Li were observed at more negative potentials and the cathodic current peak was shifted toward positive potentials. The shifts in the oxidation and reduction potentials, and thus decrease in the peak-to-peak separation, points to the electrocatalytic activity of PProDOT toward the redox reactions of DMcT-2Li. Similarly, the peak-to-peak separation for the redox reactions of DMcT-2Li was significantly decreased at a PEDOT film modified GCE as previously reported.[18] There was also a small redox couple observed at +0.45 V whose identity is not certain at this time.

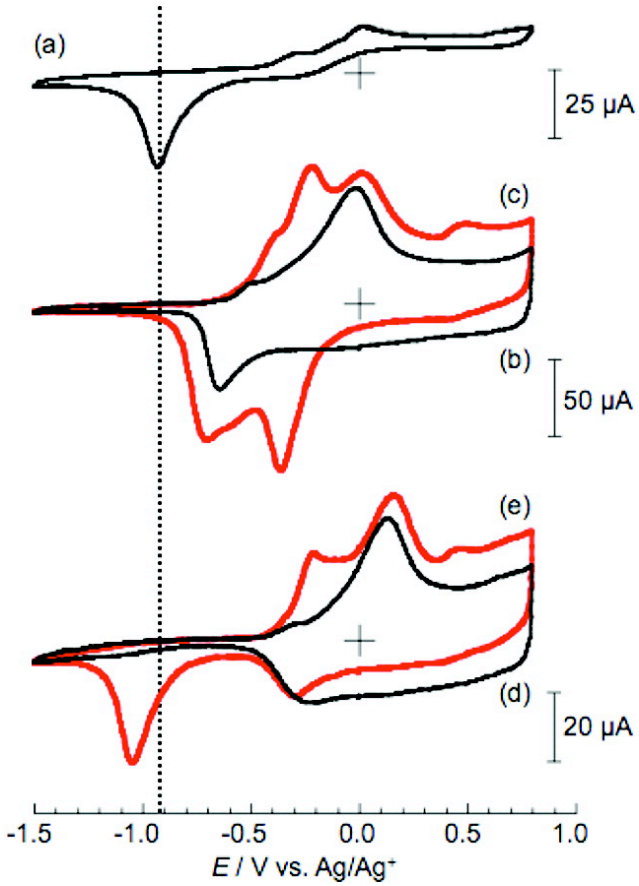

Figure 2.5. (a) Representative CV for 1 mM DMcT-2Li at a bare GCE in 0.1 M LiClO4/AN. Representative CVs for a 4 film modified GCE in 0.1 M LiClO4/AN containing (b) 0 and (c) 1 mM DMcT-2Li. Representative CVs for a 3 film modified GCE in 0.1 M LiClO4/AN containing (d) 0 and (e) 1 mM DMcT-2Li. Scan rate in all cases was 20 mV/s.

Figure 2.5e presents a representative CV for 1 mM DMcT-2Li at a PDMTh film modified GCE in 0.1 M LiClO4/AN. The CV response of a PDMTh film modified GCE in 0.1 M LiClO4/AN is also shown in Figure 2.5d for comparison. Contrary to PProDOT and PEDOT film modified GCEs, the peak-to-peak separation for the redox reactions of DMcT-2Li increased at a PDMTh film modified GCE when compared to a bare GCE (see vertical dotted line), indicating that PDMTh has no electrocatalytic activity toward DMcT-2Li and, in fact, the film appears to make the redox process

even more irreversible. PTh and PMTh film coated GCEs also exhibited no electrocatalytic activity toward the redox reactions of DMcT-2Li. These results indicate that PProDOT and PEDOT, whose windows of conductivity overlap the formal potential for dimerization of DMcT-2Li, exhibit electrocatalytic activity toward DMcT-2Li, while PDMTh, PMTh, and PTh do not. Therefore, and as we had anticipated, in order for a conducting polymer film to be able to electrocatalyze the redox reactions of DMcT-2Li, the window of conductivity of the former must overlap the formal potentials of the latter.

Quantitative Analysis of Charge Transfer Kinetics for the Dimerization Process of DMcT-2Li at Conducting Polymer Film Modified GCEs

In order to make a quantitative comparison of the electrocatalytic activity of conducting polymers toward the redox reactions of DMcT-2Li, the dimerization process of DMcT-2Li was further studied in detail via RDE voltammetry from which the standard rare constant, k^0, for the process was estimated at 3, 4, and 5 film modified GCEs. Moreover, in order to estimate k0values at conducting polymer modified GCEs and compare them with that at an unmodified GCE, the conducting polymer films were treated as an extension of the GCE.[20] In order to justify this assumption, we employed thin conducting polymer film coated GCEs. Note that the PProDOT surface coverage employed for RDE studies was 1.9×10^{-7} mol/cm2 while it was 1.1×10^{-6} mol/cm2 for CV studies.

Figure 2.6a presents linear sweep voltammograms (LSVs) for 1 mM DMcT-2Li at a PProDOT film modified rotating-disk GCE in a 0.1 M LiClO4/AN solution at different rotation rates. A LSV for a PProDOT film modified rotating-disk GCE in 0.1

M $LiClO_4$/AN is also shown in Figure 2.6a for comparison. It is worth noting that the anodic current response due to the oxidation of the PProDOT film is negligible when compared to the response due to the oxidation of DMcT-2Li in solution. It can be seen that there are two limiting current regimes corresponding to dimerization of DMcT-2Li and the further oxidation of the dimer to generate oligomers. In this study, the limiting current, i_L, was measured at –0.42 V versus Ag/Ag+ to estimate k0 for the dimerization process of DMcT-2Li.

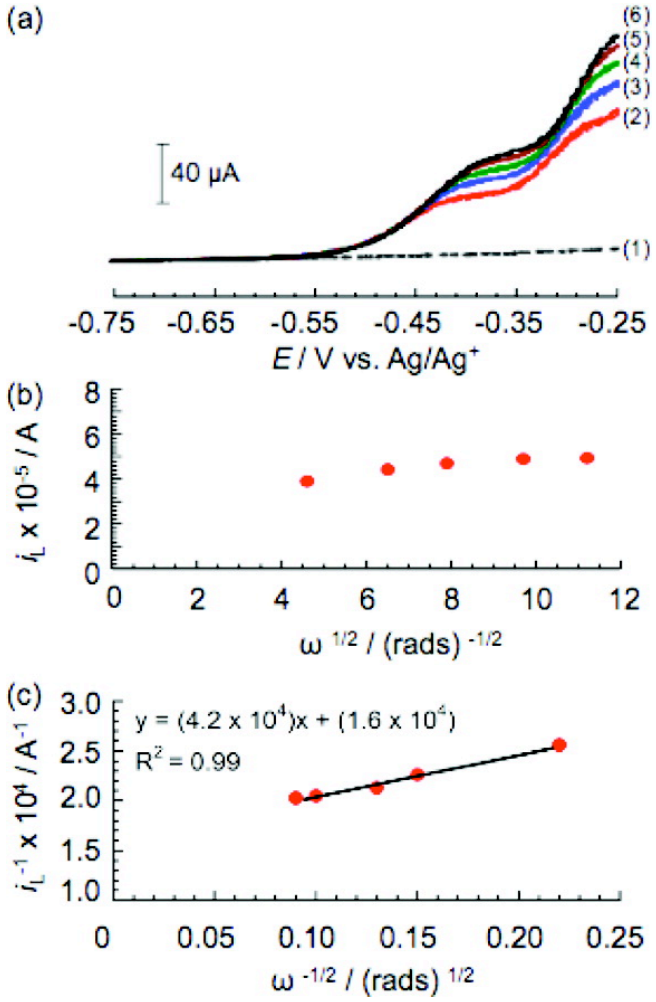

Figure 2.6. (a) LSVs for the oxidation of 1 mM DMcT-2Li at a 4 film modified rotating-disk GCE in 0.1 M LiClO4/AN. Rotation rates were (2) 200, (3) 400, (4) 600, (5) 900, and (6) 1200 rpm. (1) LSV at 1600 rpm for a PProDOT film modified GCE in

0.1 M LiClO4/AN for comparison. The scan rate in all cases was 10 mV/s. (b) Levich and (c) Koutecky–Levich plots obtained from the current values measured at –0.42 V versus Ag/Ag+.

Parts b and c of Figure 2.6 present the Levich and Koutecky−Levich (K-L) plots obtained from the LSVs shown in Figure 2.6a. The Levich plot exhibited significant curvature, consistent with a system that is kinetically limited but not transport limited. Similarly, in the K-L plot a linear relationship between i_L^{-1} and $\omega^{-1/2}$ was observed with a nonzero intercept, indicating that the oxidation of DMcT-2Li to generate the dimer is kinetically but not mass transport limited under the experimental conditions employed. The i_k value obtained from the intercept was 6.2×10^{-5}A, and thus the charge transfer rate constant at −0.42 V, $k(-0.42)$, was determined to be 3.3×10^{-3} cm/s. From that value, the standard rate constant, k^0, was estimated to be 3.2×10^{-4}cm/s.

Table 2.1 summarizes the rate constants obtained at bare and **3**, **4**, and **5** film coated GCEs. The values obtained at a bare GCE and PDMTh and PEDOT film modified GCEs were estimated through the same process as employed for the PProDOT film modified GCE. The standard rate constants for a bare GCE and PDMTh and PEDOT film modified GCEs were 6.3×10^{-5}, 6.9×10^{-5}, and 7.4×10^{-4} cm/s, respectively. These RDE voltammetry results also support the CV results that PProDOT and PEDOT exhibit electrocatalytic activity toward the redox reactions of DMcT-2Li while other polymer films do not.

Table 2.1. Standard Rate Constants for the Oxidation (Dimerization) of DMcT-2Li at a Bare GCE and 3, 4, and 5 Film Modified GCEs

electrodes	i_k/A	k^0/cm s^{-1}
bare GCE	2.7 × 10−4 a	6.3×10^{-5}
3	2.1 × 10−4 c	6.9×10^{-5}
4	6.2 × 10−5 c	3.2×10^{-4}
5	2.1 × 10−4 d	7.4×10^{-4}

(a) Estimated at −0.26 V. (b) Estimated at −0.28 V. (c) Estimated at −0.42 V.(d) Estimated at −0.40 V.

EIS Studies for Conducting Polymer Film Modified GCEs

We carried out EIS measurements for **3**, **4**, and **5** in order to ascertain the films' electrical conductivity at the formal potential for the dimerization process of DMcT-2Li. From the CV studies, the formal potential for the dimerization process of DMcT-2Li was found to be located within the windows of conductivity for PProDOT and PEDOT but outside for PDMTh. Thus, it was expected that the conductivity of PProDOT and PEDOT would be significantly higher at the formal potential of DMcT-2Li when compared to PDMTh. Figure 2.7 presents Nyquist plots, taken at −0.54 V versus Ag/Ag^+, for PDMTh, PProDOT, and PEDOT film modified GCEs in 0.1 M $LiClO_4$/AN. In the case of the PEDOT film modified GCE (Figure 2.7c), the real part of the impedance value, Z', did not change significantly over the frequency range studied, indicating that the PEDOT film is in its highly conducting state. On the other hand, the PProDOT and PDMTh films exhibited a semicircle with Z' values of 0.6 and 9.7 kΩ, respectively. From these results, it was confirmed that, as anticipated, PEDOT as well as PProDOT exhibit higher conductivity than PDMTh at the potential (−0.54 V versus Ag/Ag^+) where the oxidation of DMcT takes place.

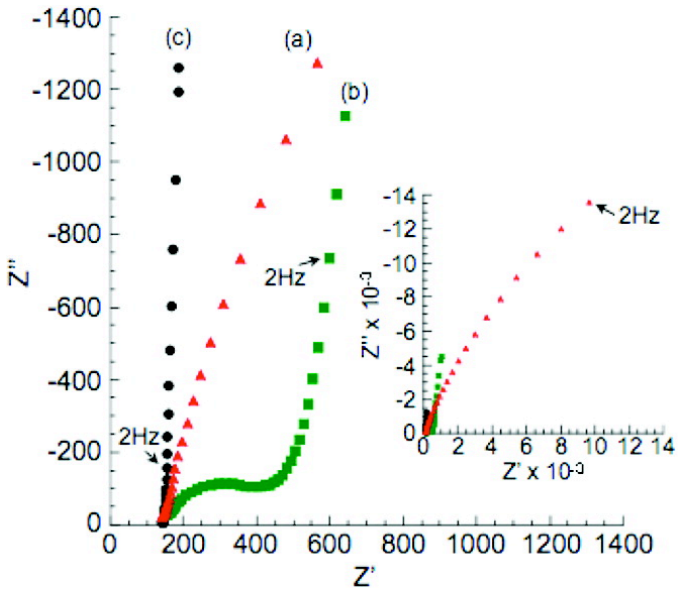

Figure 2.7. Nyquist plots for (a) 3, (b) 4, and (c) 5 film modified GCEs in 0.1 M LiClO4/AN. The inset presents the same Nyquist plots shown in the main panel but plotted over a wider range to show the impedance response of 3.

DFT Investigations of Polymer Geometries

In this study, the dimethoxy, propylenedioxy, and ethylenedioxy substituents to a Th ring (i.e., DMTh, ProDOT, and EDOT, respectively) resulted in variations of the electrochemical properties for the corresponding polymers, such as window of conductivity, and thus electrocatalytic activity toward the redox reactions of DMcT-2Li. For example, as seen in Figure 2.3, the electro-oxidation potentials for the polymers vary by over 500 mV. Interestingly, reports in the literature have demonstrated that methoxy substitution shifts the oxidation potential more negative than ethylenedioxy substitution for conjugated organochalcogen molecules,[26-27] while we see the opposite trend in the polymers' oxidation potentials (PEDOT < PProDOT < PDMTh). There are a number of possible explanations for this difference in oxidation potentials, including differing effective conjugation lengths, degree of π-electron donation, and macromolecular interactions (e.g., crystal packing). While ab initio

predictions of macromolecular interactions are still challenging,[28] DFT investigations have been shown to be particularly well suited for studying molecular and electronic structure despite placing the molecules in a markedly different environment (e.g., absolute zero and vacuum).[23,29,30] The highest occupied molecular orbital (HOMO) energy levels of the neutral oligomers in this work showed good agreement with the experimentally observed oxidation potentials, as seen in Figure 2.8. The ordering of polymer oxidation potentials and the relative energy difference between the oxidations are successfully reproduced for both short and long oligomers. This suggests that DFT electronic structure calculations probe the relevant geometric and electronic parameters and can help rationalize our experimental results. Since geometric and electronic structures are inherently coupled, investigation of both structures yields complementary information.

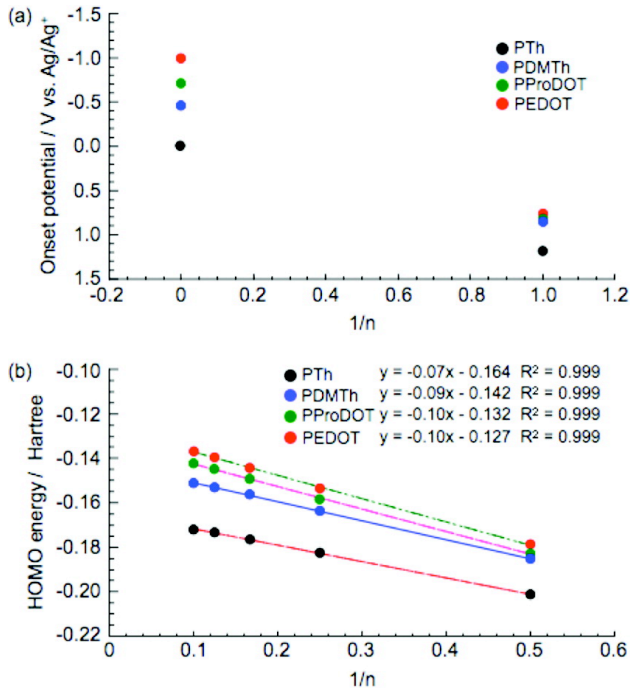

Figure 2.8. Comparison between experimental anodic onset potentials (a) and computed B3LYP/6-31G* HOMO energy levels (b) for 1, 3, 4, and 5.

The relaxed geometries of all the polymers (octamers were employed as representative) are similar and in agreement with previous theoretical reports of thiophene-based oligomers.[23,24,29,31] The C−C backbone exhibits a regular bond-length alternation with three distinct bond positions (Table 2.2). The double bond (B−C or D−E) length did not change with substitution, while the intraannular and interannular bond lengths did. The effective conjugation length of conducting polymers is expected to be sensitive to the type of bonding between Th units. From a purely tight-binding perspective, conjugation lengths are expected to be longest when electronic distribution/bond lengths are most equal along the C−C backbone,[29] and several methods have been proposed to characterize the bond length alternation. One simple indication of bonding in the backbone is the difference between interannular and intraannular bond lengths, which correlates with the degree of electron localization on individual monomer units. The difference between the intraannular and interannular bond lengths was similar for all the three substituted PTh derivatives and significantly smaller than in PTh, suggesting that the three PTh derivatives exhibit greater electronic delocalization along the backbone. The intraannular bonds of PEDOT and PTh were shorter than those in PDMTh and PProDOT, likely due to decreased steric strain from the substituents on the 3,4-positions, and the interannular bond lengths varied in the order PEDOT < PProDOT < PDMTh < PTh. Although the changes in interannular bond lengths are small, the trends are in agreement with oxidation potentials and predict that PEDOT has the most interaction between adjacent rings.

Table 2.2. Average Geometric Parameters for Optimized Octamers of 1, 3, 4, and 5

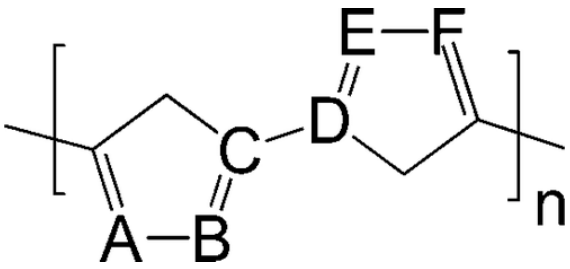

oligomer	intraannular bond[a]/Å	interannular bond[b]/Å	Δbond/Å	interannular dihedral[c]/deg
1	1.416	1.443	0.027	170.3
3	1.428	1.44	0.013	175.7
4	1.428	1.439	0.011	177.8
5	1.42	1.436	0.016	179.3

(a) Intraannular bonds: A−B and E−F. (b) Interannular bond: C−D.(c) Interannular dihedral: B−C−D−E.

The interannular dihedral angles are also expected to indicate the degree of electronic communication between adjacent monomer units, with the most conjugated molecules exhibiting the most planar backbone. Analysis of the oligomers indicated that all were close to being planar. Although previous experimental work has shown that conjugation is maintained until the angle between adjacent orbitals becomes large (>36°), there is a correlation between decreasing dihedral angle and increasing experimentally observed oxidation potential. Relaxed potential energy scans about the central dihedral angle of the Th derivatives indicated that less energy was required for small rotations in PDMTh than in PProDOT or PEDOT but that all of the derivatives were able to rotate up to 30° from their respective minima without significant energy cost (<1 kcal/mol). Thus, while ProDOT and EDOT may be more constrained to planarity, the effect is expected to be dwarfed by intermolecular interactions (e.g., crystal packing) that are not accounted for by DFT calculations.

Some additional observations may be made about the conformation of the substituents. Both ethylenedioxy and propylenedioxy substituents adopt a twisted conformation that enable the oxygens to be approximately planar with the carbon backbone while increasing the distance between the oxygen and the sulfur of the adjacent ring. On the other hand, the methoxy substituents were planar only in the monomer. Longer oligomers of DMTh had the nonterminal methoxy groups out of plane with the backbone as seen in Figure 2.9b. This nonplanarity diminishes the electronic interaction between the p orbitals of the oxygen and the π-type orbitals of the conjugated system, resulting in less electron donation from the methoxy group. The rotation of the methoxy group away from the plane of the carbons has two causes: steric interactions with the sulfur on the neighboring Th ring[32] and, as seen in Figure 2.9b, rotation of the methoxy group allows a bonding interaction between the oxygen and neighboring Th that energetically stabilizes the HOMO.[33] Similar steric limitations on electron donation have been reported for thioether groups in terthiophenes[33] and methoxy groups on substituted dibenzodioxins.[26] Conversely, attractive electrostatic interactions between the constrained oxygen of the ethylenedioxy substituent and the neighboring Th−ring sulfur have previously been used to explain the planarity of EDOT oligomers.[31-32] These effects are seen in the reversal of the relative HOMO energies for the DMTh and EDOT oligomers (data not shown). In the monomers, where the methoxy groups do not have steric hindrance, the HOMO energy of DMTh is 300 meV higher than that of EDOT; in the dimers, where substituents interact with neighboring rings, the HOMO of EDOT is nearly 200 meV less stable than that of DMTh.

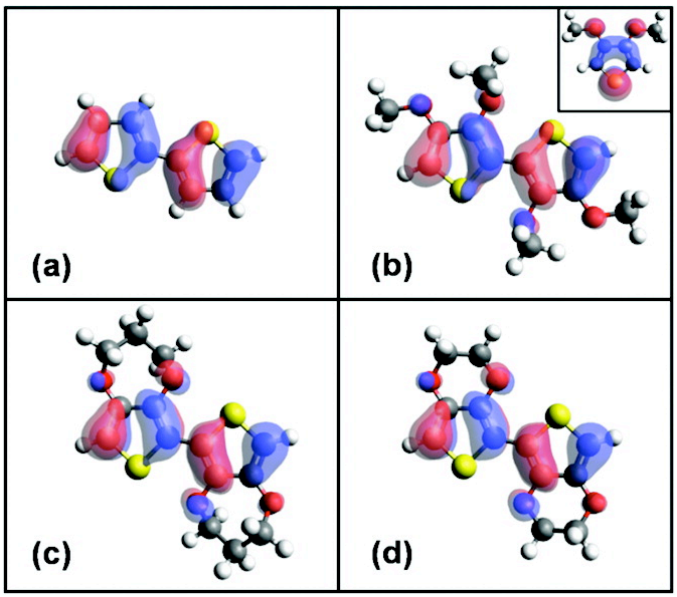

Figure 2.9. Change in HOMO with substitution. HOMO displays with iso-value of 0.05 for (a) Th, (b) DMTh, (c) ProDOT, and (d) EDOT dimer. Inset of (b) shows the monomer of PDMTh.

The results of the DFT calculations were also used to probe the influence of the different substituents on the charge density. Bader charge analysis of the monomers found a trend toward increasing charge density on the Th rings in the order DMTh < ProDOT < EDOT. While this trend agrees nicely with the order of experimental oxidation potentials, the magnitude of the charge difference (0.04 e^-/monomer) is smaller than would be expected to account for the different oxidation potentials. The trend does persist in the interior Th rings of larger oligomers, indicating that it is not an artifact of H termination. However, Bader analysis probes the charge density integrated across all energy levels, making it difficult to deconvolve a relative change in charge density near an energy of interest (e.g., the HOMO). However, as seen in Figure 2.9, visualization of the highest occupied orbital for each dimer demonstrated a clear shift in the HOMO away from the Th sulfur in the series Th > DMTh > ProDOT

> EDOT. This supports the conclusion that ethylenedioxy interacts most strongly with the π system along the carbon backbone. Finally, in addition to the favorable orbital overlap between O 2p orbitals and the carbon backbone, EDOT may also benefit from additional resonance structures that distribute charge around the entire six-membered ring.

It must be noted that these results do not preclude the influence of intermolecular interactions in charge transport.[34] These interactions are expected to be strongest in the most compact, symmetric oligomers (e.g., PDMTh < PProDOT < PEDOT).[35]

Conclusions

In this study, the redox reactions of DMcT-2Li have been investigated at GCEs modified with PTh-based conducting polymers. In particular, the effect of the position of the windows of conductivity for conducting polymers on the electrocatalytic activity toward DMcT-2Li was studied via CV, RDE voltammetry, and EIS. It was found that the electrocatalytic activity of the conducting polymers is strongly influenced by their position of window of conductivity. CV and RDE voltammetry studies revealed that PEDOT and PProDOT, whose windows of conductivity overlap well with the formal potential for the dimerization process of DMcT-2Li exhibited electrocatalytic activity toward both the oxidation and reduction processes. On the other hand, PTh, PMTh, and PDMTh showed no electrocatalytic activity because the p-doping processes of the films take place at more positive potentials than the formal potential of DMcT-2Li. EIS studies also indicated that the higher the electrical conductivity of a film at the formal potential of DMcT-2Li, the higher the

electrocatalytic activity toward DMcT-2Li. These results clearly indicated that the window of conductivity of a conducting polymer needs to overlap with the formal potentials of organosulfur compounds in order to accelerate the redox processes. Additionally, DFT calculations suggested that the electrical conduction within conducting polymers, related to the position of window of conductivity and thus the electrocatalytic activity toward DMcT-2Li, is influenced by both the geometric and electronic structure of the monomer units. This study will help the rational design of novel conducting-polymer-based electrocatalysts for organosulfur compounds to be of practical use as cathode materials for lithium ion rechargeable batteries.

REFERENCES

1. Liu, M.; Visco, S. J.; and De Jonghe, L. C.; J. Electrochem. Soc. 1991, 138 1896.

2. Trofimov, B. A.; Sulfur Rep. 2003, 24, 283

3. Novak, P.; Muller, K.; and Santhanam, K. S. V.; Haas, O.; Chem. Rev. 1997, 97, 207.

4. Liu, M.; Visco, S. J.; and De Jonghe, L. C.; J. Electrochem.Soc. 1991, 138,1891.

5. Oyama, N.; Tatsuma, T.; Sato, T.; and Sotomura, T.; Nature 1995 , 374, 196.

6. Oyama, N.; Kiya, Y.; Hatozaki, O.; Morioka, S.; and Abruña, H. D.; Electrochem. Solid-State Lett. 2003, 6, A286

7. Henderson, J. C.; Kiya, Y.; Hutchison, G. R.; and Abruña, H. D.; J. Phys. Chem. C 2008, 112,3989

8. Yu, L.; Wang, X. H.; Li, J.; Jing, X. B.; and Wang, F. S.; J. Power Sources 1998, 73,261

9. Cho, J.S.; Sato, S.; Takeoka, S.; and Tsuchida, E.; Macromol. 2001 34, 2751

10. Uemachi, H.; Iwasa, Y.; and Mitani, T.; Electrochim. Acta 2001, 46, 2305

11. Xue, L. J.; Li, J. X.; Hu, S. Q.; Zhang, M. X.; Zhou, Y. H.; and Zhan, C. M.; Electrochem. Commun. 2003, 5, 903

12. Yu, X. G.; Xie, J. Y.; Yang, J.; Huang, H. J.; Wang, K.; and Wen, Z. S.; J. Electroanal. Chem.2004, 573, 121

13. Deng, S. R.; Kong, L. B.; Hu, G. Q.; Wu, T.; Li, D.; Zhou, Y. H.; and Li, Z. Y.; Electrochim. Acta 2006, 51, 2589

14. Amaike, M.; and Iihama, T.; Synth. Met. 2006, 156, 239

15. Kiya, Y.; Henderson, J. C.; and Abruña, H. D. ; J. Electrochem. Soc. 2007, 154, A844

16. Tarascon, J. M.; and Armand, M.; Nature 2001, 414, 359

17. Kiya, Y.; Hutchison, G. R.; Henderson, J. C.; Sarukawa, T.; Hatozaki, O.; Oyama, N.; and Abruña, H. D.; Langmuir 2006, 22, 10554

18. Kiya, Y.; Henderson, J. C.; Hutchison, G. R.; and Abruña, H. D.; J. Mater. Chem. 2007, 17,4366

19. Kiya, Y.; Iwata, A.; Sarukawa, T.; Henderson, J. C.; and Abruña, H. D.; J. Power Sources 2007,173, 522

20. Kiya, Y.; Hatozaki, O.; Oyama, N.; and Abruña, H. D.; J. Phys. Chem. C 2007, 111, 13129

21. Shouji, E.; Matsui, H.; and Oyama, N.; J. Electroanal. Chem. 1996, 417, 17

22. Shouji, E.; and Buttry, D. A.; J. Phys. Chem. B 1998, 102, 1444

23. Zade, S. S.; and Bendikov, M.; Org. Lett. 2006, 8, 5243

24. Alemán, C.; Casanovas, J.; J. Phys. Chem. A 2004, 108, 1440

25. Sanville, E.; Kenny, S. D.; Smith, R.; and Henkelman, G.; J. Comput. Chem. 2007, 28,899

26. Hellberg, J.; Dahlstedt, E.; and Pelcman, M. E.; Tetrahedron 2004, 60, 8899

27. Engman, L.; Hellberg, J.; Ishag, C.; and Soderholm, S.; J. Chem. Soc., Perkin Trans. 1988, 1,2095

28. Rubeš, M.; and Bludský, O.; Phys. Chem. Chem. Phys. 2008, 10, 2611

29. Aleman, C.; Armelin, E.; Iribarren, J. I.; Liesa, F.; Laso, M.; and Casanovas, J.; Synth. Met.2005, 149, 151

30. Vogel, E.; Deger, H. M.; Hebel, P.; and Lex, J. Angew. Chem. 1980, 92, 943

31. Kim, E.-G.; and Bredas, J.-L.; J. Am. Chem. Soc. 2008, 130, 16880

32. DiCesare, N.; Belletete, M.; Leclerc, M.; and Durocher, G.; J. Mol. Struct. 1999, 467,259

33. Pozo-Gonzalo, C.; Khan, T.; McDouall, J. J. W.; Skabara, P. J.; Roberts, D. M.; Light, M. E.; Coles, S. J.; Hursthouse, M. B.; Neugebauer, H.; Cravino, A.; and Sariciftci, N. S.; J. Mater. Chem. 2002, 12, 500

34. Hutchison, G. R.; Ratner, M. A.; and Marks, T. J.; J. Am. Chem. Soc. 2005, 127, 16866

35. Zade, S. S.; and Bendikov, M.; Chem. Eur. J. 2007, 13, 3688

CHAPTER 3

ELECTROCATALYSIS OF 2,5-DIMERCAPTO-1,3,5-THIADIAZOLE BY 3,4-ETHYLENEDIOXY-SUBSTITUTED CONDUCTING POLYMERS

Introduction

Organosulfur compounds (OSC) such as 2,5-dimercapto-1,3,4-thiadiazole (DMcT) are promising cathode materials for lithium ion batteries (LiBs) due to their high theoretical capacity.[1-15] This is a consequence of the multiple electron transfers per molecule (one electron per thiolate functionality) in OSCs. Moreover, the potentials at which these processes take place indicate that the materials should also have high energy density. The theoretical capacity of DMcT (360 mAh/g), one of the most promising OSCs, is higher than most inorganic cathode materials currently commercialized (e.g. 120 to 160 mAh/g for $LiCoO_2$ and $LiFePO_4$.)[16] OSCs are also less expensive, especially when compared to cobalt. The improvement of the generally slow charge transfer kinetics of OSCs has been a goal for their successful incorporation in to LIBs. To overcome the sluggish charge transfer kinetics of OSCs, conducting polymers (CP) have been identified and employed as potential electrocatalysts.

CPs, such as polyaniline (pAN) and poly-3,4-ethylenedioxythiophene (PEDOT), have been shown to exhibit electrocatalytic activity towards DMcT.[16,17] Our group has previously reported that PEDOT film-modified glassy carbon electrodes (GCE) accelerate the redox reactions of DMcT in acetonitrile solution by a factor of at least 12,000.[18] We seek a fundamental understanding of the electrocatalytic process in order

to further enhance performance. For example, we recently reported on the effects, on the electrocatalysis of DMcT, arising from changes in the substituents in the 3,4-positions of thiophene derivatives.[19] We established that the electronic structure of the polymers is largely a result of the geometry of the electron donating groups, and that subtle geometric changes could have dramatic effects in the electrocatalytic activity towards DMcT.

Using the above studies as a point of departure, we have carried out a study on the electrocatalytic activity, towards DMcT, of CPs with identical substituents but with different heteroatoms. The polymers studied herein were: PEDOT (figure 3.1a), poly-3,4-ethylenedioxyselenophene (PEDOS) (figure 3.1b), and poly-3,4-ethylenedioxypyrrole (PEDOP) (figure 3.1c), corresponding to sulfur, selenium, and nitrogen, respectively as heteroatoms.

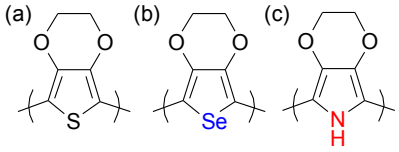

Figure 3.1. Chemical structure of poly-3,4-ethylenedioxy substituted polymers: (a) PEDOT, (b) PEDOS, and (c) PEDOP.

Upon oxidation of DMcT monomers, the thiol functionalities react to form disulfide linkages and DMcT dimers. The proposed dimerization process mechanism is presented in scheme 1.[20] Further oxidation of the dimers yields higher order oligomers. On the other hand, reduction of DMcT oligomers gives rise to cleavage of the disulfide bonds and formation of DMcT monomers. The ability of the thiolate functionality to capture Li ions allows the cleavage and formation of disulfide bonds to be incorporated into the rocking chair type mechanism of LIBs.[21]

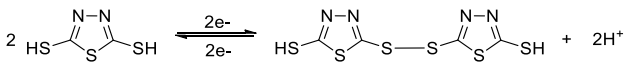

Scheme 3.1. Redox dimerization reaction of DMcT

The electronic properties and electrochemical behavior of PEDOT, PEDOS, and PEDOP were studied via cyclic voltammetry (CV) in lithium perchlorate ($LiClO_4$)/propylene carbonate (PC) solutions. The electrocatalytic activity of polymer films of the CPs mentioned above, towards DMcT, was studied qualitatively via CV and quantitative analysis was obtained using RDE voltammetry from which the heterogeneous charge transfer rate constants of DMcT at the CP film-modified GCEs were estimated. In the RDE studies, thin polymer films were used so that they could be considered as an extension of the electrode surface. SEM images of the electropolymerized CP film-modified GCEs were obtained in order to ascertain if there were morphological features that could influence the electrocatalytic activity.

Experimental

Materials:

Propylene Carbonate 98% Anhydrous (PC), Lithium Perchlorate ($LiClO_4$) (99.99%), 2,5-Dimercapto-1,3,4-thiadiazole (DMcT), 3,4-Ethylenedioxythiophene (EDOT), and 3,4-ethylenedioxypyrrole (EDOP) 2% in THF were purchased from Aldrich Chemical Co. Inc. and used as received. Sodium hydroxide (NaOH) was purchased from Mallinckrodt Chemicals and used as received. 3,4-ethylenedioxyselenophene (EDOS) was synthesized as reported by M. Bendikov et. al.[22]

Electrochemical Measurements:

CV and RDE voltammetric studies were carried out at room temperature using a Hokuto Denko Co., HABF1510m potentiostat or a BAS CV-27 model potentiostat. In RDE voltammetry studies, linear sweeps were carried out at 10 mV/s at different rotation rates using a Pine Instrument Co., model AFMSRX, rotator. Measurements were taken in a three-electrode cell configuration using glassy carbon electrodes (GCE) (for CVs, 5.0 mm diameter homemade electrodes, and for RDE, a 5.0 mm diameter electrode from Pine Instrument Co.), a large area Pt coil counter electrode, and a Ag/Ag^+ (0.05 M $AgClO_4$ + 0.1 M $LiClO_4$/AN) reference electrode without regard to the liquid junction potential, and against which all potentials are reported. The working electrodes were polished with 1.0 μm, 0.3 μm, and 0.05 μm alumina slurries (REFINETEC Ltd.), rinsed with distilled water and acetone, and dried prior to use. The electrodes were then electrochemically cleaned by cycling the potential in a 1 M NaOH solution between 0.0 V and +1.3 V versus Ag/AgCl (KCl saturated), followed by rinsing with distilled water and acetone. Unless otherwise noted, all experiments were carried out in 0.1 M $LiClO_4$/PC solutions, which were thoroughly purged for at least 10 minutes with prepurified nitrogen gas (Airgas) prior to use.

Films of PEDOT, PEDOP, and PEDOS were prepared on GCEs for CV and RDE studies by anodic electrochemical polymerization of the monomers in 0.1 M $LiClO_4$/PC solutions via potential cycling at 20 mV/s. The potential cycling was carried out over the potential regions from -0.600 V to +0.900 V for EDOT, -0.600 V to +0.800 for EDOS, and -0.600 V to +0.700 V for EDOP. The monomer concentrations employed for the polymerization of EDOS, EDOP, and EDOT were 10 mM, 10 mM, and 20 mM, respectively. After polymerization, the films were

thoroughly rinsed with a 0.1 M $LiClO_4$/PC solution and subsequently used for the characterization of the redox reactions of 5 mM and 2 mM solutions of DMcT.

SEM Measurements:

Glassy carbon slugs of 5mm and 6mm in diameter were used to generate electropolymerized films of PEDOT, PEDOS and PEDOP films. The electropolymerization of the CP onto the glassy carbon slugs was done using the same experimental conditions as used for the electrochemical experiments. After electropolymerization the glassy carbon slugs modified with the CP films were rinsed thoroughly with 0.1 M $LiClO_4$/PC solution, dried under vacuum for 30-40 minutes and heated to 50 ºC to remove the remaining solvent before transferring to the SEM chamber. Images were taken using an accelerating voltage of 3 keV. A Zeiss SEM model 1550 field emission scanning electron microscope was used to acquire the images.

Results and Discussion

Conducting polymer preparation and electrochemistry

Conducting polymer films were prepared electrochemically by anodic cycling. Anodic scans were taken in order to form oligomers and subsequently polymers. All films exhibited self-catalyzing behavior characteristic of CP film formation on the electrode surface through consecutive anodic cycles. Figure 3.2 presents steady-state CVs for PEDOT, PEDOS, and PEDOP film-modified GCEs in 0.1 M $LiClO_4$/PC solution at 20 mV/s. For the PEDOT film (figure 3.2a) one broad oxidation wave (due to p-doping) with a peak current at -0.280 V and two reduction waves (de-doping) at -0.210 V and -0.875 V respectively were observed. Figure 3.2b presents the CV for a

PEDOS film which had one broad oxidation at -0.340 V and two reduction waves at -0.400 V and -0.925 V, respectively. The CV for the PEDOP film (figure 3.2c) exhibited a broad oxidation wave at -0.770 V and two reduction waves at -0.800 V and -1.20 V. The onset of the p-doped region (window of conductivity) as determined from the CV experiments for PEDOT, PEDOS, and PEDOP began at -1.15 V, -1.35 V, and -1.50 V respectively, and was limited at positive potentials by over-oxidation of the polymer and subsequent degradation of the film. After polymerization, the CV responses of the CP films in monomer-free solutions were stable, enabling the study of electrocatalysis of DMcT at these surfaces.

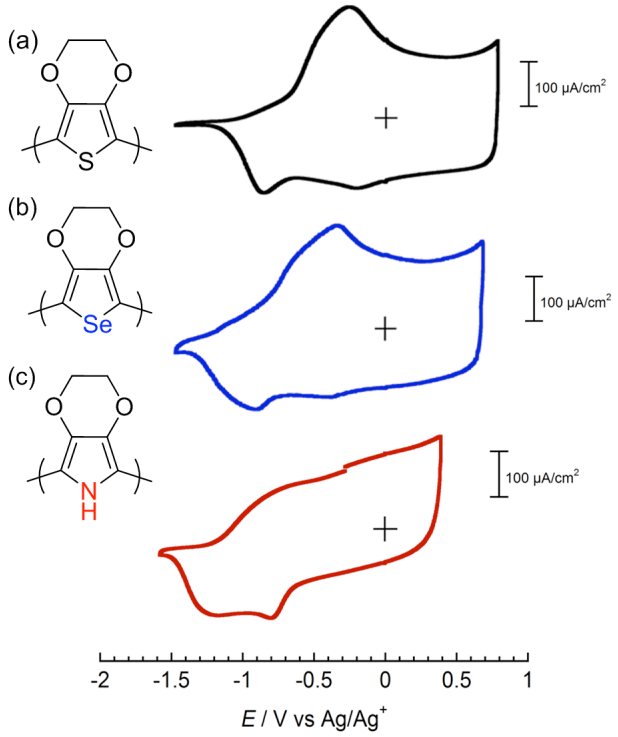

Figure 3.2. Representative steady-state CVs of film-modified GCEs: (a) PEDOT, (b) PEDOS, and (c) PEDOP; in 0.1 M $LiClO_4$/PC solution at a scan rate of 20 mV/s.

Cyclic voltammetry of conducting polymer modified GCE's in DMcT

From the structures of the monomers, it is evident that the backbone of the resulting CP films are the same and that the only difference is the heteroatom on the conducting polymer ring. The monomer units can only polymerize through the alpha position (2,5-positions) since the 3,4-substituents inhibit coupling of the monomer units through the 3,4-sites. The above results demonstrate that changes in the polymer's chemical nature can have significant effects in their electronic properties. The observed onset potential for p-doping was most positive for the PEDOP film followed by the PEDOS film and the PEDOT film, respectively. This trend in the onset agrees with computational results previously reported.[23]

We have previously reported on the importance of matching the window of conductivity of a CP with the redox reactions of DMcT for electrocatalysis to take place.[19] In this study all of the CPs films investigated had a window of conductivity that covered the potential range over which the DMcT redox reactions take place. Figure 3.3a presents the CV of a 5 mM DMcT/0.1 M $LiClO_4$/PC solution at a bare GCE. Three oxidation processes with peak potential values of +0.070 V, +0.485 V and +0.970 V were observed. These were associated with the oxidation of DMcT to form dimers followed by further oxidation to form higher order oligomers. The CV also exhibited two reduction waves at -0.640 V and -0.710 V. The peak to peak potential difference (ΔE_p), of the oxidation at +0.070 V and the reduction at -0.640 V, which corresponds to the dimerization reaction of DMcT monomers to DMcT dimers, was 710 mV indicating that this is an irreversible electrochemical process.

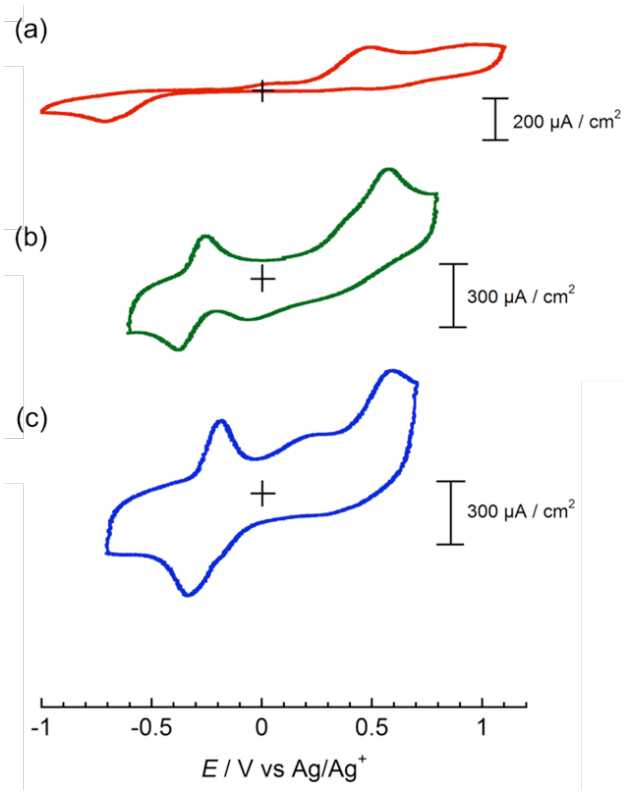

Figure 3.3. Representative steady-state CV's of (a) bare GCE, (b) PEDOS film-modified GCE (c) PEDOP film-modified GCE; in 5 mM DMcT/0.1 M $LiClO_4$/PC solution at a scan rate of 20 mV/s.

Figure 3.3b presents a steady state CV for a PEDOS film-modified GCE in 5 mM DMcT / 0.1 M $LiClO_4$/PC solution at 20 mV/s. In this CV, three main oxidation redox processes at peak potential values of -0.260 V, 0.360 V, and 0.575 V; and two reduction redox processes at peak potential values of -0.375 V and -0.060 V were observed. The peak to peak separation of DMcT disulfide bond formation (dimerization) and cleavage of the disulfide bond from the dimer to the DMcT monomer species was 115 mV which represents a dramatic diminution when compared to the value of 710 mV observed at a bare GCE. The redox process at -0.260 V is assigned to the dimerization of DMcT and this is the process that will be studied in detail by RDE experiments as described below.[20]

Figure 3.3c presents a steady-state CV of a PEDOP film-modified GCE in a 5mM DMcT/0.1 M $LiClO_4$/PC solution at 20 mV/s. The steady-state CV has three main oxidation waves with peak potential values at -0.190 V, +0.220 V, and +0.590 V; and two closely spaced reduction waves with the main peak at -0.345 V, and a small shoulder at approximately -0.180 V. The peak to peak separation for disulfide bond formation and cleavage, corresponding to the dimerization of DMcT, was 155 mV. As for the PEDOS case, this value is also dramatically smaller than the value for bare GCEs, which is consistent with a strong catalytic effect, although noticeably larger than the peak to peak separation for DMcT at PEDOS or PEDOT[20]. The oxidation corresponding to dimerization of DMcT is the one at -0.190 V. Similar electrocatalytic behavior was observed in CV experiments for PEDOT film-modified GCEs in DMcT solutions as we have described previously.[20]

The electrocatalysis observed at all of the CP films is anticipated, since the formal potentials of the redox processes of DMcT fall well within the respective windows of conductivity for PEDOT, PEDOS, and PEDOP. However the specific properties of the CPs influence the electrocatalytic activity, as can be seen from the different values of the peak-to-peak separation, and current peak potentials, for the oxidation of DMcT at different CP film-modified GCEs. Further understanding of the electrocatalytic process could enable the successful incorporation of DMcT/CP composites into LIBs.

Rotating Disk Electrode Voltammetry of Conducting Polymer Film-Modified GCE's

In order to obtain more quantitative measurements of the kinetics of the electrocatalysis, RDE voltammetry was employed in DMcT/0.1 M $LiClO_4$/PC

solutions at PEDOT, PEDOS, and PEDOP film-modified GCEs. The dimerization process of DMcT was studied in detail using this technique and the heterogeneous charge transfer rate constant ($k^{0'}$) for said process was determined. Linear sweep voltammograms (LSV) in DMcT/0.1 M $LiClO_4$/PC solutions at different rotation rates are presented in figure 3.4a where an increase in the current was observed, as expected, when the rotation rate was increased. A decrease in the baseline of the LSV can be observed over the -0.400 V to -0.300 V potential range. The baseline current decreased linearly as a function of the square root of the rotation rate indicating that it is the result of a species in solution, and is likely due to DMcT dimers, or higher order oligomers in solution, generated by air or light oxidation. It has been previously documented, in the literature, that thiolate functionalities undergo oxidation under ambient conditions to form disulfide bonds.[24] Because the reduction of DMcT dimers is also electrocatalyzed at the PEDOT and PEDOS CP films, trace disulfide species are more apparent at these films. In order to analyze these LSVs a quantitative baseline correction was necessary for the PEDOT and PEDOS CP films. Because we believe that the reduction of dimers and oligomers of DMcT could occur through the entire potential region of interest, the baseline current was subtracted from the mass-transport limited current of the DMcT oxidation. It should be noted that if the correction is not applied to the LSVs, the data sampled did not fit the Levich or Koutecky-Levich equations for RDE voltammograms. Therefore, the correction was necessary in order to calculate an appropriate value for the rate constants at PEDOT and PEDOS film-modified GCEs. At a bare GCE and PEDOP film-modified GCE, no appreciable current due to this effect was observed since the reduction of dimmers is

slow (irreversible) and thus no subtraction or treatment was necessary for the Levich and Koutecky-Levich plots. In all cases, the calculated diffusion coefficient for DMcT in PC solution was unphysically low, 2.5 x 10^{-8} cm^2/s. A possible explanation could be that the DMcT decomposes or is unstable in PC solutions, therefore the lowered activity may affect the value of the diffusion coefficient making it appear smaller than it actually is.

The heterogeneous charge transfer rate constant for the dimerization of DMcT was determined at PEDOT, PEDOS and PEDOP film-modified GCEs, as well as at a bare GCE, for comparison. Figure 3.4b presents the Levich plot at -0.200 V for a PEDOS film-modified GCE where a deviation from linearity can be observed at higher rotation rates indicating that the reaction is no longer mass-transport controlled and becomes kinetically limited. To obtain the kinetically limiting current (i_k) a Koutecky-Levich plot was employed as shown in figure 3.4c. The $k_f(E)$ was calculated for all CPs studied, but because the potentials to calculate the $k_f(E)$ were different, the standard rate constant $k^{0'}$ was calculated in order to compare values among the CPs films using the same conditions (Table 3.1). To obtain the rate constant values, the Levich and Koutecky-Levich Plots were done at different potentials to verify the rate constant, as well as the kinetically limited region. Koutecky-Levich plots at all the chosen potentials resulted in similar standard rate constant values. The value of alpha (α), used for the $k^{0'}$ calculation, was assumed to be 0.5. The estimated $E^{0'}$ for the DMcT dimerization process was -0.292 V. The $E^{0'}$ was calculated at a PEDOS film modified GCE since at a bare GCE this reaction is extremely irreversible making the estimation of the $E^{0'}$ value difficult and unreliable.

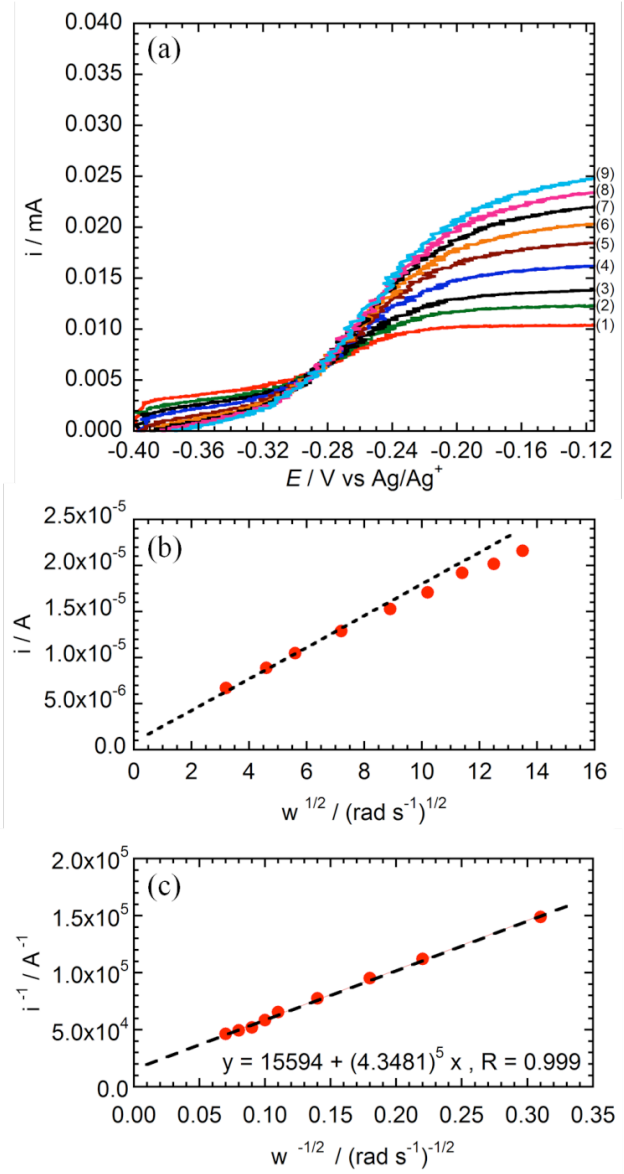

Figure 3.4. (a) Representative LSVs of a PEDOS film-modified GCE at a 2 mM DMcT/0.1 M $LiClO_4$ / PC solution at different rotation rates (1) 200, (2) 400, (3) 600, (4) 1000, (5) 1500, (6) 2000, (7) 2500, (8) 3000, and (9) 3500 rpm; scan rate was 10 mV/s. Baseline corrected (b) Levich and (c) Koutecky-Levich Plots obtained at the values measured of -0.200 V vs Ag/Ag^+.

The estimated $k^{0'}$ for PEDOS, PEDOT, PEDOP modified GCEs and at a bare GCE obtained at DMcT/0.1 M $LiClO_4$/PC solutions were 1.7 x 10^{-3} cm/s, 9.8 x 10^{-5} cm/s,

1.7×10^{-5} cm/s, and 1.8×10^{-7} cm/s respectively. The calculated rate constants show that all CP film-modified GCEs studied catalyzed the electrochemical reactions of DMcT, albeit to different extents.

In an effort to try to understand and/or rationalize the differences in the rate constant for the oxidation of DMcT at the various conducting polymers, we considered the potential effects of the conductivity of the polymers. First of all, we must recognize that the k^0 values reflect the interfacial charge transfer kinetics of DMcT at glassy carbon electrodes modified with the conducting polymers. On the other hand, the conductivity of the conducting polymer is a property inherent to the specific material. In order for the conducting polymer film to exhibit electrocatalytic activity towards DMcT, the formal potential for DMcT must fall within the window of conductivity of the conducting polymer. However, the conductivity of the polymer can be (and often is) a function of the applied potential. For example, Reynolds et. al. have studied the conductivity of PEDOP and PEDOT as a function of potential.[25] In their investigation, they observed that the conductivity of PEDOP increased as the film was oxidized (max σ ca. 20 S/cm) but after the first oxidation peak in the CV of the electropolymerized film, the conductivity started to decrease.[25] For PEDOT, the conductivity increased (max σ ca. 500 S/cm) and reached a plateau after the first oxidation peak in the polymer film.[25] However, in the region of interest in the present context, (ca. -0.25 V) the conductivity for both PEDOT and PEDOP was potential dependent and could, at least in part, affect the response. This would reflect the interplay of the current density associated with the electrocatalytic oxidation of DMcT and the conductivity of the polymer film at the specified potential.

From the RDE experiments, the electrocatalytic activity was found to be dependent on the nature of the polymer film. The values of the rate constant could be correlated with the conductivity value and its potential dependence for the PEDOT and PEDOP films. These chemical and conductivity differences in the CPs films exhibited variations in the $k^{0'}$ spanning two orders of magnitude. The RDE measurements suggest that using PEDOT/DMcT and PEDOS/DMcT composites may enable faster charge/discharge rates in a LIB and may improve the cyclability of devices. If the DMcT partially decomposes in the PC solvent as the RDE experiments suggest, it may be fruitful to use a different electrolyte system in a practical LIB device.

Table 3.1. Estimated heterogeneous charge transfer rate constants; $k_f(E)$ and $k^{0'}$ of bare GCE, PEDOT, PEDOP and PEDOS film modified GCEs:

Electrode	$k_f(E)$ (Potential in V)	$k^{0'}$
PEDOT film	3.3×10^{-4} cm/s (-210 mV)	9.8×10^{-5} cm/s
PEDOS film	1.8×10^{-3} cm/s (-200 mV)	1.7×10^{-3} cm/s
PEDOP film	1.5×10^{-4} cm/s (-180 mV)	1.7×10^{-5} cm/s
Bare GCE	8.3×10^{-5} cm/s (25 mV)	1.8×10^{-7} cm/s

SEM

Electrochemically prepared polymer films were characterized by SEM to establish the film morphology and determine if the chemical structure of the polymers affected the resulting film morphology. The effects of film morphology on the electrocatalysis of CP films towards DMcT have not been previously documented in the literature and we were interested in determining if there was any correlation between film morphology and electrocatalytic activity. The effects of the switching potential on the

electropolymerization of EDOT have been previously investigated by Ivaska et. al.[26] In their investigation, they determined that higher switching potentials gave rise to macroporous films due to the higher kinetics for the electropolymerization reaction. The fast kinetics in the electropolymerization reaction causes fast growth conditions, in which lower packing of the films is observed, therefore creating a macroporous film. In our investigations all the films were prepared using potentials where macroporous films would be expected. In this way the morphology of the film should only be affected by the inherent properties of the CP and not by the electropolymerization conditions (i.e. reaction kinetics).

SEM images of PEDOT, PEDOS, and PEDOP films are shown in figure 3.5. Figure 3.5a presents a PEDOT polymer film at different magnifications, and a macroporous structure can be observed. PEDOS (Figure 3.5b) exhibited a similar macroporous structure. However regions in the film can be observed where there are larger aggregates when compared to PEDOT. We believe that these regions are composed of denser polymeric material. SEM images at different magnifications for the PEDOP polymer film are presented in figure 3.5c. For this polymer film the macroporous structure was observed but, compared to the other polymers under study, the feature size in this structure was the largest. The bigger feature size in the macroporous structure of PEDOP could be due to hydrogen bonding interactions between the NH functionalities of the conducting polymer films.

Comparing these data to the CV and RDE experiments, where the kinetics of DMcT at the CP film-modified GCEs were determined, it appears that the smaller macroporous structure of PEDOT and PEDOS polymer films can be correlated with

higher electrocatalytic activity. Clearly, the heteroatom affects both the interaction of the CP film with DMcT, as well as the morphology of the electropolymerized CP. We believe that the resulting electrocatalytic activity of the CP film reflects a delicate interplay of these aspects. Having this macroporous morphology in the CP films should provide better contact with DMcT making for a better device.

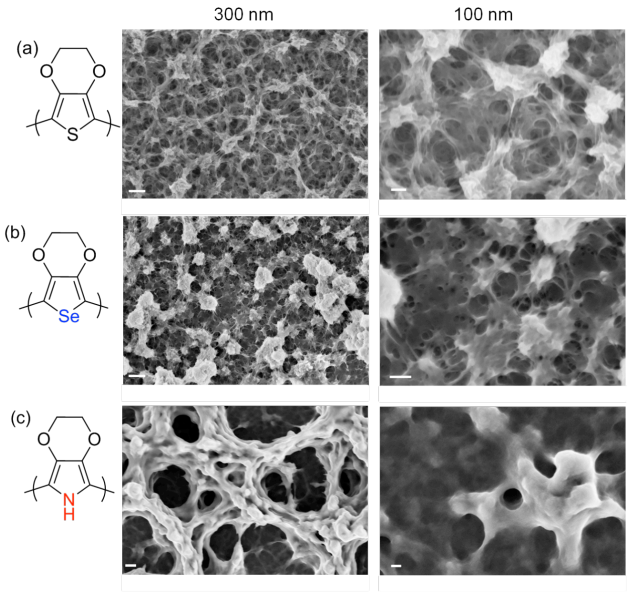

Figure 3.5. Representative SEM images for electrochemically prepared PEDOX (X = Se, S, NH) polymer film-modified GCEs at different magnifications: (a) PEDOT, (b) PEDOS, and (c) PEDOP polymer films.

Conclusions

The electronic properties and electrochemical behavior of PEDOT, PEDOS, and PEDOP films have been studied at CP film-modified GCEs. The electrocatalytic activity of PEDOT, PEDOS, and PEDOP film-modified GCEs towards DMcT was studied qualitatively via CV and quantitatively via RDE. The heterogeneous charge transfer rate constants were measured at the CP films and from those, the PEDOS film-modified GCE had the highest $k^{0'}$ value. The morphology of the electrochemically

modified GCEs was studied via SEM. It appears that polymers with smaller macroporous structures (PEDOT and PEDOS), which, in turn, resulted in smaller features, exhibited the highest electrocatalytic activity towards DMcT. The fact that all poly-3,4-ethylenedioxy-substituted CPs electrocatalyzed the redox reactions of DMcT, further confirms that a good overlap of the window of conductivity with the redox process in question is key for electrocatalytic activity. In addition, the heteroatom was found to play an important role in the electrocatalysis of DMcT, likely through specific chemical interactions, potential dependent conductivity differences and morphological effects. Our findings indicate that having the appropriate CPs should improve the DMcT performance in a LIB. From the polymers studied, PEDOT and PEDOS seemed to be better suited for a CP/DMcT composite cathode material.

REFERENCES

1. Liu, M.; Visco, S. J.; and De Jonghe, L. C.; J. Electrochem. Soc. 1991, 138, 1896.

2. Trofimov, B. A. ;Sulfur Rep. 2003, 24, 283.

3. Novak, P.; Muller, K.; Santhanam, K. S. V.; and Haas, O.; Chem. Rev. 1997, 97, 207.

4. Liu, M.; Visco, S. J.; and De Jonghe, L. C.; J. Electrochem. Soc. 1991, 138, 1891.

5. Oyama, N.; Tatsuma, T.; Sato, T.; and Sotomura, T.; Nature 1995, 374, 196.

6. Oyama, N.; Kiya, Y.; Hatozaki, O.; Morioka, S.; and Abruña, H. D.; Electrochem. Solid-State Lett. 2003, 6, A286.

7. Henderson, J. C.; Kiya, Y.; Hutchison, G. R.; and Abruña, H. D.; J. Phys. Chem. C 2008, 112, 3989.

8. Yu, L.; Wang, X. H.; Li, J.; Jing, X. B.; and Wang, F. S.; J. Power Sources 1998, 73, 261.

9. Cho, J. S.; Sato, S.; Takeoka, S.; and Tsuchida, E.; Macromolecules 2001, 34, 2751.

10. Uemachi, H.; Iwasa, Y.; and Mitani, T.; Electrochim. Acta 2001, 46, 2305.

11. Xue, L. J.; Li, J. X.; Hu, S. Q.; Zhang, M. X.; Zhou, Y. H.; and Zhan, C. M.; Electrochem. Commun. 2003, 5, 903.

12. Yu, X. G.; Xie, J. Y.; Yang, J.; Huang, H. J.; Wang, K.; and Wen, Z. S.; J. Electroanal. Chem. 2004, 573, 121.

13. Deng, S. R.; Kong, L. B.; Hu, G. Q.; Wu, T.; Li, D.; Zhou, Y. H.; and Li, Z. Y.; Electrochim. Acta 2006, 51, 2589.

14. Amaike, M.; and Iihama, T.; Synth. Met. 2006, 156, 239.

15. Kiya, Y.; Henderson, J. C.; and Abruña, H. D.; J. Electrochem. Soc. 2007, 154, A844.

16. Kiya, Y.; Henderson, J. C.; Hutchison, G. R.; and Abruña, H. D.; J. Mater. Chem. 2007, 17, 4366.

17. Oyama, N.; Tatsuma, T.; Sato, T.; and Sotomura, T.; Nature 1995, 374, 196.

18. Kiya, Y.; Hatozaki, O.; Oyama, N.; and Abruña, H. D.; J. Phys. Chem. C 2007, 111, 13129.

19. Rodríguez-Calero G. G., Lowe M. A., Kiya Y., and Abruña H. D.; J. Phys. Chem. C 2010 114 13, 6169.

20 Kiya Y., Hutchison G. R., Henderson J. C., Sarukawa T., Hatozaki O., Oyama N., and Abruña H. D.; Langmuir 2006, 22, 10554.

21 Tarascon, J. M.; and Armand, M. Nature 2001, 414, 359.

22. Patra A., Wijsboom Y. H., Zade S. S., Li M., Sheynin Y., Leitus G., and Bendikov M., J. Am. Chem. Soc. 2008, 130, 6734–6736

23. Burkhardt S. E., Rodríguez-Calero G.G., Lowe M. A., Hennig R. G., and Abruña H. D.; J. Phys. Chem. C. 2010, 114, 16776.

24. Kalimuthu P., Kalimuthu P., and Abraham John S. Nature Precedings 2007 available from nature precedings <http://hdl.handle.net/10101/npre.2007.734.1>

25 Groenendaal L., Zotti G., Aubert P.-H., Waybright S. M., and Reynolds J.R., Adv. Mater., 2003, 15, 855.

26. Niu L., Kvanström C., Fröberg K., and Ivaska A., Synthetic Metals 2001, 122, 425.

CHAPTER 4

UNDERSTANDING THE ELECTROPOLYMERIZATION AND FILM ELECTROCHEMISTRY OF REDOX ACTIVE SUBSTITUTED CONDUCTING POLYMERS: THE CASE OF POLY-3,4-ETHYLENEDIOXYTHIOPHENE / 5,5 – BIS(METHYLTHIO)- 2,2 –BITHIOPHENE (PEDOT-BMTbT) COMPOSITES

Introduction

Since their discovery in the 1970's by MacDiarmid, Heeger, and Shirakawa, conducting polymers (CPs) have been thoroughly investigated by the scientific community.[1-8] These Nobel Laureates doped polyacetylene and discovered they could increase the conductivity of this polymer by 7 orders of magnitude.[1] Due to the metallic-like conductivity of CPs and the inherent properties of organic materials (i.e. inexpensive, tunable, mechanically flexible, abundant), they have been widely studied for many applications. The application space for CPs ranges from energy generation and storage (i.e. batteries and photovoltaics) to molecular electronics (i.e. organic field effect transistors).

Among CPs, poly-3,4-ethylenedioxythiophene (PEDOT) has attracted much attention. PEDOT was developed by BASF in the 1980's. By protecting the beta-positions in thiophene monomers they were able to increase the electrochemical and chemical stability of polythiophene based compounds. The electrochemical properties of PEDOT make it promising for electrochemical energy storage, electrochromic devices, biosensors, and photovoltaics. [10-15]

In our group, we have studied CPs to use them in electrical energy storage applications.[12,16-18] We have also designed and developed small redox active molecules to use the as cathodes in electrical energy storage.[18-20] Of particular interest is 5,5'-bis(methylmethio)-2,2'-bithiophene (BMTbT), a small organic molecule that undergoes a two electron oxidation at ca. 4 V vs Li/Li^+. We have also developed redox active substituted conducting polymers (RAS-CPs) as an attractive platform for electrical energy storage devices.[12]

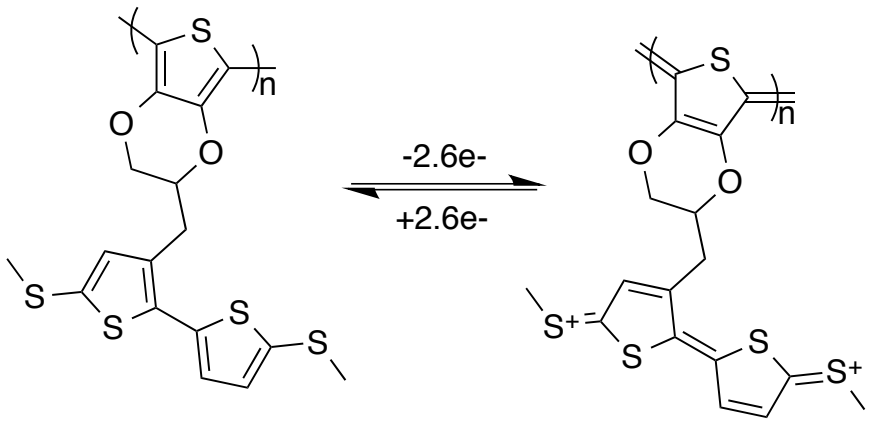

Scheme 4.1. Electrochemical reaction representation of a PEDOT-BMTbT CP film.

During our investigations we have observed that the electrochemical response of RAS-CPs is dependent on the solvent and the electrolyte salt. In particular, the electropolymerization reaction can yield a redox active film or an insulating film depending on the electrolyte media chosen. These experiments aim to investigate the effects of the solvent and electrolyte salt on the redox reactions of BMTbT, EDOT-BMTbT and PEDOT-BMTbT and then use them as a model system for other RAS-CPs. Scheme 4.1 shows the redox reactions of a PEDOT-BMTbT film.

First, we employed the use of cyclic voltammetry to study the redox reactions of BMTbT and the electropolymerization reaction of EDOT-BMTbT. The criteria

necessary for the yield of redox active RAS-CPs were established. The Raman spectra for the following synthesized compounds: BMTbT, EDOT-BMTbT and PEDOT-BMTbT are reported. Finally, *in situ* Raman spectroelectrochemistry was carried out to study the chemical changes that occur as a product of the electrochemical cycling of PEDOT-BMTbT films.

Experimental

Materials and Reagents

Unless otherwise noted all chemicals and reagents were purchased from Sigma-Aldrich and used as received. BMTbT and EDOT-BMTbT were synthesized as stated in references 18 and 19 respectively.

Electrochemical Measurements

Cyclic voltammograms (CVs) were taken using a 3-electrode setup using a Hokuto Denko (HSV-100), Hokuto Denko (HABF 1580m), or a Bio-Analytical Systems (BAS) CV-27 potentiostat. The reference electrode used for the CV experiments was a home-built Ag/Ag^+ using a silver wire, a fritted tube and a 50mM $AgClO_4$ / 0.1 M $LiClO_4$ / AN inner solution and it was stored in a 0.1 M $LiClO_4$/AN solution. The working electrodes were GCE electrodes.

Raman Measurements

Raman measurements were done using a 3 electrode setup using a PEDOT-TAPD film modified GCE as the working electrode, a Pt coil counter electrode and a Ag wire quasi reference electrode. An inVia Renishaw confocal Raman spectrometer using a

785nm excitation wavelength laser at 5% of the intensity using a 20x objective in a Leica microscope was employed.

Results and Discussion

BMTbT Solvent Dependent Electrochemistry

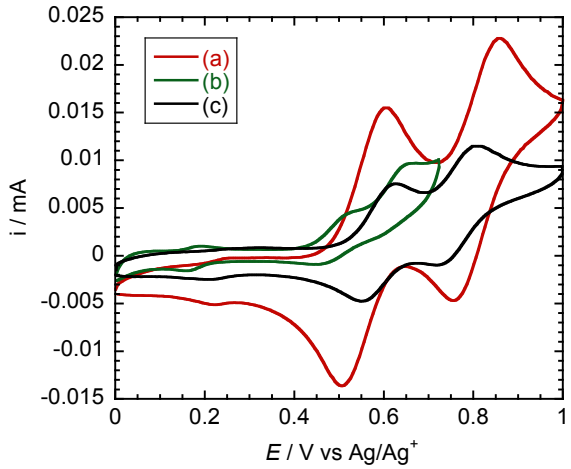

Figure 4.1. Cyclic voltammetry of 1 mM BMTbT in (a) 0.1 M TBAH / NB, (b) 0.1 M TBAH / PC, and (c) 0.1 M TBAP / NB. Sweep rate for all CV measurements was 50 mV/s.

We started this investigation because we observed that depending of the electrolyte media in which the CV of BMTbT was carried out, there were significant differences in the electrochemical response. Specifically, the shape, peak position and peak currents significantly changed (we carried out the experiments at the same molecule concentration and the same concentration of supporting electrolyte).

The cyclic voltammetry of a 1 mM BMTbT solution in different solvents and electrolyte salts is presented in Figure 4.1. As can be observed the redox reactions of BMTbT are chemically reversible in 0.1 M TBAH / NB electrolyte medium. The formal potential for the first chemically reversible redox couple, where BMTbT goes from its neutral form to the radical cation, is at +0.55 V. The $E^{0'}$ for the second

oxidation process, where BMTbT's radical cation is oxidized to the di-cation, is at +0.81 V. The peak-to-peak separation for the first redox process is 100 mV, and the peak-to peak separation for the second redox process is 80 mV; indicating that the charge transfer kinetics are slower for the first redox process when compared to the second charge transfer process.

We then proceeded to investigate the effects of the counter ion on the redox reactions of BMTbT. For these experiments we chose 0.1 M TBAP / NB as the electrolyte medium. The CV for a 1mM BMTbT solution in 0.1 M TBAP / NB is shown in Figure 4.1b. The effects of the anion on the redox reactions of BMTbT were investigated. The peak currents for a 1mM BMTbT solution in this electrolyte concentration are smaller than in the case of 0.1 M TBAH / NB. We believe that this is due to slight differences in the weighted mass of BMTbT, and not a sign of a more complicated mechanism. However, the CV shape is approaching a steady state response. Although somewhat speculative on our part, we believe this is due to higher ion paring effects with perchlorate anions than with hexafluorophosphate anions. The first and second oxidation formal potentials ($E^{0'}$) are at +0.56 V and +0.76 V respectively. The peak-to-peak separation for the first and second redox processes was 125 mV in both cases.

Finally, we proceeded to investigate the effects of the solvent using hexafluorphosphate as the electrolyte. Figure 4.1c presents the CV of a 1mM BMTbT solution in 0.1 M TBAH / PC solution. In this case the redox reactions of BMTbT are chemically and electrochemically irreversible. At 20 mV/s a reverse peak cannot be observed. This is likely due to the nucleophilic character of carbonate-based solvents

(PC in this case). Even at higher sweep rates of 200 mV/s, there was no observable reverse peak in the voltammogram. The peak potentials for the first and second oxidations are +0.5 V and +0.63 V respectively.

From these experiments the best electrolyte medium for the study of the electrochemical reactions of BMTbT is 0.1 M TBAH / NB. This electrolyte medium gave the smallest peak-to-peak separation and the largest (in terms of current) reduction waves, which means higher chemical and electrochemical reversibility, in addition to higher charge transfer kinetics. With these results in mind, we proceeded to study the electrolyte media effects on the electropolymerization reactions of EDOT-BMTbT.

Solvent effects on the electropolymerization of EDOT-BMTbT

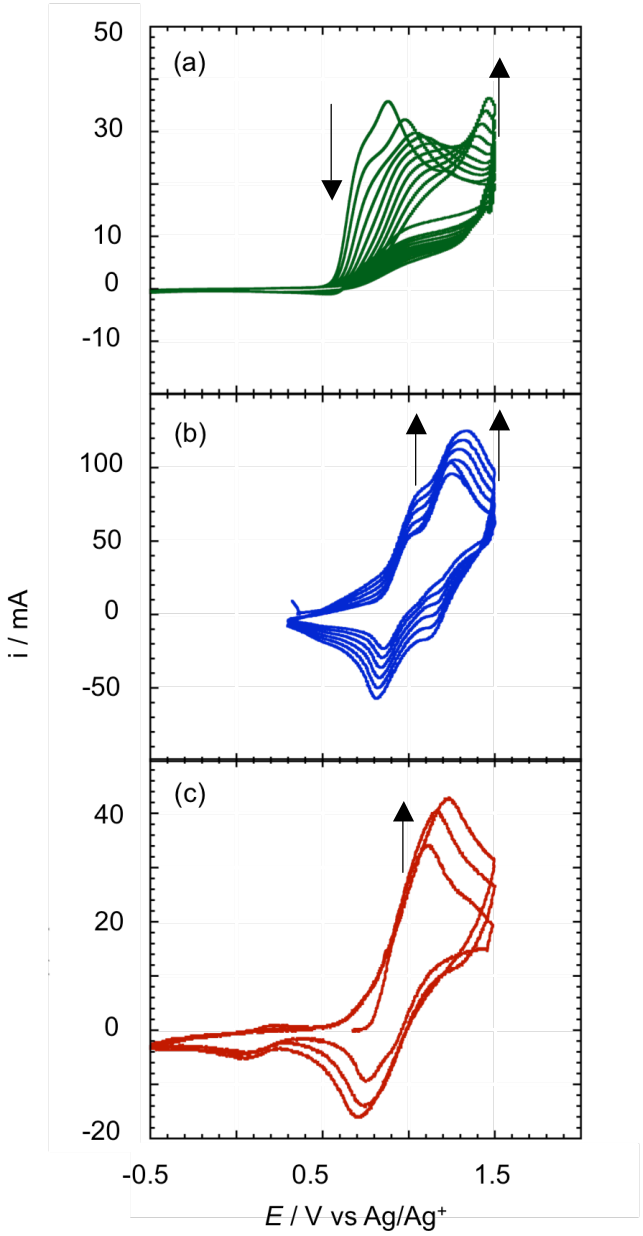

Figure 4.2. Consecutive CVs of 10 mM EDOT-BMTbT in (a) 0.1 M TBAH / PC, (b) 0.1 M TBAH / NB, and (c) 0.1 M TBAP / NB solutions. Sweep rate in all cases was 20 mV/s.

The electropolymerization of 10 mM EDOT-BMTbT monomers was carried out using the same electrolyte media as in the previous section. We wanted to establish relationships between BMTbT's electrochemical reaction stability and reversibility

with the electropolymerization reaction of EDOT-BMTbT. The electropolymerization was carried out using CV and doing anodic scans in 10 mM EDOT-BMTbT solutions (Figure 4.2).

Figure 4.2a illustrates the electropolymerization profile of EDOT-BMTbT in 0.1 M TBAH / PC. There are 2 oxidation peaks at +0.7 V and +0.85 V corresponding to the BMTbT pendant of the EDOT-BMTbT monomer. When the potential is swept over the selected range these two oxidation peaks decrease as the number of cycles increases. The appearance and growth of a third oxidation peak at ca. +1.45 V can be observed as the number of cycles increases. However, there is no evidence that indicates the formation of a redox active CP film when using these experimental conditions and parameters.

The electropolymerization was then carried out in 0.1 M TBAH/NB electrolyte medium. The consecutive CVs show two oxidation peaks at +1.05 V and +1.2 V, respectively. The reduction of those peaks is at ca. +0.7 and +1.1 V respectively. There is an increment in the peak currents (both in the oxidation and the reduction) as the number of CV cycles increases. This observable evidences the formation of a redox active CP film on the electrode surface. Interestingly, there must be an interaction between the BMTbT pendant and the EDOT component of the molecule since there is not a third oxidation due to the EDOT Monomer and there has to be an EDOT radical cation for the electropolymerization to take place. This behavior is different from other reported PEDOT based RAS-CP where the oxidation and reduction of the pendant occurs first and the EDOT component occurs later.[16]

We then proceeded to investigate the effects of the anion on the electropolymerization of EDOT-BMTbT. For these experiments NB was used as the solvent since we had good pendant (i.e. BMTbT) electrochemistry and the electropolymerization reaction in 0.1 M TBAH / NB yielded a redox active film. The electropolymerization profile for an EDOT-BMTbT in 0.1M TBAP / NB electrolyte medium is presented in Figure 4.2c. Two oxidation processes are convoluted into one broad oxidation wave that can be observed at ca. 1.2 V. The peak current increases as the number of CV cycles increases evidencing the formation of an electroactive CP film on the electrode surface. Similar to the case of BMTbT's molecule electrochemistry the resolution of the peaks is less, most likely due to ion pairing effects.

In general, it appears that the electropolymerization of RAS-CP type materials yields electroactive films if the electrochemistry of the pendant is chemically and electrochemically reversible in the electropolymerization reaction electrolyte media. In this case, EDOT-BMTbT, the electrolyte media in which BMTbT exhibited the best electrochemical behavior (or electrochemical stability) was 0.1 M TBAH / NB. The pendant of the molecule needs to be stable if we are to electropolymerize the monomer backbone successfully.

PEDOT-BMTbT Film Electrochemistry

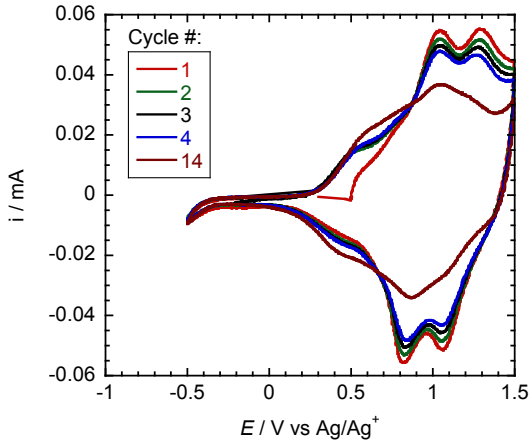

Figure 4.3. CV of a PEDOT-BMtBT film in a 0.1 M TBAH / NB solution at a sweep rate of 20 mV/s.

The film electrochemistry of PEDOT-BMTbT in 0.1 M TBAH / NB is presented in Figure 4.3. This RAS-CP film exhibits features characteristic of PEDOT with the redox reactions of BMTbT super imposed on the pseudocapacitive current from the CP backbone. The onset for the p-doped conductivity is observed at ca. +0.3 V. The oxidation redox reactions of BMTbT are at +1.05 V and +1.3 V respectively; the corresponding reductions of the aforementioned oxidation processes are at +1.1 V and +0.8 V. There is a significant fade in the current corresponding to the redox reactions of the BMTbT pendant as the number of cycles increases. In contrast, the pseudocapacitance of the polymer persists even after the redox processes of BMTbT have decreased. This means that possible degradation pathways for the capacity fade are most likely due to instabilities in the pendant and not the CP backbone.

Raman Spectroelectrochemistry of PEDOT-BMTbT

The Raman spectra for BMTbT, EDOT-BMTbT, PEDOT film-modified GCE, and PEDOT-BMTbT film-modified GCE are presented in Figure 4.4. We used PEDOT and BMTbTs spectra as a reference spectra to identify spectral changes in

EDOT-BMTbT and PEDOT-BMTbT including *in situ* Raman spectroelectrochemistry. We also report for the first time the Raman spectra of BMTbT.

BMTbT has several Raman peaks of interest. The thiophene ring (C-S-C) def can be observed at ca. 700cm^{-1}. There is also a big peak at 1450 cm^{-1} corresponding to asym. C=C str. transition. There are smaller peaks at 1340 cm^{-1} 1045cm^{-1} 1000 cm^{-1} and 950cm^{-1} which are likely due to the following modes: sym. C=C, C-C str., and C-C interring respectively. BMTbT's peak assignment was carried out by comparing the Raman spectra from BMTbT to other similar molecules reported in the literature.[21-23]

EDOT-BMTbT Raman spectra preserve much of the characteristics of BMTbT spectra; the peaks at 1450 cm^{-1} (very strong) and the following smaller peaks 1340 cm^{-1} 1045cm^{-1} 1000 cm^{-1} and 950cm^{-1}. Interestingly, the strong peaks at ca. 700 cm^{-1} are smaller when compared to BMTbT, most likely due to the loss of symmetry in the molecule.

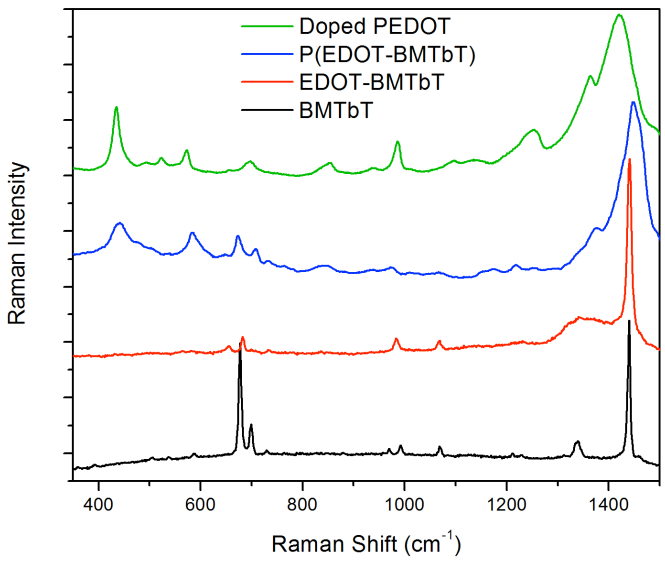

Figure 4.4. Raman spectra of PEDOT (green), BMTbT (black), EDOT-BMTbT (red) and PEDOT-BMTbT (blue).

PEDOT-BMTbT films on the other hand exhibit largely the Raman spectra of PEDOT films. There are small peaks corresponding to BMTbT superimposed on PEDOTs spectrum (specifically the double peak at 700 cm^{-1}). There also appears to be a small shoulder at 1450 cm^{-1}, which also corresponds to the BMTbT pendant.

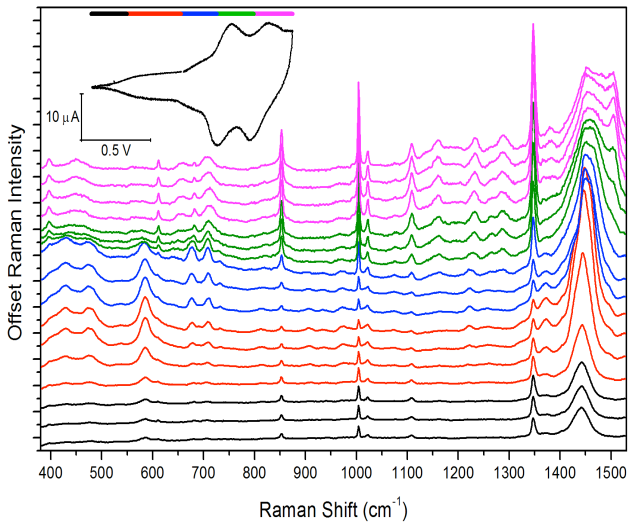

Figure 4.5. Raman spectroelectrochemistry of PEDOT-BMTbT in 0.1 M TBAH / NM solution at a sweep rate of 10 mV/s.

The *in situ* Raman spectroelectrochemistry of PEDOT-BMTbT is presented in Figure 4.5. At low potentials, where PEDOT-BMTbT is undoped, the peaks correspond to those of an undoped PEDOT film. At higher potentials, where the PEDOT-BMTbT is being doped, there is the emergence of one peak at 600cm^{-1}, two peaks at ca. 700cm^{-1}, and one peak at 1360cm^{-1}. There is a broadening of the peaks around 1450 cm^{-1} corresponding to the quinoid-like bonding that polythiophenes assume when oxidized. At potentials just before the first oxidation of the BMTbT pendant, the one peak at 600cm^{-1}, two peaks at ca. 700cm^{-1}, and one peak at 1360cm^{-1}

intensity grows, and the polythiophene peaks at the 1400cm^{-1} range keep broadening; this is consistent with higher doping levels of the CP.

When the applied potential is enough to oxidize the BMTbT pendant, the peak at 600 cm^{-1} diminishes and the emergence of two peaks at 1275 cm^{-1} and one peak at 1500 cm^{-1} can be observed. These peaks are likely due to changes in the bi-thiophene moiety of BMTbT. At very oxidizing potentials, where BMTbT is in its di-cation and the polymer is highly doped very doped, the intensity of the peaks at 1350cm^{-1} and 1000cm^{-1} increases significantly. The emergence of an intense peak at 850 cm^{-1} can also be observed at these potentials. When the potential is cycled back to potentials where PEDOT is undoped and BMTbT is in its neutral form, the Raman spectra obtained at the start of the experiment is recovered, evidencing the stability of PEDOT-BMTbT films cycled in 0.1 M TBAH / NB electrolyte medium.

The experiments detailed herein serve to illustrate the subtle interplay that the electrolyte salt and the solvent media have on the redox reactions of BMTbT and the electropolymerization of electroactive CP films (in this case RAS-CPs). Small changes in the electrolyte medium can give rise to events that range from reversible electrochemical processes to chemical irreversibility. In addition, the electropolymerization reactions of EDOT-BMTbT depend on the stability of the BMTbT pendant. We speculate that this is true for all RAS pendants in RAS-CP films. If BMTbT or the pendant of the RAS-CP is unstable, then electropolymerization will not occur. Even more surprising are the more subtle effects that ion pairing have on the redox reactions of BMTbT. We observed that in cases where the electrochemistry of BMTbT was less reversible due to what we attribute to ion paring effects, the electropolymerization reaction profile was also significantly affected.

Conclusions

The redox reactions of BMTbT have been studied in detail using different electrolyte media. We have established that highly nucleophilic solvents such as PC create a reactive environment for BMTbT's cation and dication. This was evidenced by the irreversible character of the CVs in this electrolyte medium. In addition, the electrolyte anion interaction with BMTbT also affected the redox reactions of the molecule. We discovered trends that perchlorate anions interact stronger with BMTbT's cation and dication when compared with hexafluorophosphate anions.

Moreover, we uncovered that in order for the electropolymerization of EDOT-BMTbT to yield an electroactive CP film, the pendant (in this case BMTbT) cation and di-cation have to be stable in the electrolyte media selected for the successful electrosynthesis of an electroactive CP film. We then measured the Raman spectra of BMTbT, EDOT-BMTbT, as well as the Raman spectroelectrochemistry of PEDOT-BMTbT. The peak assignment for BMTbT, EDOT-BMTbT and the Raman spectroelectrochemistry of PEDOT-BMTbT was carried out. The Raman spectroelectrochemistry yielded insights into the electrochemical reaction mechanism of the RAS-CP film. Most importantly, these experiments serve to illustrate the required conditions, experimental parameters and observables if the successful electropolymerization and reversible electrochemical reactions of RAS-CPs are expected.

REFERENCES

1. Hiang, C. K.; Fincher, C. R., Jr.; Park, Y. W.; Heeger, A. J.; Shirakawa, H.; Louis, E. J.; Gau, S. C.; and MacDiarmid, A. G.; Physical Review Letters 1977, 39, 1098.

2. McCullough, R. D.; Advanced Materials 1998, 10, 93.

3. Groenenedaal, L.; Jonas F.; Freitag, D.; Pierlarzik, H.; and Reynolds, J.R.; Adv. Mater. (2000) 12, 481.

4. Heeger, A.J.; Kivelson, S.; Schrieffer, J.R.; and Su, W.-P.; Rev. Mod. Phys. 1988, 60, 781.

5. Sirringhaus, H.; Kawase, T.; Friend, R.H.; Shimoda,T.; Inbasekaran, M.; Wu, W.; and Woo, E.P.; Science 2000, 290, 2123.

6. Gustafsson, G.; Cao, Y.; Treacy, G.M.; Klavetter, K.; Colaneri, N.; and Heeger, A.J.; Nature 1992, 357, 477.

7. Novák, P.; Müller, K.; Santhanam, K.S.V.; and Haas, O.; Chem. Rev. 1997, 97, 207.

8. Heywang, G.; and Jonas, F.; Adv. Mater. 1992, 4, 116.

9. Patil, A.O.; Heeger, A.J.; and Wudl, F.; Chem. Rev. 1998, 88, 183

10. Groenendaal, L.; Zotti, G.; Pierre-Henri, A.; Waybright, S.M.; and Reynolds, J.R.; Adv. Mater. (2003) 15, 855.

11. Burkhardt, S.E.; Rodríguez-Calero, G.G.; Lowe, M.A.; Kiya, Y.; Hennig, R.H.; and Abruña, H.D.; J. Phys. Chem. C. 2010, 114, 16776.

12. Conte, S.; Rodríguez-Calero, G.G.; Burkhardt, S.E.; Lowe, M.A.; and Abruña H.D.; RSC Adv. 2013, 3, 1957

13. Perepichka, I.F.; Perepichka, D.F.; Meng, H.; and Wudl, F.; Adv. Mater. 2005, 17, 2281.

14. Mortimer, R.J.; Chem. Soc. Rev. 1997 26, 147

15. Thompson, B.C.; and Fréchet, J.M.J.; Angew. Chem. Int. Ed. 2008, 47, 58

16. Burkhardt, S. E.; Lowe, M. A.; Conte, S.; Zhou, Weidong; Qian, H.; Rodríguez-Calero, G. G.; Gao, Jie; Hennig, Richard G.; and Abruña, H. D.; Energy & Environmental Science 2012, 5, 7176.

17. Rodríguez-Calero, G. G.; Lowe, M. A.; Kiya, Y.; and Abruna, H. D.; Journal of Physical Chemistry C 2010, 114, 6169.

18. Kiya, Y; Iwata, A.; Sarukawa, T.; Henderson, J. C.; and Abruña, H. D. Journal of Power Sources 2007, 173, 522.

19. Kiya, Y.; Henderson, J. C.; Hutchinson, G. R.; and Abruña, H. D. J. Phys. Chem. C 2008, 112, 3989.

20. Kiya, Yasuyuki; Henderson, J. C.; Hutchison, G. R.; and Abruna, H. D.; Journal of Materials Chemistry 2007, 17, 4366.

21. Burkhardt, S. E.; Conte, S.; Rodríguez-Calero, G. G.; Lowe, M. A.; Qian H.; Zhou, W.; Gao, J.; Hennig, R.; and Abruña, H. D.; Journal of Materials Chemistry 2011, 21, 9553.

22. Lowe, M. A.; Kiya, Y.; Henderson, J. C.; and Abruña, H. D.; Electrochemistry Communications 2011, 13, 462.

23. Lapkowski, M.; and Pron, A.; Synthetic Metals 2000, 110, 79.

24. Garreau, S.; Louarn, G.; Buison, J.P; Froyer, G.; and Lefrant, S.; Macromol. 1999, 32, 6807.

CHAPTER 5

A NEW BREED OF ORGANIC CATHODE MATERIALS FOR ELECTROCHEMICAL ENERGY STORAGE

Introduction

The search for efficient, high energy density, high power density, inexpensive, safe, and electrochemically reversible electrochemical energy storage (EES) materials is one of the greatest challenges facing the academic and industrial communities.[1] It has been challenging for EES materials to concurrently meet all of these criteria. In the search for alternative materials, we determined that organic compounds could meet most of these challenges.[2-6] Organic materials are very promising electrode materials due to the easy tuning of their energy levels (thus their formal potential, $E^{0'}$) using organic synthesis, and because they lack heavy metals that generally compromise most of the metal oxides in traditional electrodes, they can also achieve higher capacity and lower costs while being more environmentally benign (this is especially true when considering metals such as cobalt). [1-7] In addition, since the charge/discharge processes do not involve intercalation, they can sustain high C-rates and thus achieve high power density.

Interest in the use of organic materials for electrochemical energy storage has increased recently within in the scientific community, with most of the work concentrating on carbonyl functionalities.[8-14] For example, some research groups have synthesized, from plants, carbonyl based organic molecules and used them as

electrode materials demonstrating promising performance,[8] in terms of electrochemical reversibility and capacities. Moreover, these molecules are environmentally safe, and are derived from renewable feed stocks. However, these molecules generally suffer from low formal potentials (since carrying out reductions at positive potentials is a difficult task to accomplish), solubility issues, and poor conductivity leading to poor energy densities, albeit, their gravimetric charge storage capacities can be high.

Among organic materials, conducting polymers (CP) have also been studied as materials for positive electrodes in LIBs.[16-22] However, they suffer from low capacities (e.g. 20-30 mAh/g) due to the fact that only a fraction of an electron is transferred per monomer unit. However, they do offer high conductivity, no solubility into the electrolyte and high cycling ability. In our group, we have also employed them as electrocatalysts for organosulfur compounds for EES applications.[24-27]

In this manuscript we thoroughly investigate and elucidate the electrochemical mechanism of a test molecule serving as the prototype for a new class of materials, that can preserve all of the attributes that make organic compounds attractive, while overcoming some of the drawbacks that typical organic electrode materials have such as low electronic conductivities and solubility into the electrolyte. We recently published on a promising material that combines a conducting polymer with a redox active substituent. The material uses a tetra-alkylated phenylenediamine (TAPD) redox active substituent (RAS) in combination with a poly-3,4-ethylenedioxythiophene (PEDOT) conducting polymer backbone (CP). [28]

The use of this approach (combining RAS with CPs) eliminates one of the main drawbacks of using traditional CP (low capacities and hence low energy densities), by increasing the number of electrons transferred per monomer unit from 0.6 e^- to 2.6 e^-, while preserving their conductivity and insoluble properties (Scheme 1). Moreover, these redox processes take place at potentials exceeding 3 V vs Li/Li^+. The CP (PEDOT) now serves as the conducting additive and binder (in addition to providing some modest capacity), while the RAS (TAPD) contributes a high number of electrons transferred at high formal potentials ($E^{0'}$), resulting in high energy densities.

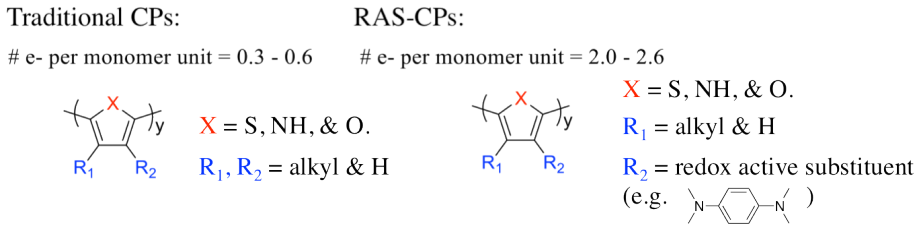

Scheme 5.1. Redox Active Substituted – Conducting Polymers (RAS-CP) concept.

We also previously discussed the design criteria employed for the selection of this material, the methodology for the synthesis and some electrochemical characterization. In this manuscript we expand on our previous work by investigating, in detail, the electrochemical processes involved in PEDOT-TAPD redox reactions, their dependence on the electrolyte system, elucidating the mechanisms of the electrochemical reactions using spectroelectrochemical techniques, understanding the capacity fade phenomena, and controlling material morphology. Most importantly, we have designed a methodology to incorporate RAS-CPs into traditional coin cell electrodes, while demonstrating that PEDOT-TAPD by itself (without conducting

additives or binders) can yield high capacity at high C-rates. To the best of our knowledge, PEDOT-TAPD has the highest capacity of any CP-type based positive electrode material reported to date. A scheme for the electrochemical reactions is presented in Scheme 2.

In the mechanistic investigations, we have employed Raman and ultra-violet visible spectroelectrochemical methods. To further investigate transport in the RAS-CP films, we performed electrochemical quartz crystal microbalance (EQCM) measurements, to assess the morphology dependence on the electropolymeriaztion conditions, we used scanning electron microscopy (SEM) images, and finally we performed device testing characterization to incorporate PEDOT-TAPD in common device tests (i.e. coin cell testing).

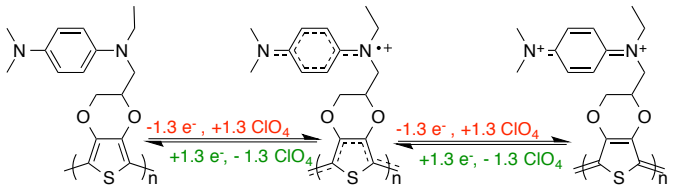

Scheme 5.2. Electrochemical reaction of PEDOT-TAPD films.

Experimental

Materials

The synthesis of PEDOT-TAPD was done as reported in Ref. 27. All other chemicals, unless otherwise noted, were purchased from Sigma-Aldrich and used as received. The glassy carbon electrodes were purchased from CH instruments. ITO glass slides were from NANOCS (the resistance of the ITO electrodes was 10 Ohms).

Electrochemical and In Situ Measurements

Cyclic voltammograms were taken using a 3-electrode configuration using a Hokuto Denko (HSV-100), Hokuto Denko (HABF 1580m), or a Bio-Analytical Systems (BAS) CV-27 potentiostat. Electrochemical impedance spectroscopy was done using a Solartron potentiostat. The reference electrode used for the CVs and EIS experiments was a home-built Ag/Ag^+ using a silver wire, a fritted tube and a 50mM $AgClO_4$ / 0.1 M $LiClO_4$ / AN inner solution and was kept in a 0.1 M $LiClO_4$ storing solution. The working electrodes were GCE electrodes.

AT-cut quartz crystals (5 MHz) of 24.5 mm diameter with Au electrodes deposited over a Ti adhesion layer (Maxtek) were used for EQCM measurements. An asymmetric keyhole electrode arrangement was used, in which the circular electrodes' geometrical areas were 1.370 cm2 (front side) and 0.317 cm2 (back side), respectively. The electrode surfaces were overtone polished. The quartz crystal resonator was set in a probe (TPS-550, Maxtek) made of Teflon, in which the oscillator circuit was included, and the quartz crystal was held vertically. The probe was connected to a conventional three-chamber electrochemical cell by a home-made Teflon joint. One of the electrodes of the quartz crystal resonator, in contact with the solution, was also used as the working electrode. The frequency response measured with a plating monitor (PM-740, Maxtek) and the current measured with the potentiostat were simultaneously recorded by a personal computer which was interfaced to the above instruments using LabVIEW (National Instruments). The admittance of the quartz crystal resonator was measured near its resonant frequency by an impedance analyzer (HP4194A, Hewlett-Packard) equipped with a test lead (HP16048A). A probe similar to the one used in the EQCM measurements, but which

did not include an oscillator circuit inside, was used to accomplish a direct connection between the quartz crystal resonator and the impedance analyzer.

A diagram of the electrochemical cells used for Raman spectroelectrochemistry experiments is shown in the supporting information. The UV-Vis experiment was done in a quartz cuvette, using a silver quasi reference electrode, a Pt coil as the counter electrode and a PEDOT-TAPD film-modified ITO electrode. Spectra were taken both while cycling the potential at 10mV/s taking spectra every 10s, and at specific potentials in the voltammetric profile. The UV-Vis spectroelectrochemistry experiments were carried out using a Hewlett Packard spectrophotometer (model 8453).

Raman measurements were done using a 3 electrode setup using a PEDOT-TAPD film modified GCE as the working electrode, a Pt coil counter electrode and a Ag wire quasi reference electrode. An inVia Renishaw confocal Raman spectrometer using a 785nm excitation wavelength laser at 5% of the intensity using a 20x objective in a Leica microscope was employed.

Device Testing Measurements

All electrochemical device measurements were conducted in CR2032 coin cells. The cathodes were prepared using the electrochemical methodology discussed below. The electropolymerized films were dried under vacuum at 80 ºC overnight, and cut into circular electrodes with a typical area of 0.71 cm^2. They were then pressed onto nickel foam used as a current collector. Coin cells were assembled in an argon-filled glove box with lithium foil as the anode, Celgard 2320 as the separator, and a

solution of LiTFSI, $LiClO_4$ (1.0M) in ethylene carbonate/diethylcarbonate (EC/DEC) (1:1 by volume) and TEGDME as the electrolyte. Galvanostatic discharge/ charge tests were carried out with an Arbin battery testing system. The cells were discharged to 3.0 V vs Li/Li^+ at 60 mA/g and charged to 4.1 V vs Li/Li^+ at 60mA/g for each cycle. The capacity was normalized to the overall mass of the PEDOT-TAPD composite.

Scanning Electron Microcopy

Glassy carbon slugs 5 or 6 mm in diameter, were used to generate electropolymerized films of PEDOT-TAPD films. The electropolymerization of the CP onto the glassy carbon slugs was done using the same experimental conditions as used for the electrochemical experiments. After electropolymerization, the glassy carbon slugs, modified with the CP films, were rinsed, dried under vacuum for 30-40 minutes and heated to 50 ºC, to remove any remaining solvent, before transferring to the SEM chamber. Images were taken using an accelerating voltage of 3 keV. A Zeiss SEM model 1550 field emission scanning electron microscope was used to acquire the images.

Results and Discussion

Electropolymerization

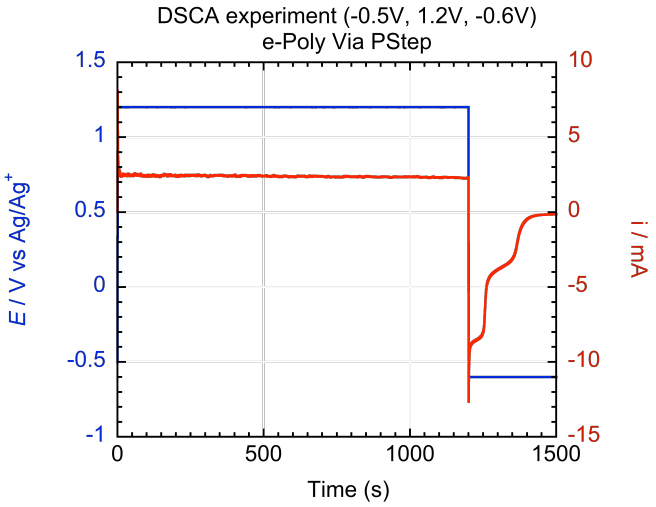

Figure 5.1.1. Double potential step chronoamperometry (DPSCA) experiment for the electrodeposition of PEDOT-TAPD.

PEDOT-TAPD films were prepared using two distinct electropolymerization techniques. The first was anodic cycling between -0.5 V and 1.1 V vs Ag/Ag^+. Electropolymerization CV profiles are shown in Figure 5.1.2. The second electropolymerization method employed was double potential step chronoamperometry (DPSCA). In this experiment two potential steps were carried out using a Au coated Al current collector and analytical GCEs, in a solution containing 10mM EDOT-TAPD monomer and 1 M $LiClO_4$ in acetonitrile (Figure 5.1.1). The initial potential was held at -0.5 V (i.e. the open circuit potential) vs Ag/Ag^+ for 30s, and then a first step to 1.2 V vs Ag/Ag^+ was applied for 20 mins to oxidize EDOT-TAPD monomers and make PEDOT-TAPD films on the electrode. Afterwards a second potential step to -0.6 V vs Ag/Ag^+ was applied for 5 mins to reduce the PEDOT-TAPD monomer and de-dope the film. The solution was thoroughly purged with high purity nitrogen gas prior to and during the experiments, and stirred with a magnetic stirrer through out the experiment. The resulting films from both

electropolymerization methods exhibited similar electrochemical responses. The electrochemical response was studied in thinner RAS-CP films on analytical electrodes (film thicknesses of ca. 500 nm). The morphological dependency on the electropolymerization technique employed is discussed below (vide-infra).

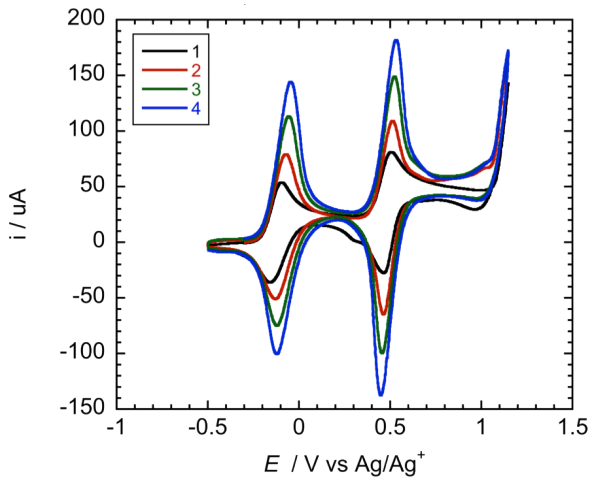

Figure 5.1.2: Concecutive CVs during the electropolymerization of EDOT-TAPD (10mM) in a 0.1 M $LiClO_4$ / AN solution at a GCE. Scan rate employed was 20 mV/s.

Cyclic Voltammetry

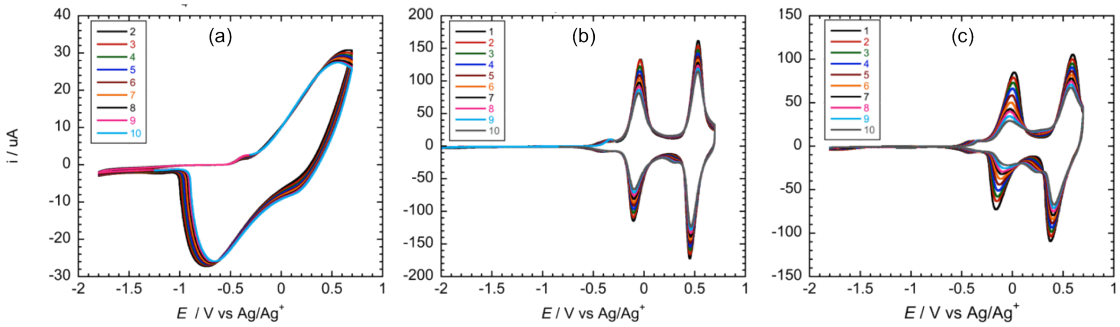

Figure 5.2. Consecutive CVs of a PEDOT-TAPD film-modified GCE at 0.1 M $LiClO_4$: (a) THF, (b) AN, and (c) PC solutions. Scan rate in all cases was 20 mV/s.

The electrochemical behavior of PEDOT-TAPD films was investigated in solvents with varying dielectric constant (THF, AN, and PC with dielectric constants

of 8, 37, 68 respectively) (Figure 5.2). To keep the morphology and structure of the films similar in all cases, all the PEDOT-TAPD films studied herein were prepared in 10 mM EDOT-TAPD, 0.1 M TBAP, acetonitrile electrolyte solutions, using anodic cycling (as described in the supporting information).

The cyclic voltammograms of PEDOT-TAPD films in THF (Figure 5.1a) are very resistive as evidenced by the large peak-to-peak potential (ΔE_p) separation. The second redox process (at ca. 0.5 V) of the polymer film could not be observed unless the potential was swept to quite positive values. However, we decided to compare the electrochemical response of all the films over the same potential range. The onset of conductivity for the polymer can be observed at ca. -0.5 V vs Ag/Ag^+, while the onset for the first redox couple (TAPD to $TAPD^{\cdot+}$) is at -0.3 V vs Ag/Ag^+. The peak current potential for this redox process is at +0.4 V vs Ag/Ag^+. The corresponding reduction of the pendant $TAPD^{\cdot+}$ cation can be observed to have a peak current at -0.75 V vs Ag/Ag^+. The peak-to-peak separation for the processes associated with the first oxidation and reduction of the TAPD RAS is 1.15 V, providing further evidence as to the solution resistance of this electrolyte medium.

The PEDOT-TAPD film studied in AN (Figure 5.2b), exhibited much faster charge transfer kinetics when compared to the film studied in THF. This agrees well with the fact that THF is much more resistive than the AN (as shown by the measured solution resistances using EIS presented in the supporting information). The onset of conductivity for the polymer was at -0.65 V vs Ag/Ag^+. The peak current potentials for the cation and dication were -0.1 V and +0.5 V vs Ag/Ag^+ respectively. The peak current potentials for the reverse processes where the film goes from the dication to

the cation, and from the cation to the neutral molecule, were +0.45 V and -0.15 V vs Ag/Ag^+ respectively. There is a small over-potential of ca. 50 mV in both redox processes. Although somewhat speculative on our part, this is likely due to limitations in the charge-transfer between polymer chains and conductivity limitations caused by the smaller effective conjugation length caused by the steric hindrance of having the RAS covalently bound to the CP backbone. This is further evidenced and consistent with the positive shift of 500 mV in the onset of conductivity between PEDOT and PEDOT-TAPD.

The electrochemical cycling of PEDOT-TAPD films in PC (Figure 5.2c) exhibited charge transfer kinetics intermediate between those of THF and AN. The onset of conductivity for the CP backbone was -0.65 V vs Ag/Ag^+ and the peak current potentials for the oxidation of the neutral and cationic TAPD RAS were at 0.0 V vs Ag/Ag^+ and +0.6 V vs Ag/Ag^+, respectively. The corresponding reduction peak current potentials for the dication and cation or TAPD were at +0.4 V and -0.3 V vs Ag/Ag^+. In addition, the capacity fade, or decrease in the charge underneath the peaks, was more evident in this electrolyte medium. The capacity fade seemed to correlate with the dielectric constant, solvation ability, and nucleophilicity of the electrolyte medium used; with electrolytes that had a higher values of these properties exhibiting lower charge retention (i.e. higher capacity fade).

UV-Vis Spectroelectrochemistry

The UV-Vis spectroelectrochemistry of electropolymerized PEDOT-TAPD film-modified ITO electrodes was investigated and is presented in Figure 5.3. UV-Vis spectroelectrochemistry was chosen because it provides information about the

electronic structure of the material and provided spectra of the expected redox pathways (assuming that the UV-Vis spectrum for PEDOT-TAPD is a convolution of PEDOT and TMPD spectra), yielding mechanistic insights. The UV-Vis spectra were taken at the specified potentials that represented different oxidation state regions in the CV profile of PEDOT-TAPD film-modified GCEs. The UV-Vis spectrum taken at -500mV was predominantly that of undoped PEDOT with a broad peak at ca. 650nm. At this point, the electrode potential is not sufficient to oxidize the TAPD RAS to the cation radical ($TAPD^{\bullet+}$). As we apply more positive potentials (-0.25 V and 0.00 V) the absorption of undoped PEDOT starts bleaching out, since the polymer is going from the undoped state to the doped polaron and bipolaronic states.[29] The emergence of the characteristic absorptions of the TAPD cation at +0.5 V (having strong peak absorbances at 525nm and 625nm) can be observed at potentials close to or beyond the first faradaic process.[30] At the most positive potentials (+0.75 V and +1.0 V) the disappearance of the TAPD radical cation peaks could be observed. At these positive potentials, the majority of the absorbance is due to the polaron and bipolaron states of the polymer. In the cases where the potential was cycled, the same trends were observed with no, or minimal decrease in the absorbances. At this time we are not certain about the origin of the sharp peaks at 675nm, 1000nm and 1100nm. In general, UV-Vis proved insightful in the determination of the redox species present at different applied potentials. It could be observed that the PEDOT-TAPD spectra behaved similarly to PEDOT and TAPD. However, no further evidence about the mechanism could be derived from these experiments.

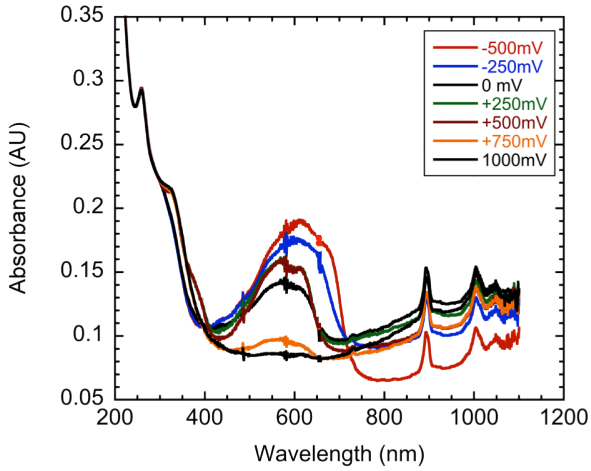

Figure 5.3. UV-Vis spectroelectrochemistry of a PEDOT-TAPD film-modified ITO electrode. Spectra taken at the specified potentials in a 0.1 M $LiClO_4$ / AN solution.

Raman Spectroelectrochemistry

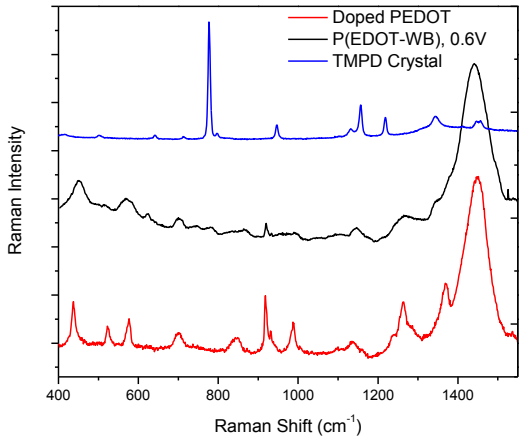

Figure 5.4.1: Reference Raman Spectrum for a PEDOT film (red), TMPD (blue) and a PEDOT-TAPD film (black).

The Raman spectroscopy was used to probe structural changes within a set of molecules (TMPD, PEDOT and PEDOT-TAPD) or within the same molecule under different conditions (PEDOT-TAPD at different electrochemical potentials). Several

previous reports have employed *in situ* Raman spectroscopy to probe the electrochemical reactions of conducting polymers.[31-33] Confocal Raman is particularly relevant and useful for spectroelectrochemical studies since the signal arises primarily from species at the focal point (e.g. the electrode surface). In this work, we employed *in situ* confocal Raman spectroscopy to probe structural changes in the RAS-CP PEDOT-TAPD, confirming the nature of the electrochemical reactions and detecting possible modes of polymer degradation. The Raman spectra for the molecules under study is illustrated in Figure 5.4.1.

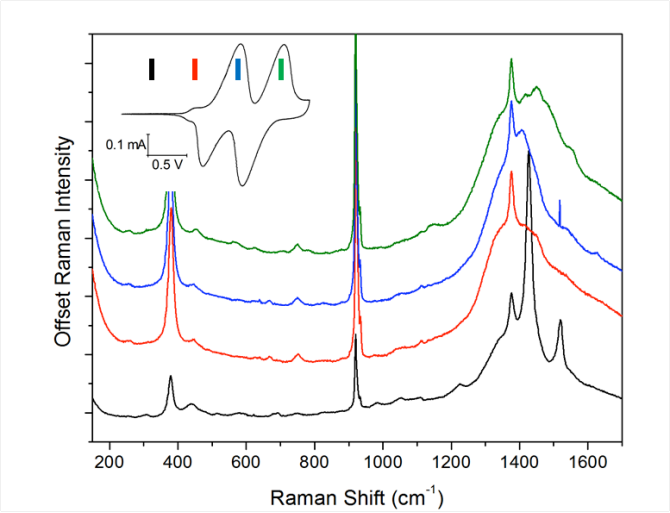

Figure 5.4.2 Raman spectra of PEDOT-TAPD film-modified GCEs at different potentials.

Figure 5.4.2 shows spectra collected from the polymer film at the specified oxidation states shown in the inset CV. The spectra are dominated by the response of the PEDOT backbone and, a bit surprisingly, the electrolyte solution. The peaks from acetonitrile are much more intense than typically observed for other conducting polymers, including PEDOT, which may indicate a more open film morphology and/or more solvent incorporation into the polymer film. This observation can be

rationalized, at least in part, due to the higher anion incorporation expected in PEDOT-TAPD films than in traditional conducting polymers (since the number of electrons transferred, in these films (ca. 2.6) is ca. 5 times that of PEDOT films). During oxidation, the peaks from the conjugated backbone (~1400 cm^{-1}) first broaden and move to lower energies, consistent with the backbone becoming more quinoid-like,[29,31] and then shift to higher energies as the oxidation state of the polymer increases. In the highly oxidized polymer (green spectrum), several peaks are observed due to a distribution of double bonds in polaronic and bipolaronic states of the CP backbone

A weak signal from the TAPD pendant is apparent in the neutral and oxidized polymer (Figure 5.4.2 black and red traces) at 750 cm^{-1}. At the potential of the first oxidation peak (Figure 5.4.2 blue trace), a characteristic signal from a ring-stretching mode of the TAPD radical cation appears at 1628 cm^{-1}, and this signal then disappears after the second oxidation peak (Figure 5.4.2 green trace).[32] These observations are in agreement with the assignment of the peaks to the first and second oxidations of the pendant TAPD. Peak assignments are presented in Table 5.1, and reference spectra for PEDOT and TMPD are presented in the supporting information section.

Table 5.1. Raman Shifts for PEDOT, TAPD and PEDOT-TAPD

undoped PEDOT	nature of transition	neutral TAPD	nature of transition	undoped PEDOT-TAPD	nature of transition
Raman shift in cm-1 (corresponding vibration)					
1520 1431 1369 1270 1226	asym. C=C str, sym C=C, C-C str, C-C interring	1220	C-H stretching	broad 1400	asym. C=C str, sym C=C, C-C str, C-C interring (from CP component)
1111	C-O-C def	1340	N-CH3 asym. stretch	750	TAPD ring breathing/deforma-tion
991	oxyethylene ring def				
692	C-S-C def, oxyethylene ring def.	778	ring breathing		
571		620	ring deformation		

* peaks at 375 cm^{-1} and 1375 cm^{-1} are due to AN, and peak at 933 cm^{-1} is due to ClO_4^-

Additional insights into the reaction mechanism can be derived through the correlation of the electrochemical and spectroscopic datasets, as shown in Figure 5.5. Panel A shows the current as a function of time while panel B shows the integrated peak areas from the doping anion (ClO_4^-, 933 cm^{-1}) and from the undoped polymer backbone (C=C asymmetric stretch, 1520 cm^{-1}). As expected, the signal from the doping anion increases throughout film oxidation and decreases during film reduction, while the signal from the un-doped polymer is seen when the film is in the un-doped state.

However, closer inspection reveals additional details. First, the doping / un-doping does not appear to be uniformly distributed between the first and second oxidation peaks. Rather, most of the change in anion concentration (~60%) appears before the second oxidation (40 and 275 s). Second, the film appears to retain an

excess of anions even at the end of the window of conductivity (160 and 400 s). This is supported by the observation that the signal from the un-doped polymer backbone continues to increase even in the non-conducting region (160-180 s and 400-420 s). At the end of the second cycle, the film shows much more ion incorporation and much less signal from the un-doped backbone, suggesting a relaxation of the film.

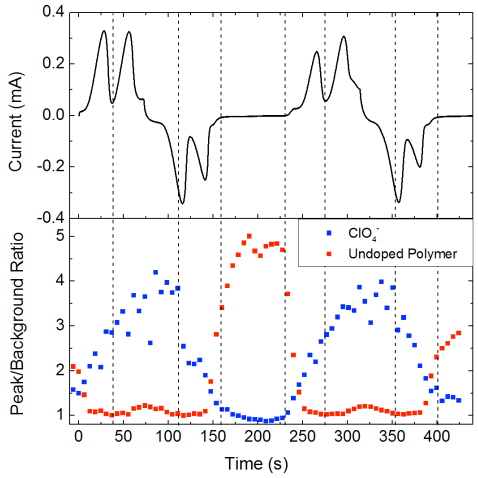

Figure 5.5. (a) Current vs potential/time profile (sweep rate of 10mV/s) of a PEDOT-TAPD film-modified GCE. (b) Integrated ClO_4^- and CP ring peaks (from Raman spectra) as a function of time.

The *in situ* Raman suggests the presence of ion trapping within the film. Holding the electrode at reducing potentials, between scans at different sweep rates, should allow for the deconvolution of the time scale of ion trapping and contributions from chemical reactivity. The dynamics of ion trapping and solvent incorporation at different potentials were further investigated as described below using EQCM studies.

Electrochemical Quartz Crystal Microbalance

In order to better understand the ion and solvent incorporation dynamics of oxidizing and reducing the PEDOT-TAPD films, EQCM experiments were carried

out. EQCM allowed us to monitor the frequency change (that can be related to mass-changes using the Sauerbrey equation) at different doping levels in PEDOT-TAPD films.[33] In these experiments, we swept the potential and monitored the frequency changes as a function of the applied potential. Figure 5.6, shows the CV of the PEDOT-TAPD film-modified EQCM electrode (Au deposited on quartz) and the corresponding frequency/mass changes. As the potential is swept positive, one can observe that, as anticipated, the frequency starts decreasing after -0.65 V vs Ag/Ag^+, since this is the onset of doping for PEDOT-TAPD films, and anions (ClO_4^-) and solvent are being incorporated into the film. At more positive potentials, when the TAPD RAS becomes oxidized, we observe a rapid decrease in frequency associated with the additional incorporation of anions and solvent molecules into the PEDOT-TAPD film. The frequency keeps decreasing although at a slower rate from 0 V vs Ag/Ag^+ to +0.3 V vs Ag/Ag^+, indicating that the polymer is being doped at slower rates at these potentials. Once the onset for oxidation of the TAPD cation is achieved, the frequency decreases further down at a faster pace. Interestingly, even though the PEDOT-TAPD film is being oxidized by the same amount as in the first redox process (i.e. by one electron) the frequency change is roughly half that of the first oxidation of the neutral to the cation radical redox process. Similar results have been previously found for poly-vinyl ferrocene films and are explained by the difference in solvation effects and trapping of anions when going from a neutral to a 1+ cation.[34] We believe that the same is true here, and that the change in frequency is larger in the first oxidation of the TAPD RAS due to the increased solvation needed for this process (giving rise to a higher influx of solvent molecules in the process). During the reverse

sweep, the potential dependent frequency changes are mirror to those for the forward sweep. However, upon full un-doping of the PEDOT-TAPD film, the frequency is lower than the initial frequency. The lower frequency indicates that solvent and perhaps some electrolyte ions are still trapped within the film. These results agree with the *in situ* Raman spectroelectrochemical measurements described earlier. From these observations, both *in situ* Raman and EQCM, we believe that the major cause for the lack of cyclability and/or capacity fade is charge trapping inside the PEDOT-TAPD films.

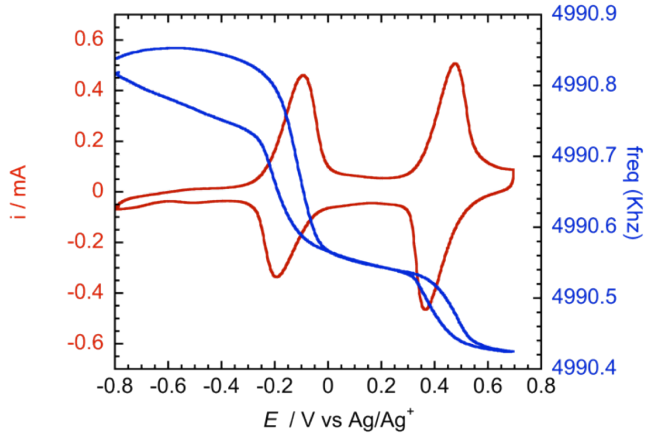

Figure 5.6. EQCM profile for a PEDOT-TAPD film-modified EQCM electrode. The red trace represents the CV at 50 mV/s of a PEDOT-TAPD film in a 0.1 M TBAP / AN solution. The blue trace represents the frequency as a function of potential.

Scanning Electron Microscopy

The effects of electropolymerization conditions on film morphology were studied using SEM. The different electropolymerization methods (i.e. potential steps and CV) can probe the effects of reaction kinetics on polymer film growth and how

those affect the resulting film morphology. It has been shown that fast growth generally yields more porous polymer films.

Potential step methods, in which the potential is stepped to +1.2 V vs Ag/Ag^+, will cause fast growth conditions. PEDOT-TAPD films prepared using this method exhibited a porous morphology (Figure 5.7a), with pores of ca. 100nm. For films deposited via anodic cycling, polymer growth was at a lower rate allowing the film time to unwind during doping and un-doping of the CP film. Films prepared by this electropolymerization method yielded a smooth morphology (Figure 5.7b). Control over the polymer film morphology is most attractive since one could control, to some extent, the polymer density and the film morphology by simply changing the electrochemical deposition parameters. For device testing, we chose to use open film morphologies (similar to Figure 5.7b), since we believe that a more open film morphology is likely beneficial to the desired cycling performance.

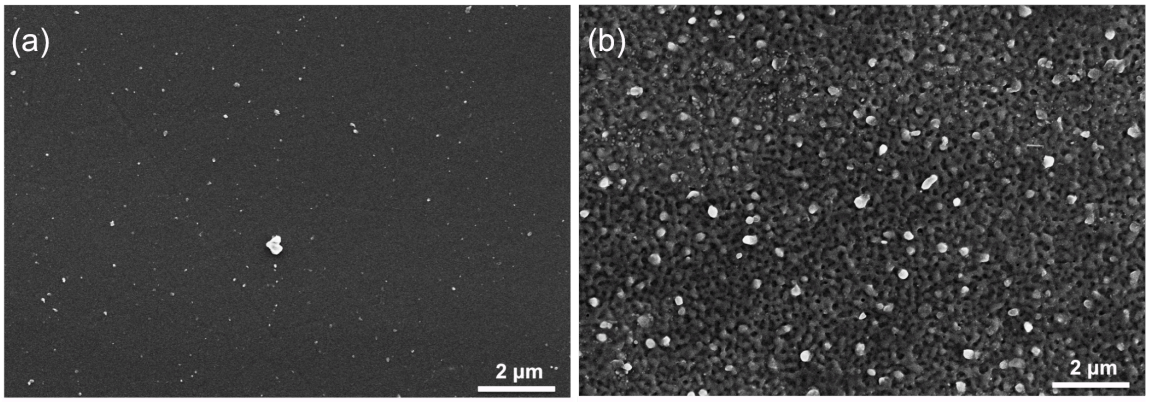

Figure 5.7. PEDOT-TAPD SEM images for films prepared using (a) CV and (b) potential step methodologies.

Device Testing

Electropolymerized PEDOT-TAPD films were tested in a traditional half-cell configuration. The resulting electropolymerized films had a mass of ca. 1 mg, demonstrating that even at these smaller scales, electropolymerization approaches are attractive for practical applications. It is important to note that the resulting films had a thicknesses of 10-30 microns and that film thicknesses could be controlled by varying the electropolymerization time, in the case of potential steps, and by the number of cycles in the case of the scanning potential method.

The charge / discharge profiles at 1 C are presented in figure 5.8a. This PEDOT-TAPD film was tested in a low dielectric solvent (TEGDME) to preserve cyclability, as demonstrated from the CV experiments in the first section of the results and discussion of this chapter. The first charge capacity was 140 mAh/g and the first discharge was 64 mAh/g (27% of the theoretical capacity). To the best of our knowledge this is the highest capacity for a CP-based material. The theoretical capacity for PEDOT-TAPD, assuming 2.6 e^- per monomer unit, is 220 mAh/g. The cycling performance for the PEDOT-TAPD half-cell is presented in Figure 5.8b. It can be observed that the capacity fades abruptly during the first 10 cycles and stabilizes around 20mAh/g after 90 cycles.

The plateaus at 3.3 and 3.8 V vs Li/Li^+ on the first charge/discharge cycle are in good agreement with the 3 electrode setup CV measurements. In addition, the fact that the charge in the forward sweep is higher than in the subsequent discharge is also in good agreement with CV measurements. We believe that the capacity fade is likely due to charge trapping inside the RAS-CP films. We speculate that this is more evident in the device testing measurements, than in the analytical electrodes, due to the

increased film thicknesses in the electrodes used for device testing. Thicker films were necessary so as to have an accurate mass measurement in these experiments.

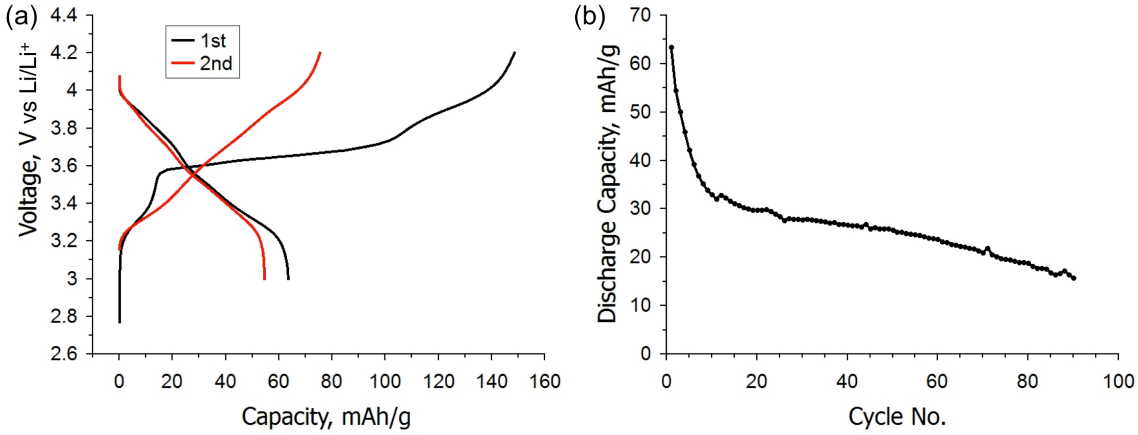

Figure 5.8. (a) Charge / discharge curves for a PEDOT-TAPD film modified current collector (100 % active material). (b) Capacity retention of the PEDOT-TAPD half-cell.

The compilation of results presented herein suggests that RAS-CPs are an attractive alternative for cathode materials in electrical energy storage systems. They can offer higher capacities that purely CP devices while retaining their high C-rates. We demonstrated that we can precisely control the materials morphology. Moreover , we developed an electrochemical method, that in our view is scalable to the industrial level, in which these electrodes can be incorporated into prototype coin-cells without the need of electrode additives (i.e. binder and carbon black). However, the PEDOT-TAPD model compound suffered from charge trapping effects that limited the materials cycling. We believe that thinner films of PEDOT-TAPD in higher surface area supports can significantly improve the cycling of these films (as evidenced by the CVs of the film-modified GCEs). We are currently investigating

electropolymerization conditions to achieve conformal coatings on high surface area supports.

Conclusions

In this manuscript we have presented a detailed investigation of the electrochemical reactions of PEDOT-TAPD films, used as a model compound of RAS-CPs. The solvent dependent electrochemistry was studied in THF, AN, and PC. The electrochemical responses and charge retention correlated with the dielectric constant and the nucleophilicity of the solvent, where the use of more nucleophilic and higher dielectric solvents (for example PC) resulted in the poorest charge/capacity retention. We also confirmed the presence of TAPD cations using UV-Vis spectroelectrochemistry, in which the results represented a convolution of the PEDOT CP backbone and the TAPD molecule in solution. The capacity fade mechanism for the PEDOT-TAPD films was determined to be largely due to charge trapping in the RAS-CP films as evidenced by Raman and EQCM measurements. Film morphology, as assessed via SEM, could be controlled by the use of different electrochemical techniques or electropolymerization parameters. Furthermore, the PEDOT-TAPD composites were assembled into a half-cell and the capacity obtained (i.e. 64 mAh/g) was the highest for a CP-type material. We note that extensive investigations are being carried out to achieve a higher percentage of the theoretical capacity of the PEDOT-TAPD films since in our device testing we only achieved 27%. We believe that the results presented in this manuscript illustrate the validity of the RAS-CP approach for EES technologies. More importantly, we believe that this work demonstrates that

through the careful choice of materials and processing methods one can make organic electrodes composed entirely of active material that perform well in real devices.

REFERENCES

1. United States Department of Energy Report, Basic Research Needs for Electrical Energy Storage: Report of the Basic Energy Sciences Workshop for Electrical Energy Storage, 2007.

2. Liang, Y.; Tao, Z.; and Chen.; J. Adv. Energy Mater. 2012, 1, 1.

3. Burkhardt, S. E.; Lowe M. A.; Conte, S.; Zhou, W.; Qian, H.; Rodriguez-Calero, G. G.; Gao, J.; Hennig, R. G.; and Abruña, H. D.; Energy. Environ. Sci. 2012, 5, 7176.

4. Poizot, P.; and Dolhem, F.; Energy Environ. Sci. 2011, 4, 2003.

5. Chen, H.; Armand, M.; Courty, M.; Jiang, M.; Grey, C. P.; Dolhem, F.; Tarascon, J.-M.; and Poizot, P.; J. Am. Chem. Soc. 2009, 131, 8984.

6. Gao, J., Lowe M. A., Conte S., Burkhardt, S. E., and Abruña H. D.; Chem. Eur. J. 2012, 18, 8521.

7. Tarascon, J. M.; and Armand, M.; Nature 2001, 414, 359.

8. Chen, H.; Armand, M.; Demailly, G.; Dolhem, F.; Poizot. P.; and Tarascon, J.-M.; ChemSusChem. 2008, 1, 348.

9. Walker, W.; Grugeon, S.; Mentre, O.; Laruelle, S.; Tarascon, J.-M.; and Wudl, F.; J. Am. Chem. Soc. 2010, 132, 6517.

10. Xiang, J.; Chang, C.; Li, M.; Wu, S.; Yuan, L.; and Sun, J.; Cryst. Growth Des. 2008, 8, 280.

11. Song, Z.; Zhan, H.; and Zhou, Y.; Angew. Chem. Int. Ed. 2010, 49, 8444.

12. Armand, M.; Grugeon, S.; Vezin, H.; Laruelle, S.; Ribiere, P.; Poizot, P.; and Tarascon, J.-M.; Nature Mat. 2009, 8, 120.

13. Song, Z.; Zhan, H.; and Zhou, Y.; Chem. Commun. 2009, 448.

14. Zhou, W.; Hernandez-Burgos, K.; Burkhardt, S. E.; Qian, H.; and Abruña, H. D.; J. Phys. Chem. C 2013, 117, 6022.

15. Williams, D. L.; Byrne, J. J.; and Driscoll, J. S.; J. Electrochem. Soc. 1969, 116, 2.

17. Henderson, J. C.; Kiya, Y.; Hutchison, G. R.; and Abruña, H. D.; J. Phys. Chem. C 2008, 112, 3989.

18. Rudge, A.; Raistrik, I.; Gottesfeld, S.; and Ferraris, J. P.; Electrochim. Acta 1994, 39, 273.

19. Mirmohseni, A.; and Solhjo, R.; Eur. Pol. J. 2003, 39, 219.

20. Gurunathan, K.; Murugan, A.V.; Marimuthu, R.; Mulik, U.P.; and Amalnerkar, D.P.; Materials Chemistry and Physics 1999, 61, 173.

21. Musiani, M.; Electrochim. Acta 2000, 45, 3397.

22. Burkhardt S.E.; Rodríguez-Calero, G.G.; Lowe, M.A.; Kiya, Y.; Hennig, R.G.; and Abruña, H.D.; J. Phys. Chem. C 2010 114, 16776.

23. Novak, P.; Müller, K.; Santhanam, K.S.V.; and Haas, O.; Chem. Rev. 1997, 97, 207.

24. Rodríguez-Calero, G. G.; Kiya, Y; Lowe, M. A., and Abruña H. D.; J. Phys. Chem. C 2010, 114, 13.

25. Oyama, N.; Kiya, Y.; Hatozaki, O.; Morioka, S.; and Abruña, H. D. Electrochem. Solid-State Lett. 2003, 6, A286.

26. Rodríguez-Calero G.G.; Lowe, M.A.; Brukhardt, S.E.; and Abruña, H. D.; Langmuir 2011, 27, 13904.

27. Kiya, Y.; Hutchison, G.R; Henderson, J.C.; Sarukawa, T.; Hatozaki, O.; Oyama, N.; and Abruña, H. D.; Langmuir 2006, 22, 10554.

28. Conte, S.; Rodríguez-Calero, G.G.; Burkhardt, S. E.; Lowe, M.A.; and Abruña, H. D. ; RSC Adv. 2013, 3, 1957.

29. Lapkowski, M.; and Pron, A.; Synthetic Metals 2000, 110, 79.

30. Petr, A.; Dunsh, L.; and Neudeck, A.; J. Electroanal. Chem. 1996, 412, 153.

31. Garreau, S.; Louarn, G.; Buison, J.P; Froyer, G.; and Lefrant, S.; Macromol. 1999, 32, 6807.

32. Jeanmaire, D.J.; and Van Duyne, R. P; J. Electroanal. Chem. 1975, 66, 235-247

33. Buttry, D.A.; and Ward, M. D.; Chem. Rev. 1992, 92, 1355.

34. Inzelt, G.; and Bacskai, J.; Electrochim. Acta 1992, 37, 647.

CHAPTER 6

SYNTHESIS AND CHARACTERIZATION OF POLY-3,4-ETHYLENEDIOXYTHIOPHENE / 2,5-DIMERCAPTOTHIADIAZOLE (PEDOT-DMCT) COMPOSITES

Introduction

The energy crisis, and the attendant consequences of the continued use of fossil fuels, has ignited a renewed interest in the research for alternative and renewable energy technologies. The intermittent nature of all renewable energy sources necessitates the development of devices that can store the energy so that there is uninterrupted access. Of particular importance are electrical energy storage (EES) devices.[1-3] One of the most promising candidates for EES are batteries. Among these, Li-ion batteries have, to date, the highest energy density among all secondary batteries.[4-6] However, several reports in the literature have highlighted the importance of improving this already successful technology, if we are to use them in a broader application space (e.g. grid-energy storage).[7-10] In order to improve EES technologies we have focused on cathode materials, since today, the cathode limits the cell capacity.

Traditional cathode materials are composed of metal oxides. These are generally intercalation materials that accommodate lithium ions in their lattices during the charge and discharge process of the battery. The most successful and currently commercialized cathode material is $LiCoO_2$.[11] This material can exchange up to 1

electron per formula unit. However, in practice it is limited to about 0.5 e^-, because the inherent instability. The practical capacity of $LiCoO_2$ is thus around 130 mAh/g. Due to their relative low capacity, low reaction rate (largely due to the intercalation processes), structural instability, resource availability, safety concerns, and price of metal oxides such as $LiCoO_2$, we have decided to study a new family of materials that can in principle address the limitations that most metal oxides inherently possess.

This new family is composed of redox-active small organic compounds. The availability and sustainability of using such materials, accompanied by their high theoretical capacity, high power and broad modifying ability, through organic synthesis, makes them prime candidates as alternative cathodes.[12-16] There are several reports in the literature were organic compounds have been extracted from plants and/or easily synthesized and which exhibit excellent electrochemical performance.[17-18] The most commonly used materials in the literature has been carbonyl based (e.g. quinones). However, other redox active functionalities such as alkyl-amines and nitro groups have been studied as well.[19-20] Another promising family of materials is organosulfur compounds (OSCs).[20-23] This later one is the one under study in this manuscript.

Among OSCs we have chosen the di-lithium salt of 2,5-dimercapto-1,3,4-thiadiazole (Li_2DMcT) as our redox active component. The electrochemical reaction of Li_2DMcT is depicted in Scheme 6.1. During the charge process (oxidation process of the positive electrode), the thiolate from the monomer of Li_2DMcT is oxidized, forming a disulfide bond formation and generating poly-DMcT. During the discharge process (reduction of the cathode), the disulfide bond is cleaved upon reduction,

giving rise to the thiolate monomer form of Li_2DMcT. During these processes polymerization/de-polymerization of the DMcT is occurring. The electrochemical reactions of these processes are slow at carbon electrodes, with rate constants of ca. 1 x 10^{-7} cm/s.[24] However, our group, among several other groups, has studied the electrocatalytic properties of conducting polymers (CPs) towards the redox reactions of OSCs, including Li_2DMcT.[25-27] Among all CPs, PEDOT has shown the best electrocatalytic performance, accelerating the reaction rate of Li_2DMcT by a factor of 12,000.[28]

In this manuscript we have combined PEDOT with Li_2DMcT to create a PEDOT-DMcT composite hybrid material that aims to mitigate some of the limitations of Li_2DMcT, specifically, the conductivity and dissolution problems that OSCs possess. Moreover, by using PEDOT we would also accelerate the reactions of Li_2DMcT, which would give us an enhanced rate capability. A novel strategy for the modification of polymers for EES applications is discussed and shown to be effective for Li_2DMcT. The strategy takes advantage of the post-polymerization modification reaction to modify a CP (i.e. PEDOT-OTs; OTs is tosylate) with a redox active component (i.e. Li_2DMcT) and form a CP that can exchange a higher number of electrons per monomer unit. The theoretical capacity of this material is 130mAh/g (a number that is higher than any traditional CP and which matches the practical capacity of $LiCoO_2$) for 1.5 e^- per monomer unit. The scheme of the electrochemical reactions undergone by the composite material studied herein is depicted in Scheme 2. The source of the electrons in this PEDOT-DMcT composite derives from oxidation and

reduction processes that accompany the formation and cleavage of the disulfide bond in the DMcT pendant.

We present and discuss the synthesis of the PEDOT-OTs precursor, the monitoring of the post-polymerization modification reaction where PEDOT-OTs is reacted with Li_2DMcT to form the PEDOT-DMcT hybrid material, the *in situ* spectroelectrochemistry and the device testing for this composite. Finally, we demonstrate that the material has excellent capacity retention (specially when compared to PEDOT/DMcT) and high power capabilities, albeit the post polymerization modification yield for the electrode films is low and needs to be optimized if the theoretical capacity is to be achieved. However, that optimization is beyond the scope of this manuscript.

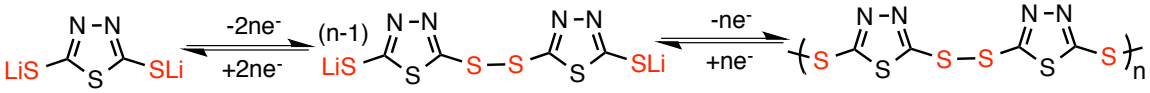

Scheme 6.1. Electrochemical reactions of the thiolate and disulfide bonds of Li_2DMcT monomers and poly-DMcT.

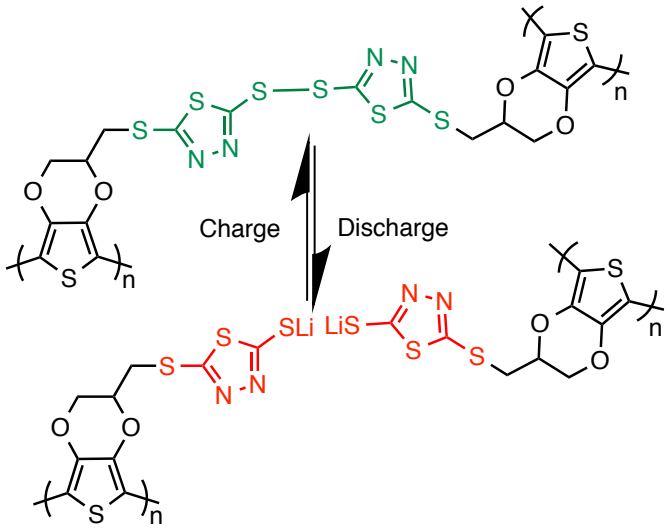

Scheme 6.2. Electrochemical reactions of PEDOT-DMcT composites during charge/discharge (i.e. oxidation and reduction reactions).

Experimental

Synthesis and Reagents

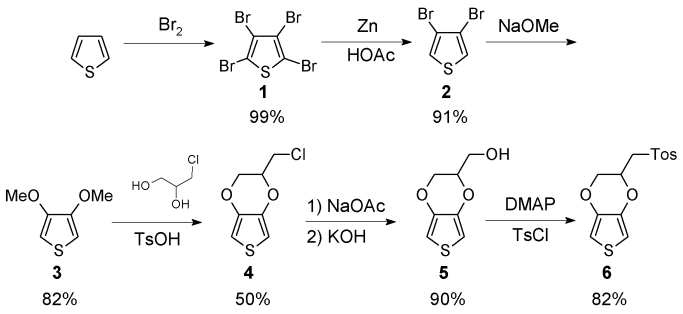

Scheme 6.3. Synthesis strategy for alcohol derivative of EDOT monomer.

Reagents and Materials Purchased

2,5-Dimercapto-1,3,4-thiadiazole di-lithium salt (Li_2DMcT) (battery grade) was purchased from Toyo Kasei Co. (Japan) and used without further purification. High-purity HPLC-grade acetonitrile were purchased from Burdick and Jackson and dried over 3 Å molecular sieves. Triethylamine (TEA) (reagent grade) and dimethylformamide (DMF) (SPECTRANALYZED) were purchased from Fischer Chemicals. Other chemicals were purchased from Aldrich Chemical Co. Inc. and used as received.

Synthesis and Characterization of Individual Species

(2,3-Dihydrothieno[3,4-b][1,4]dioxin-2-yl)methanol (5)

2-(Chloromethyl)-2,3-dihydrothieno[3,4-b][1,4]dioxine **4** (7.30 g, 38.3 mmol) was dissolved in 100 ml of DMSO with three equivalents of anhydrous sodium acetate (9.42 g, 115 mmol) and the resulting solution stirred at 110 °C overnight. The reaction was then poured onto water, extracted with diethyl ether, dried over $MgSO_4$, and the solvent removed *in vacuo* to give 9.30 g of the crude oil. To the crude product was added 120 ml of a mixture of H_2O:EtOH (1:2) and four equivalents of KOH (8.59 g,

150 mmol) and stirred at room temperature for 3 hours after which it was acidified with concentrated HCl and worked up as mentioned above. The reactions could be monitored by TLC as with the starting material at $R_f = 0.62$, the acetate at $R_f = 0.14$, and the alcohol at $R_f = 0.0$ (1:1 dichloromethane:hexanes). The reaction yielded 5.50 g (83% crude) of a crude oil that was carried on to the next step without purification.

(2,3-Dihydrothieno[3,4-b][1,4]dioxin-2-yl)methyl 4-methylbenzenesulfonate (6)

To a solution of (2,3-dihydrothieno[3,4-b][1,4]dioxin-2-yl)methanol **5** (5.50 g, 31.73 mmol), TEA (5.80 ml, 57.42 mmol), and 4-dimethylaminopyridine (DMAP) (0.10 g, 0.77 mmol) in dichloromethane at 0°C was added TsCl (8.76 g, 45.94 mmol) in small portions and the reaction was warmed to room temperature overnight. The reaction was subsequently washed with water and the organic phases combined, dried over $MgSO_4$, and the solvent removed *in vacuo*. The tosylated EDOT (Ts-EDOT) was purified by flash chromatography on silica with solvent changing from 1:2 to 1:0 dichloromethane:hexanes to yield 10.36 g. (82% from the chloro-derivative **4** over three steps) as an oil which slowly gave a white solid under prolonged vacuum. It exhibited a sharp melting point range of 80.5–81.5°C. ^{1}H NMR (300 MHz, $CDCl_3$) δ 7.80 (d, J = 8.2, 2H), 7.37 (d, J = 8.2, 2H), 6.32 (d, J = 3.7, 1H), 6.26 (d, J = 3.8, 1H), 4.36 (dddd or appqd, J = 6.5, 2.3, 1H), 4.20 (m or 3 overlapping dd, 3H), 4.03 (dd, J = 11.6, 6.5, 1H), 2.46 (s, 3H). ^{13}CNMR (100 MHz, $CDCl_3$) δ 145.5, 141.1, 140.6, 132.5, 130.2, 128.3, 100.4, 71.0, 67.1, 65.1, 21.9.

PEDOT-DMcT post-polymerization modification

10 mM solutions of EDOT-OTs in 0.1 M $LiClO_4$/AN were used for the electropolymerization of PEDOT-OTs. The working electrodes were glassy carbon for

the analytical measurements (CV and Raman spectroelectrochemistry) and Au-coated Al foil for the scanning electron microscope (SEM) and coin-cell testing. The PEDOT-OTs electrodes were placed in a 0.5 M Li_2DMcT/DMF solution at 90 °C for 30 minutes. Longer reaction times did not result in a higher yield for the reaction as evidenced by the CV monitoring.

Raman Spectroscopy

Raman measurements were done employing a 3-electrode configuration using a CP film-modified GCE as the working electrode, a Pt coil counter electrode and an Ag wire quasi reference electrode for all the *in situ* measurements. An inVia Renishaw confocal Raman spectrometer using a 785nm excitation wavelength laser at 5% of the intensity using a 20x objective in a Leica microscope was employed.

Electrochemical Measurements

Cyclic voltammograms (CVs) were taken using a 3-electrode setup using a Hokuto Denko (HSV-100), Hokuto Denko (HABF 1580m), or a Bio-Analytical Systems (BAS) CV-27 potentiostat. The reference electrode used for the CV experiments was a home-built Ag/Ag^+ using a silver wire, a fritted tube and a 50mM $AgClO_4$ / 0.1 M $LiClO_4$ / AN inner solution and it was stored in a 0.1 M $LiClO_4$/AN solution. The working electrodes were GCE electrodes.

Scanning Electron Microscope

Au-coated Al foil was used to generate electropolymerized films of PEDOT-OTs. The electropolymerization of the CP onto the Au-coated Al foil was done using the same experimental conditions as used for the electrochemical experiments. After electropolymerization, the electrodes modified with the CP films were reacted, using

the same conditions as the post-polymerization modification discussed herein, rinsed, dried under vacuum for 30-40 minutes and heated to 50 ºC to remove any remaining solvent before transferring to the SEM chamber. Images were taken using an accelerating voltage of 3 keV. A Zeiss SEM model 1550 field emission scanning electron microscope was used to acquire the images.

Device Testing

All electrochemical device measurements were conducted in CR2032 coin cells. The cathodes were prepared using the electrochemical methodology discussed below. The electropolymerized films were dried under vacuum at 80 °C overnight, and cut into circular electrodes with a typical area of 0.71 cm^2. They were then pressed onto nickel foam used as a current collector. Coin cells were assembled in an argon-filled glove box with lithium foil as the anode, Celgard 2320 as the separator, and a solution of $LiClO_4$ (1.0M) in TEGDME as the electrolyte. Galvanostatic discharge/ charge tests were carried out with an Arbin battery testing system. The cells were discharged to 2.0 V vs Li/Li^+ and charged to 4.0 V vs Li/Li^+ at 1 C for each cycle. The capacity was normalized to the overall mass of the PEDOT-DMcT composite.

Results and Discussion

EDOT-OTs and PEDOT-OTs Electrochemistry

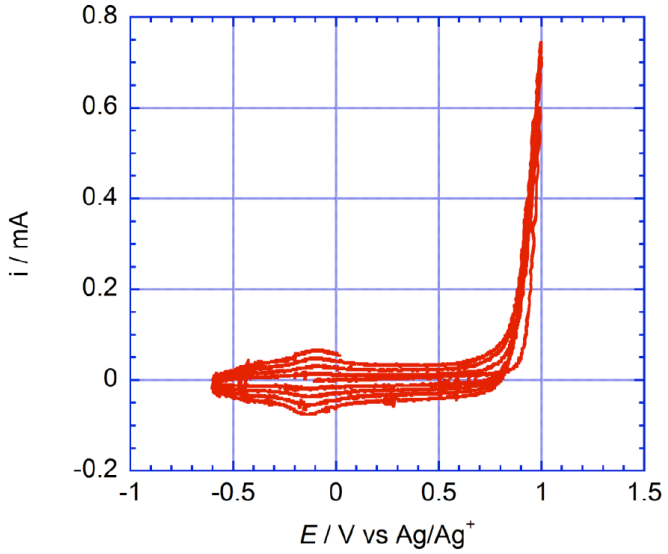

Figure 6.1. Electropolymerization profile for EDOT-OTs (10 mM) in a 0.1 M $LiClO_4$ / AN solution at a GCE. Sweep rate for the electropolymerization was 20 mV/s.

We have employed, to the best of our understanding, for the first time, a post-polymerization modification reaction for the synthesis of EES electrodes. The first step was to synthesize a monomer with a good leaving group (i.e. EDOT-OTs). This was accomplished using the reaction pathway shown in Scheme 6.3. The electropolymerization reaction of EDOT-OTs was conducted via CV as shown in Figure 6.1, were consecutive anodic scans were performed. The incremental cycles exhibited the characteristic electropolymerization profile of CPs. Contrary to EDOT, EDOT-OTs has an onset for oxidation at ca. 0.85 V vs 0.8 V for EDOT. The resulting polymer film CV can be observed in figure 6.2 (0min). In here the onset for p-doped conductivity is ca. -0.8 V, which is more positive than PEDOT by ca. 200 mV. The main doping and de-doping peak are at -0.15 V, which in contrast to PEDOT, are both at the same electrochemical potential.

Post-Polymerization Reaction and PEDOT-DMcT Composites Electrochemical Response

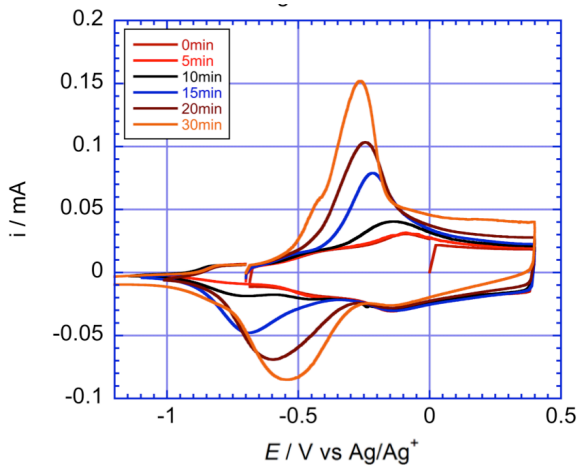

Figure 6.2. PEDOT-DMcT film-modified GCE at different post-polymerization modification reaction times in a 0.1 M $LiClO_4$/AN solution at a sweep rate of 20 mV/s.

Once the PEDOT-OTs films were generated, the film-modified GCEs were immersed in a three-neck reaction flask, sealed under argon, with the reagents needed for the post-polymerization modification reaction (Scheme 6.4). The reaction monitoring via CV is presented in figure 6.2, where the majority of the reaction takes place between 15-25 minutes, with no noticeable changes after 30 minutes.

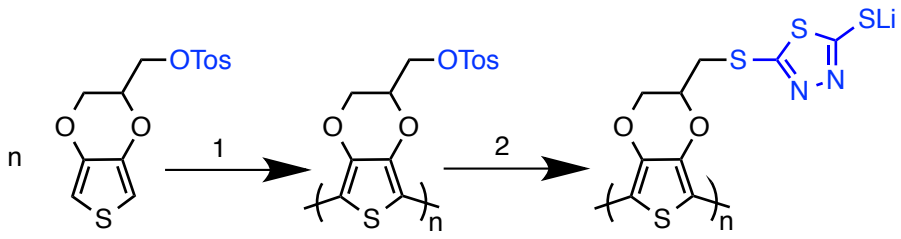

Scheme 6.4. PEDOT-DMcT composite synthetic scheme. (1) electropolymerization in 10 mM EDOT-OTs / 0.1 M $LiClO_4$ at 20 mV/s (2) 0.5 M Li_2DMcT / DMF solution under an Ar atmosphere.

The resulting PEDOT-DMcT composite electrochemistry can be observed in the 30 min CV in figure 6.2. The formal potential for the faradaic processes for this reaction is approximately -0.35 vs Ag/Ag+. This is ca. 3 V vs Li/Li^+, which makes it very attractive as a cathode material for LIBs, especially considering other organics struggle to have an operating voltage above 3 Volts vs Li/Li^+. The percentage of the post-polymerization modification is ca. 5% of all the PEDOT-OTs sites (calculated from the coverage of the polymer vs the area underneath the oxidation peak corresponding to the DMcT oxidation). The electrochemical reactions undergone by the PEDOT-DMcT composite are presented in Scheme 6.2. The oxidation of the thiolate occurs at -0.25 V, and the reduction of the disulfide bond happens at -0.55 V. The rest of the oxidative and reductive current after the oxidation of the thiolate is due to the pseudocapacitance of the CP, which contributes to the overall capacity of the composite.

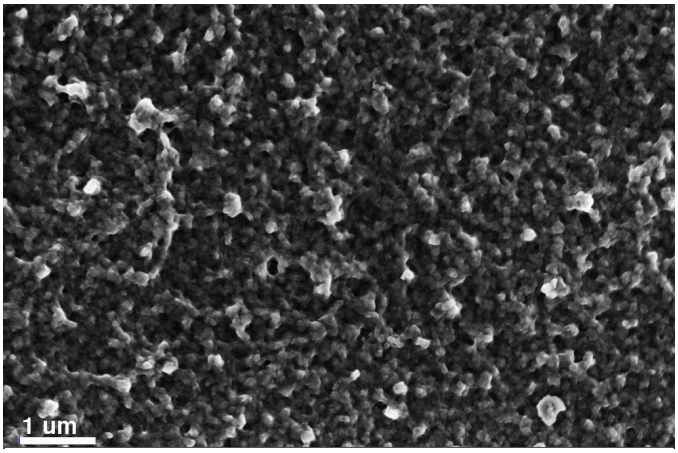

Figure 6.3. SEM image of a PEDOT-DMcT film.

The morphology for the resulting films can be observed in figure 6.3. The SEM image shows that PEDOT-DMcT composites have a mesoporous morphology,

similar to other conducting polymers, with pore sizes around 100 nanometers in size. The mesoporous structure allows, in theory, for good solvent infiltration, and thus, allows higher power densities to be achieved.

Raman Spectroscopy

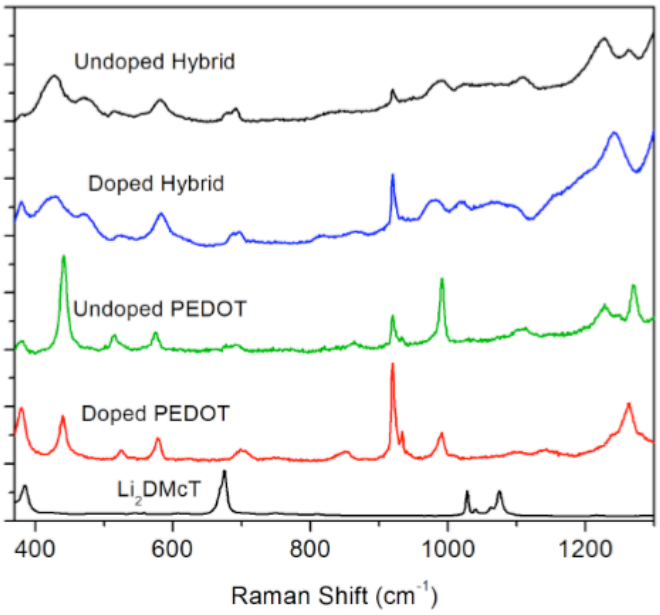

Figure 6.4. Raman spectra of the individual components of the PEDOT-DMcT composite.

Due to the complexity of the system we decided to use standards (i.e. undoped and doped PEDOT films, and Li_2DMcT) and use them to characterize the resulting PEDOT-DMcT composite Raman spectra. The peak assignments for the PEDOT and DMcT spectra can be found in Table 6.1 and the approximate vibration descriptions were obtained from the literature.[22, 30-34] From these spectra we can surmise that the PEDOT-DMcT composites are a convolution of the DMcT and PEDOT Raman spectra (Figure 6.4). However, since we have low yields they are largely dominated by the CP peaks. This is further evidenced by the large peaks above 1200 cm^{-1} that are

due to the bonds in the thiophene ring of the CP backbone. These peaks broaden as the composite is oxidized since the thiophene bonds acquire a quinoid character upon oxidation. We notice the emergence of some peaks between 1000 and 1100 cm^{-1} that are most likely due to the presence of the DMcT in the PEDOT-DMcT composite. There is a peak at 360 cm-1 that has been attributed to bending and torsion modes of the DMcT.

Table 6.1. Raman Shifts for PEDOT, Li_2DMcT and PEDOT-DMcT

undoped PEDOT	approx. vibration description	Li_2DMcT salt	approx. vibration description	PEDOT-DMcT	approx. vibration description
Raman shift in cm^{-1} (corresponding vibration)					
1520 1431 1369 1270 1226	asym. C=C str, sym C=C, C-C str, C-C interring	1375	C=N	region 1100-1300	asym. C=C str, sym C=C, C-C str, C-C interring
		1072	A1 Ring Mode		
1111	C-O-C def	1024	N-N	region 1000-1100	A_1 ring mode, (N-N) (from DMcT)
991	oxyethylene ring def	671	C-S-C		
692 571	C-S-C def, oxyethylene ring def.	532	S-S	region 300-600	(C-S-C), (S-S)

In situ Raman Spectroelectrochemistry

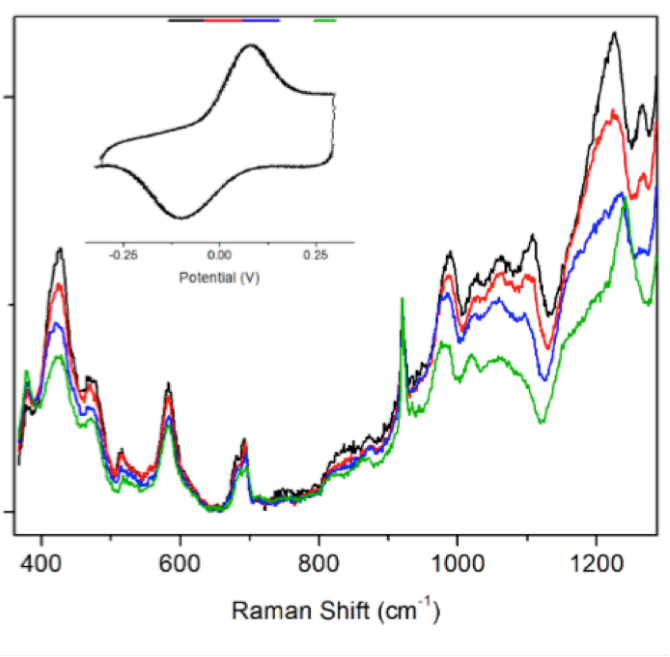

Figure 6.5. Raman spectroelectrochemistry of a PEDOT-DMcT film-modified GCE in a 0.1 M $LiClO_4$ / AN solution at a sweep rate of 10 mV/s.

The redox reactions of PEDOT-DMcT composites were tracked using Raman spectroelectrochemistry (figure 6.5). The experiment was done using a PEDOT-DMcT film-modified GCE as the working electrode, a Pt wire as the counter electrode and a Ag wire as a quasi-reference electrode. The electrochemical cell used was custom built. The electrochemical potential was swept at 10mV/s while collecting Raman spectra. Because we were only interested in monitoring the redox reactions of the DMcT pendant we only swept the potential over a 600 mV range where the DMcT redox activity was observed.

There are three spectral regions that show the majority of the changes in the Raman spectra. The first spectral range is at lower wavenumbers from 400-600 cm^{-1}. This region is involved with the disulfide bond vibrations and the bending and torsional modes of the DMcT and the C-S-C bonds of the thiophene ring. These

changes are expected since we are oxidizing the polymer and we are also oxidizing the DMcT, which will change the intensity and bending modes of the mentioned bonds. The second region that is undergoing significant changes in the Raman spectra is the region from 1000-1100 cm^{-1}. The changes here are predominantly from the DMcT unit since PEDOT has little Raman activity over this spectral range. The vibrations are from the thiadiazole ring, and the changes are due to the oxidation of the thiadiazole ring and the associated changes in bonding of the said ring. This is clear evidence that we are, in fact, oxidizing the DMcT pendant. The last spectral range that has significant changes with the applied potential is the 1100cm^{-1} – 1300 cm^{-1} region. These changes in the spectra are due to the thiophene neutral form to quinoid-type thiophene ring that PEDOT undergoes at higher doping levels.

Interestingly, DMcT dimers have a peak around 532 cm^{-1} corresponding to the disulfide bond. In this case, we could not resolve a peak from the disulfide bond formation that we expected when DMcT was oxidized. This could suggest that the low percentage of modification with DMcT in the samples used for Raman is not sufficient to detect the formation of the disulfide bond. There is no conclusive evidence as to what chemical mechanism is happening in the PEDOT-DMcT composite, however since we indeed have spectral signatures from the DMcT, the proposed mechanism should still be the disulfide bond formation and cleavage even if we do not observe the disulfide bond peak at 532 cm^{-1}.

Device Testing

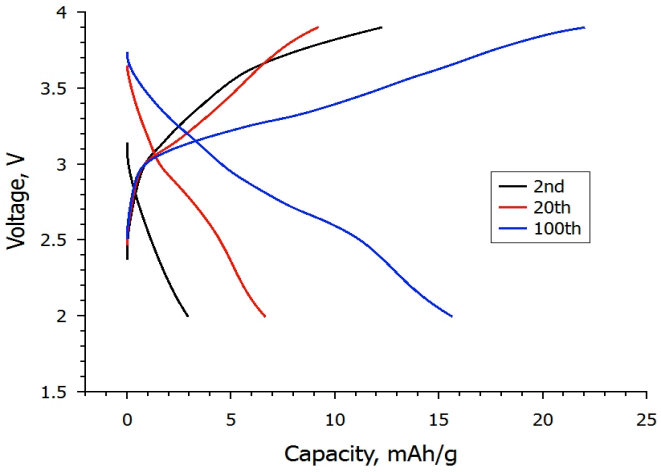

Figure 6.6. Half-cell charge / discharge curves for a PEDOT-DMcT film-modified in 1M LiTFSI / TEGME solution discharge/charge rate of 1C.

The electrosynthesis of PEDOT-DMcT films was then modified to produce higher mass and thicker (ca. 30 μm) polymer films. This was necessary to obtain higher accuracy in the mass measurements. We produced films that weighted between 1-2 milligrams. The electrode in this case was an Au coated Al foil (used as the current collector). The electropolymerized films were placed into half-cells to perform device testing. The theoretical capacity of PEDOT-DMcT should be 130 mAh/g assuming 1.5e- per monomer unit (this accounts for the 1e- oxidation of the thiolate to the disulfide and for the 0.5 electrons due to the pseudocapacitance of the PEDOT electrode). The charge discharge tests had a plateau at 2.7 V vs Li/Li^+ where the formal potential of DMcT oxidation/reduction is (Figure 6.6). The capacity retention of the PEDOT-DMcT electrodes is significantly enhanced and no significant decrease in the capacity can be observed. The practical capacity obtained was 17 mAh/g which is ca. 13% of the theoretical gravimetric capacity. We believe this is due to the large

thickness of the polymer film and that by slightly modifying the post-polymerization modification conditions higher percentage of modification can be obtained.

More importantly, we have significantly improved the electrochemical stability and by consequence the battery cycling ability of DMcT type compounds. We believe the enhanced stability is due to the insoluble and conducting PEDOT backbone. It is important to note that the capacity remains constant even after 100 cycles. This is comparable to the traditional performance of conducting polymers by themselves, except that in this case we have a purely faradaic process dominating the capacity. Moreover, the electrode is only composed of active material, further improving the electrode capacity by precluding the need for conductive additives or binders. Furthermore, one can imagine utilizing this approach to modify films, via post-polymerization modification, with compounds that possess more than one redox couple. This would increase the overall capacity of the films significantly, producing an electrode with improve gravimetric energy density.

Conclusions

We have developed a new strategy to modify CPs for electrochemical energy storage applications that takes advantage of a post-polymerization modification approach. The electrochemical characterization of these PEDOT-DMcT composite hybrids has been carried out and the response for the electrochemical reactions of the DMcT can be observed superimposed on the pseudocapacitance of the CP. The formal potential (or operating voltage) for this material is 3V vs Li/Li^+ as evidenced by the CV and device testing experiments. The *in situ* Raman spectroelectrochemistry shows evidence of the DMcT pendant. However, due to the low modification percentage, the

disulfide bond formation and cleavage was not unambiguously observed. Finally, The device testing measurements show that we are only accessing 13% of the 130 mAh/g theoretical capacity. We believe that small changes to the post-polymerization modification reactions would increase the yield of such reaction and in turn significantly improve the practical capacity while retaining the same electrochemical cycling properties.

REFERENCES

1. United States Department of Energy Report, Basic Research Needs for Electrical Energy Storage: Report of the Basic Energy Sciences Workshop for Electrical Energy Storage, 2007.

2. Goodenough, J. B.; and Kim, J.; Chem. Mater. 2010, 22, 587

3. Tarascon, J. M.; and Armand, M.; Nature 2001, 414, 359.

4. Bruce, P. G.; Scrosati, B.; and Tarascon, J.-M.; Angew. Chemie Int. Ed. 2008 47 2930

5. Liu, C.; Li, F.; Ma, L.-P.; and Cheng, H.-M.; Adv. Mater. 2010, 22, E28

6. Etacheni, V.; Marom, R.; Elazari, R.; Salitra, G.; and Aurebach, D.; Ener. Environ. Sci. 2011, 4, 3243

7. Dunn, B.; Kamath, H.; and Tarascon, J.-M.; Science 2011, 334, 928

8. Skyllas-Kazacos, M.; Chakrabarti, M. H.; Hajimolana, S. A.; Mjalli, F. S.; Saleem, M.; J. Electrochem. Soc. 2011, 158, R55

9. Cheng, F.; and Chen, J.; Chem. Soc. Rev. 2012 41, 2172

10. Conte, M.; Fuel Cells 2010, 10, 806

11. Armand, M.; Grugeon, S.; Vezin, H.; Laruelle, S.; Ribiere, P.; Poizot, P.; and Tarascon, J.-M.; Nature Mat. 2009, 8, 120.

12. Zhou, W.; Hernandez-Burgos, K.; Burkhardt, S. E.; Qian, H.; and Abruña, H. D.; J. Phys. Chem. C 2013, 117 (12), 6022.

13. Walker, W.; Grugeon, S.; Mentre, O.; Laruelle, S.; Tarascon, J.-M.; and Wudl, F.; J. Am. Chem. Soc. 2010, 132, 6517.

14. Novak, P.; Müller, K.; Santhanam, K.S.V.; and Haas, O.; Chem. Rev. 1997, 97, 207.

15. Song, Z.; Zhan, H.; and Zhou, Y.; Chem. Commun. 2009, 448.

16. Rudge, A.; Raistrik, I.; Gottesfeld, S.; and Ferraris, J. P.; Electrochim. Acta 1994, 39, 273.

17. Chen, H.; Armand, M.; Demailly, G.; Dolhery, F.; Poizot, P.; Tarascon, J.-M.; Chem. Sus. Chem. 2008, 1, 348.

18. Yao, M.; Senoh, H.; Yamazaki, S.-I.; Siroma, Z.; Sakai, T.; and Yasuda, K.; J. Pow. Sour. 2010, 195, 8336.

19. Nishide, H.; Iwasa, S.; Pu, Y.-J.; Suga, T.; Nakahara, K.; and Satoh, M.; Electrochim. Acta 2004, 50, 827.

20. Conte, S.; Rodríguez-Calero, G.G.; Burkhardt, S. E.; Lowe, M.A.; and Abruña, H. D. RSC Adv. 2013, 3, 1957.

21. Visco, S. J.; Maihe, C. C.; De Jonghe, L. C.; and Armand, M. B.; J. Electrochem. Soc. 1989, 136, 661.

22. Pope, J. M.; Sato, T.; Shoji, E.; Buttry, D. A.; Sotomura, J.; and Oyama, N.; J. Pow. Sour. 1997, 68, 739.

23. Kiya, Y.; Henderson, J. C.; Hutchison, G. R.; and Abruña, H. D.; J. Mater. Chem. 2007, 17 4366.

24. Rodríguez-Calero, G. G.; Kiya, Y; Lowe, M. A., and Abruña H. D.; J. Phys. Chem. C 2010, 114, 13.

25. Oyama, N.; Kiya, Y.; Hatozaki, O.; Morioka, S.; and Abruña, H. D. Electrochem. Solid-State Lett. 2003, 6, A286.

26. Rodríguez-Calero G.G.; Lowe, M.A.; Brukhardt, S.E.; and Abruña, H. D.; Langmuir 2011, 27, 13904.

27. Kiya, Y.; Hutchison, G.R; Henderson, J.C.; Sarukawa, T.; Hatozaki, O.; Oyama, N.; and Abruña, H. D.; Langmuir 2006 22, 10554.

28. Kiya, Y.; Hatozaki, O.; Oyama, N.; Abrun˜a, H. D.; J. Phys. Chem. C 2007, 111, 13129

29. Gao, J.; Lowe, M.A.; Conte, S.; Burkhardt, S. E.; and Abruña, H. D.; Chem. Eur. J. 2012, 18, 8521

30. Lapkowski, M.; and Pron, A.; Synthetic Metals 2000, 110, 79.

31. Petr, A.; Dunsh, L.; and Neudeck, A.; J. Electroanal. Chem. 1996, 412, 153.

32. Garreau, S.; Louarn, G.; Buison, J.P; Froyer, G.; and Lefrant, S.; Macromol. 1999, 32, 6807.

33. Van Wart, H. E.; Lewis, A.; Scheraga, H.A.; and Saeva, F.P.; Proc. Nat. Acad. Sci. 1973, 70, 2619

34. Edwards, H. G. H.; Johnson, A. F.; and Lawson, E. E.; J. Mol. Spec. A 1995, 351, 51

35. John Xavier, R.; and Dinesh, P.; Spectrochim. Acta A 2013, 113, 171

CHAPTER 7

CONCLUSIONS

In this dissertation I detailed strategies for the successful use of conducting polymers (CPs) in electrochemical energy storage (EES) cathode materials. The electrocatalytic effect of CPs towards organosulfur compounds was determined to be dependent on the position of the window of conductivity of the CP with respect to the formal potential of the organosulfur compound. Among polythiophene derivatives, poly-3,4-ethylenedioxythiophene (PEDOT) was the best electrocatalyst. Furthermore, the heterogeneous charge transfer kinetics rate constant varied by an order of magnitude in CPs in which the formal potential of the organosulfur compound was within the window of conductivity of the selected conducting polymer. This suggests that there are other chemical effects governing the electrocatalysis phenomena.

The concept of redox active substituted conducting polymers (RAS-CP) was established and the theoretical capacity of conducting polymers was increased at least threefold. The electropolymerization reaction conditions for successful CP film formation were detailed. It was found that to yield a redox active CP film, the redox active substituent oxidized products have to be stable in the electropolymerization media. For these studies PEDOT-bismethylmethiobithiophene (PEDOT-BMTbT) was used as a model compound. The electrochemical cycling of the films was studied via Raman spectroelectrochemistry. RAS-CPs were then designed with higher capacities and greater electrochemical stability. The resulting RAS-CP was PEDOT-

tetraalkylphenylenediamine (PEDOT-TAPD). The *in situ* characterization was carried out to determine the material's failure pathways. The major failure pathway in the PEDOT-TAPD RAS-CP film was found to be charge trapping inside the CP film. The methodology for testing this RAS-CP in coin-cells was developed. More importantly, the practical capacity obtained for PEDOT-TAPD films was ca. 70 mAh/g, which is higher than any other CP presented in the literature. The electrode was only composed of active material, which precludes the need for binders and conductive additives, further evidence that RAS-CPs are attractive cathodes for EES.

Finally, a new methodology was developed for the synthesis of RAS-CPs. The post-polymerization modification approach was carried out for the first time in a CP based cathode material. PEDOT-tosylate (PEDOT-OTs) was used to modify PEDOT with 2,5-dimercaptothiadiazole (DMcT). This approach covalently binds PEDOT and DMcT to prevent capacity fade due to the dissolution of the DMcT into the electrolyte solution in the battery.

This dissertation illustrates the strength of electropolymerization as a tool for the study of CPs. There is a large parameter space that can be explored and fine-tuned by changing the electropolymerization conditions. Morphology, film thickness, polymer composition and crystalinity are among the important properties that can be easily altered in electropolymerization experiments. Further studying these electropolymerization parameters could aid the design of RAS-CPs with improved properties.

The use of CPs as electrochemical energy storage platforms has been described in detail in this dissertation. The electropolymerization technique proved to be key for

the successful incorporation of these materials into prototype devices. Materials were designed that had practical capacities and improved performance when compared to the contemporary literature.

Moving forward, the design, synthesis and characterization of CP based materials with improved capacity and energy density should be carried out. If film thicknesses are high enough to cause capacity fade due to charge trapping in CP films, high surface area electrodes and thin films should be used to mitigate these undesired effects. The investigations carried out in this dissertation should be used as a starting point to design materials that have improved electrochemical stability, higher voltages and higher gravimetric capacities for electrochemical energy storage applications.

THE END